Iridoplasts as a photonic structure

By

HUGH PERRYMAN

UNIVERSITY OF BRISTOL

A dissertation submitted to the University of Bristol in accordance with the requirements of the degree of DOCTOR OF PHILOSOPHY in the Faculty of Science.

JUNE 2022

Word count: 24497

Abstract

Photonic structure is used extensively in nature to achieve colourful displays for visual signalling in diverse inter- and intra-specific relationships. This has been well studied for many animal and plant species with the use of structural colouration ranging from camouflage, signalling for warning, mating, seed dispersal, pollination and even social status.

This research sets out to investigate the modified chloroplast found commonly in Begonia species which, using ordered multilayer structures acts as a photonic structure to manipulate its interaction with light. Crucially, whilst the photonic structure here does cause colouration which can be visible under specific conditions, it is not likely to be the primary purpose. Previous research has shown that the photonic structure in iridoplasts may contribute towards an increased photosynthetic yield in low light conditions. Here iridoplasts in Begonia species have been investigated using Fourier-plane microspectrometry, autofluorescence confocal microscopy and transmission electron microscopy to measure structural properties and compare optical modelling to measured spectra. Novel green-reflecting iridoplasts have been characterised and their optical properties compared to more common blue-reflecting iridoplasts showing that these structures may be far more common in nature as they are not visible to the naked eye. The response of iridoplast ultrastructure was tested in acclimation to different wavelengths of light showing that the photonic structure is conserved under greatly varying spectral quality, unlike mesophyll chloroplasts which show drastic ultrastructural changes. In one species iridoplasts grown under blue light showed a consistent structural response indicating some wavelength tuning is possible. The effects of natural disorder found in real iridoplast images was analysed and discussed in comparison to recent theoretical studies. The findings show that the optical characteristics are robust against even the highest levels of disorder and, in contrast to a recent theoretical study, this work finds no strong evidence for the presence of correlated disorder which may have implications for the way iridoplasts form.

Dedication and acknowledgements

Many people contributed their expertise and assistance to me during this work. First and foremost I would like to thank both of my supervisors, Ruth Oulton and Heather Whitney for all the support they provided. I would like to thank Alanna Kelly for her tireless work and her endless and vital expertise on plants. Nathan Masters, O-Phart Phrathep, Sverre Tunstad, Rox Middleton, Hilary McCarthy and Alex Liu provided countless hours of fruitful discussion and moral support for which I am very grateful.

COVID-19 Statement

The COVID-19 pandemic caused planned research in this thesis to be curtailed due to lack-of-access to research facilities during periods of national restrictions, this resulted in the decision to only include two research chapters in the final thesis.

In March 2020 I had been preparing for ten weeks to undertake experimental work on single-celled green algae. This included preparing and testing different growth media, growing cultures of relevant species to learn the process and gathering pilot data using various microscopy techniques. This work was going to form a second research topic, in addition to work I planned to do on iridoplasts in Begonia plant species. It would have constituted at least one research chapter, in addition to two chapters on iridoplasts in Begonia species.

The work on Begonia species naturally entailed growing plants via leaf/stem cutting propagation. At least two of the species of Begonia I planned to work with had growing seasons between April-July in which the propagation of plants would be reliable in terms of growth and expression of iridoplasts (even when using controlled growth rooms). The work on green algae would have worked well to utilise the research time during the winter months, when some of the Begonia species were not reliable to work with.

Research using Begonia plants was planned for the early summer months of 2020. I first was able to return to using the research facilities in the Life Sciences building in July of 2020. After preparatory work ordering and testing many different bulbs and light filters, and after the 4-6 week propagation time of Begonia plants I was able to start gathering experimental work from late August. I carried out work until late October and attempted to grow one important species - B. sutherlandii in December (between the lockdowns in November and late December). Due to its growing season (April-July) the work on B. sutherlandii was unsuccessful. The experimental work carried out between late August and late October was also of limited use. It was valuable as a trial run for the next growing season but was not of a quality to go in the thesis. This work took priority over any work on green algae as it was the work most relevant and well established for the thesis.

In December 2020 the funding body UKRI made a communication to all current postgraduate students with the suggestion *"you should now talk to your supervisor in order to plan your project in a way that allows you to complete it within your funded period. "*. With the looming prospect of another lockdown at the end of December the decision was made by myself to cease any work on green algae and focus all of my available time left on iridoplasts in Begonia.

After the unsuccessful work growing B. sutherlandii out of season I also was considering not

attempting to grow it again to prioritise research time towards the main experimental work as I already had some data for B. sutherlandii. After the January-March lockdown in 2021 I consolidated my decision to not collect any more experimental results on B. sutherlandii so that I could prioritise my time and consumables budget (for TEM and confocal microscopy) towards the planned experimental work which now constitutes chapter 4. This decision meant that there were significant contributions to *in vivo* reflectance measurements, TEM structural data and modelling in chapter 3 that were not possible.

Finally, since almost all of the experimental work for this thesis was carried out between September 2020 - November 2021 (the third year of my degree) it meant that I could only use one academic year's consumables budget (£1000 per annum) rather than spread the work over two years of budget. This impacted TEM microscopy most significantly and lead to the decision not to use any cryo-EM techniques which may have significantly augmented the findings for the structural measurements and optical modelling. This is discussed in chapter 4.

AUTHOR'S DECLARATION

I declare that the work in this dissertation was carried out in accordance with the requirements of the University's Regulations and Code of Practice for Research Degree Programmes and that it has not been submitted for any other academic award. Except where indicated by specific reference in the text, the work is the candidate's own work. Work done in collaboration with, or with the assistance of, others, is indicated as such. Any views expressed in the dissertation are those of the author.

SIGNED: ..... DATE: .....

TABLE OF CONTENTS

List of Figures

CHAPTER 1

INTRODUCTION

The use of colour in biology has been widely studied and is most commonly associated with inter- and intra-specific communication or signalling. Many species use colour as a warning to predators [1], to attract mates [2], deter competing individuals [3] and it can be an indicator of social status [4]. Camouflage and mimicry seen widely among arthropods use colouration along with a host of other physiological features [5]. Plants use colour to attract pollinators [6] or dispersers [7], and many examples of these are co-evolutionary adaptations for species recognition [8].

Colour may be a by-product of some other mechanism, the most prominent example being photosynthesis. The prevalence of the green pigments chlorophyll-a and -b in photosynthetic membranes colours the foliage of most plants green. Heavy red pigmentation with anthocyanins has been proposed as a mechanism of photoprotection [9]. Carotenoids, a family of orange and yellow pigments, as well as anthocyanins play a role in optimising the resorbtion of nutrients during autumn leaf senescence in many trees [10, 11].

1.1 Physical basis of colour in nature

Colour is fundamentally governed by the relative amounts of different wavelengths of light in a spectrum, for humans and most mammals the perceivable range of wavelengths is between $400 - 700nm$, known as visible light. Many species can perceive wavelengths of light outside of this range. Shorter wavelength ultraviolet light ($280 - 400nm$) is used by pollinating insects to find flowers [12, 13] and some species of fish use far-red and near-infrared light (700 – 1100nm) in the deep sea or turbid (cloudy) waters [14, 15].

Colour is also a property of the material, independent of the thing perceiving it. Visible light can

interact with many biological materials through scattering or absorption, or may be transmitted if it is transparent. A biological entity might emit its own light though bioluminescence, which is usually based on chemiluminescent reactions. This is present in an extremely broad range of species across cyanobacteria, algae, insects and worms [16, 17], but is most prevalent in the deep sea [18] where sunlight is negligible.

1.1.1 Pigment Colour

Pigments are biological molecules which have strong absorption in narrow wavebands of the visible spectrum. The absorption spectra of pigments are dictated by the molecular structure and chemical makeup.

Electrons in molecules exist in discrete energy levels associated with the allowed electronic states in that system. A photon of light can interact with the electronic states in a molecule if the photons energy is equal to the difference between an electrons current energy (generally the ground state energy is considered), and another energy level in the system. The photon, and its energy will be absorbed by the electronic state, causing a transition to an excited vibrational state after which a number of processes can occur.

The excited vibrational state can lose its excess energy to vibrational modes, either within the molecule or to surrounding molecules. This is known as vibrational relaxation. It is the dominant process and as no photons are re-emitted this is considered as absorption. The excited state may drop back down to the ground state in a reverse process of the initial excitation, in which case a photon is re-emitted with the same energy and this is known as elastic scattering. If the excited state drops down to the ground state in more than one step the energy of the emitted photon must be lower than the initial photon and this is known as fluorescence. Phosphorescence follows a similar transition to fluorescence but is much less common in biological molecules. Fluorescence and phosphorescence are not considered as forms of colouration in biology as the amount of light emitted by these processes compared to elastic scattering is negligible. The absorption process of pigments does subtract a significant amount of light at specific wavelengths so is considered a form of biological colouration.

During the emissive processes, photons are emitted isotropically, meaning equally in all directions and can not have any relationship to the initial photon apart from energy. This is why iridescence (which will properly explained in the next section) is not possible using only pigment colouration.

Another method used in nature to produce colouration is structural colour which is based on the interference of light with structures on the scale of the wavelength of light.

1.1.2 Structural Colour

Structural colour refers to a broad range of phenomena where interference effects cause different wavelengths of light to be selectively reflected, absorbed or transmitted based on material substructure on the scale of the wavelengths of light. This can cause brilliant colouration without the presence of pigments. Interference effects in organic structures generally arise from thin films, stratified media, opal structures and diffraction gratings.

When light travels through a translucent dielectric material, it will travel at a reduced speed governed by the refractive index of the material. This in turn causes the wavelength of light in that material (λ_n) to reduce by a factor of the refractive index (n), given by $\lambda_n = \lambda/n$. When it meets the interface of two regions of different refractive index the light will be partially reflected, and partially transmitted, depending on the magnitude of the difference between the two regions. Reflections of individual rays are always specular (meaning the angle of reflection is equal to the angle of incidence) but transmitted light will be refracted, that is, its direction of propagation will be deflected if the refractive indices differ.

If a structure is made up of many regions of differing refractive index then as light is partially reflected and transmitted at each interface the superposed waves will combine, or interfere, and exactly how they do is governed by the relative phase of the waves. A phase change of 180° (half a wavelength) occurs at the reflection of a wave travelling from a region of higher to lower refractive index, and the phase of a wave changes continuously during propagation through a material. Reflection of a wave going from a region of low to high refractive index and the transmission of a wave through an interface causes no phase change.

It can be shown that if a structure has periodic change in refractive index on a length scale similar to the wavelength of light then constructive interference can dominate in the reflected waves. The outgoing waves are said to have a coherent phase relationship in this case, as the phase difference of the superposed waves usually corresponds to half-, quarter- or some integer factor of the wavelength. The structure with ideal parameters for maximal constructive interference is called the Bragg reflector (see figure 1.1). It is distinguished as a multilayer structure made up of alternating layers with different refractive indices, n_1 and n_2, and thicknesses that create an optical path length of $\lambda/4$. The optical path length (OPL) takes in to account the change in wavespeed and therefore wavelength in a medium and is useful to consider when dealing with interference effects as it can tell us how much the phase of a wave has changed over a given distance. It is given by $OPL = dn$, where d is the physical distance and n is the refractive index of that medium. Given that the optical path length of each layer in the Bragg reflector is $\lambda/4$, the phase change through one layer is 90°, or $\pi/2$. Upon reflection from an interface of lower to higher refractive index an additional phase change of 180° occurs, and travelling back through the same

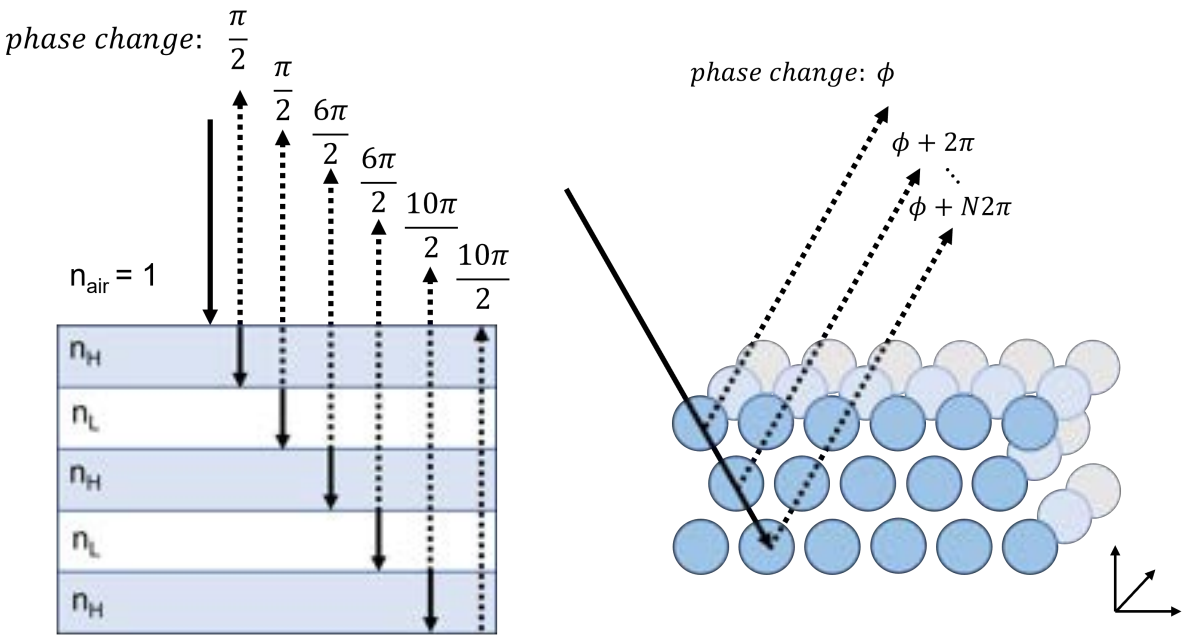

FIGURE 1.1. Coherent phase relationships of light reflected from different photonic structures. **LEFT** 1D multilayer photonic crystal with biphasic layering, using the quarter-wave structure of a Bragg reflector (each layer has thickness equal to the optical path length of a quarter wavelength, see section 1.1.2. Each pair of arrows shows the subsequent partial transmission (bold line) and reflection (dotted line) of the same initial beam, separated laterally for clarity. The additional phase gained by the each of the reflected beams when they leave the structure vertically are shown in radians above the beams. **RIGHT** An example of a 3D photonic crystal made up of close-packed spheres acting as scattering centres. Axes in bottom right to denote 3D.

layer gives another phase change of 90°. This means that for rays reflected from all layers except the first, the overall phase change experienced will be some integer of 360°, a full wavelength, leading to complete constructive interference. An example of this can be seen in figure 1.1. The absolute reflectance is determined by both the number of layers, and the refractive index contrast between the layers [19]. The refractive index contrast has a strong influence on how much light is reflected, since higher contrast leads to greater partial reflectance at each interface. Structures with high refractive index contrast ($|n_1 - n_2| = 0.6$) can approach 100% reflectance in 10-13 layers, whilst lower contrast ($|n_1 - n_2| = 0.05$) may take as many as 60 layers to achieve the same [20]. The amount of light that is reflected and transmitted at an interface of two regions of different refractive index is governed by the Fresnel coefficients for reflectance and transmittance.

The multilayer structure is an ideal reflector when it has a quarter-wave optical thickness,

but will still lead to significant amounts of reflectance when the dimensions are not exact. It is also apparent that light travelling through a distributed Bragg reflector at an angle may come close to complete constructive interference for a different wavelength of light, as the path length is changed. This can lead to iridescence, which is defined as the changing of reflected wavelengths, as the viewing angle changes. Whilst iridescence can only arise due to the presence of photonic structure, photonic structures do not always give rise to iridescence (see incoherent scattering, below, polycrystals and quasi-ordered arrays, section 1.3.1).

The distributed Bragg reflector is an example of a 1D photonic crystal, since the material variation is periodic in only 1 dimension. However, the same physics can apply to 2D or 3D photonic crystals, as in the case of opal-like structures, shown in figure 1.1. Here spherical scattering bodies are arranged in a close packed ordered structure where the crystal planes can act as the layers in a multilayer structure. This gets its name from the mineraloid, Opal, which is made up of transparent silica spheres. Generally these are amorphous but may have extremely well ordered domains, leading to significant photonic effects.

Photonic crystals with differently ordered domains, referred to as quasi-ordered arrays or polycrystals can also achieve structural colour based on coherent scattering even with the introduction of long range disorder. In this case iridescence may not be strong or present at all.

Diffraction gratings are another photonic structure with a coherent phase relationship. In this case light is incident on a surface of periodic parallel striations, or transmitted though a periodic grating of parallel lines. The reflected or transmitted waves at each line in the grating can be thought of as new point sources, undergoing diffraction-like interference if the period of the grating allows. Here it is even more clear that light travelling at different angles will have different path lengths that allow for coherent interference over a continuous range of wavelengths – leading to iridescence.

There are also examples of incoherent scattering, which produce colour by optical effects but do not show a coherent phase relationship in the outgoing waves. Rayleigh scattering, Tyndall scattering and Mie scattering all arise from a system of randomly and sparsely distributed particles which act as scattering centres. These are differentiated by the size of the particle relative to the wavelength of light. For particles much smaller than the wavelength of light (Rayleigh scattering), the photon may be absorbed and re-emitted at the same energy, in a two-photon process. In this case the mean free path, related to the scattering cross-section is inversely proportional to the wavelength of light. This is demonstrated by the blue colouration of the sky: white sun-light is scattered by gas molecules in the atmosphere and the shorter (blue) wavelengths are scattered much more readily than longer (red) wavelengths. Tyndall scattering accounts for the regime

where the particle size is similar to the wavelength of light and Mie scattering is a special case solution for spherical particles. In these cases the scattered light may be weakly angle-dependent, but this does not derive from the same coherent phase relationships as iridescence.

1.2 Analysing structural colour

Detailed characterisation of biophotonic systems can lead to a deeper understanding of the purposes or evolution of structurally coloured regions in plants, algae and animals, as well as providing inspiration for biomimetic applications. Over the years this field of research has implemented a range of techniques such as optical measurement, imaging of the substructure using electron microscopy and optical modelling. Since many photonic structures in biology are iridescent, a common way to analyse the optical response is to measure the reflectance spectrum over a wide range of angles, usually in one angular dimension. This must be achieved by different methods for macroscopic and microscopic measurements.

For macroscopic measurements, the sample, or detected light may be rotated using goniometric apparatus, allowing for measurement of the angular reflectance properties. Broadband light is essential as the reflected wavelength varies with angle in iridescent structures. The waveband may be different depending on the sample, for example flowers may have significant reflectance in the UV whereas many bird feathers may only reflect in the visible spectrum. Collimated light conserves intensity over distance and is necessary to determine the scattering angle accurately. However for microscopic measurements requiring an illumination spot on the order of microns or less, rotation of the sample will introduce undesirable effects. The rotation of the sample will move the illumination spot unless it is at precisely the centre of rotation, and a circular spot may be stretched into an elliptical spot, changing the illumination area and making it more difficult to compare the optical response at different angles accurately. In this case it is much more suitable to measure the angle-resolved reflectance spectrum using a Fourier plane microspectrometry set up.

It is well known in optics that a thin lens will produce a spatial Fourier transform of an object in the front focal plane at its back focal plane (BFP) [21]. In practise, the most useful aspect of this transformation is that parallel rays leaving the object at a particular angle in the front focal plane of a lens will be focused at a particular spatial position in the BFP. Therefore, for iridescent samples all of the angular range supplied and collected by the objective lens is presented in a spatially resolved flat plane which can be collected by a spectrometer to measure the angular reflectance spectra. This is usually done in a 4F configuration, where the BFP of an objective lens is projected out, using a series of lenses, to a location where it can be magnified and collected, either by a camera to collect the full image [22], or by spectrometer. One can collect the light for a

spectrometer using an optical fibre which acts as a small aperture only collecting a small area of the BFP. In this way the angular reflectance spectrum can be built up by collecting spectra at different positions in the BFP. These same principles can also be used to measure the sample in transmission [23]. The optics of this measurement system is described in detail in section 2.2.1. The 4F system also makes it easier to incorporate spatial filters, spectral filters or polarisation filters in the beam line which introduces a diverse array of ways to probe the sample [23].

When no spatial or angular information is required, backscattering or transmission measurements such as integrating spheres or bifurcated optical fibres can provide a simpler way to collect information. Backscattered or transmitted light from a sample can be projected onto an integrating sphere, usually a hollow spherical cavity coated in diffuse reflective coating. In this way scattered light can be integrated over an entire hemisphere and collected by a spectrometer. A bifurcated optical cable can couple light from a light source, illuminate and collect light at the probe end and send the collected light to a spectrometer. Both of these methods have poor or zero angular resolution but can be used cheaply and simply to collect many spectra quickly [19, 24]. A novel implementation of this method was demonstrated by Goodling *et al* [25], whereby the hemispherical backscattering light from a flat plane of oil droplets was projected on to half a ping-pong ball and imaged with a camera.

Imaging of micro or nanostructures involved in structural colour is vital to understanding how they may be scattering light. The size of features in a photonic structure scattering visible light is usually on the order of 100-1000nm [19] with some finer details sometimes as small as 5-10nm [26]. Conventional light microscopy does not have the resolution to image such fine structures. Electron microscopy can deliver the resolution and magnification needed, but some consideration is needed to choose the best method. Scanning electron microscopy (SEM) is a surface scanning imaging technique, therefore to image anything in cross section a modified technique is needed. Transmission electron microscopy (TEM) offers better resolutions than SEM and inherently allows imaging of cross-sections as ultrathin (70nm) slices are cut from a sample fixed in a resin block. The chemical fixation method commonly used in TEM can introduce shrinkage to a sample possible distorting any structural dimensions. Cryogenic fixation methods can be used to mitigate this factor for both TEM and SEM but introduce more special considerations depending on the type of sample [23, 24]. A more detailed discussion of EM is found in section 2.2.

If the dimensions and refractive index of a structure are known, the optical response can be calculated using a number of optical modelling techniques. Maxwell's equations of electromagnetism or classical optical theory can be combined with the geometry of the structure and characteristics of the light such as polarisation in a number of matrix formulations [24, 27, 28]. In particular the

transfer matrix model can calculate the reflectance, transmission and therefore absorptance for stratified structures such as multilayers or thin films [29]. Another tool is finite-difference-time-domain simulation. This method calculates the evolution of the electromagnetic wave through a structure by solving Maxwell's equations in a nearest-neighbour calculation, cell by cell through a user defined mesh. This has the advantage of being able to deal with any arbitrary structure even in three dimensions, which has been aided by the advent of 3D electron microscopy techniques such as SBF-SEM, electron tomography and more [30–32].

A powerful tool for identifying the photonics and ordering of quasi-ordered arrays uses the 2D fast Fourier transform (2DFFT) on electron microscopy images of such structures. Quasi-ordered structures here refer to those which have a consistent size and spacing of scattering regions, but lack longer range ordering [33]. In other words, these are structures which have some degree of ordering, enough to coherently scatter light, but in general are much more disordered than perfectly periodic structures. Electron microscopy images of such structures can be difficult to visually identify as quasi-ordered or completely disordered. However, the 2D FFT converts a real space image to the corresponding 2D power density spectrum of its spatial frequencies, making it possible to identify any underlying real-space periodicity as a peak in the frequency-space image. Prum *et al* further developed this method with the inclusion of refractive index information such that it was possible to predict the reflectance spectrum to be compared with measurement [33]. They went on to identify examples of coherent scattering of quasi-ordered arrays in avian, mammal, dragonfly and and butterfly species [34–38].

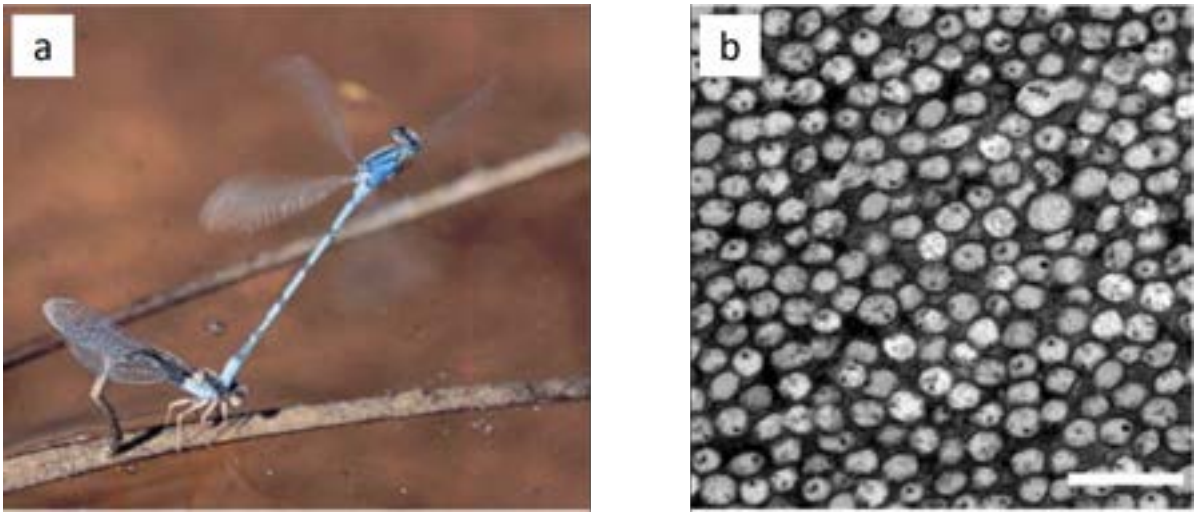

FIGURE 1.2. Mating pair of damselflies (*Enallagma civile*) with non-iridescent, blue structural colouration **(a)** caused by a quasi-ordered array of light scattering nanospheres **(b)**. Prum *et al* used 2D Fourier transform analysis to show that the structural colouration in this species was likely caused by coherent scattering, as opposed to incoherent Tyndall scattering. Scale bar 500nm. Figure adapted from [37].

1.3 Biological Photonic Structures

1.3.1 Photonic structures in animals

Structural colour can be used to achieve highly reflective areas, highly saturated colours, iridescence or even dull non-iridescent colour all in the absence of pigment molecules. The materials used to create structural colour is restricted by bioavailability but nonetheless the species which utilise them are extremely diverse. In beetles, chitin arranged into multilayer stacks can act as multilayer reflectors, and in some cases the alignment of chitin microfibrils shows continuous rotation layer-by-layer resulting in a helicoidal stack [39].

Broadband reflectance is achieved by having a range of multilayer periodicities. These can be chirped multilayers, where the periodicity is continuously changed through the stack, chaotic multilayers or simply a collection of different, well ordered multilayers [40]. Similarly, multilayers of guanine crystals are found in many fish species, commonly as broadband reflectors which appear silvery [41]. This is thought to act as a camouflage by mimicking the caustics (seen as bright flashes) and shimmering caused by light passing through the undulating water surface [42].

Lepidoptera show an incredible intricacy in how the multilayer structure is achieved [38, 43].

The Morpho butterfly is perhaps the most famous example, using a unique christmas tree-like shape to create striking blue colouration which is visible over extreme distances [44]. There are also butterfly species which have been shown to utilise polarised light as a mating signal [45], which may be an advantage in dense forests where the light spectral and intensity distribution is highly variable, but the background is unpolarised. The use of polarised light is not restricted to Lepidoptera, with polarising photonic structures found in fish and beetle species [46], which, in some cases, appear to enhance the overall reflectance.

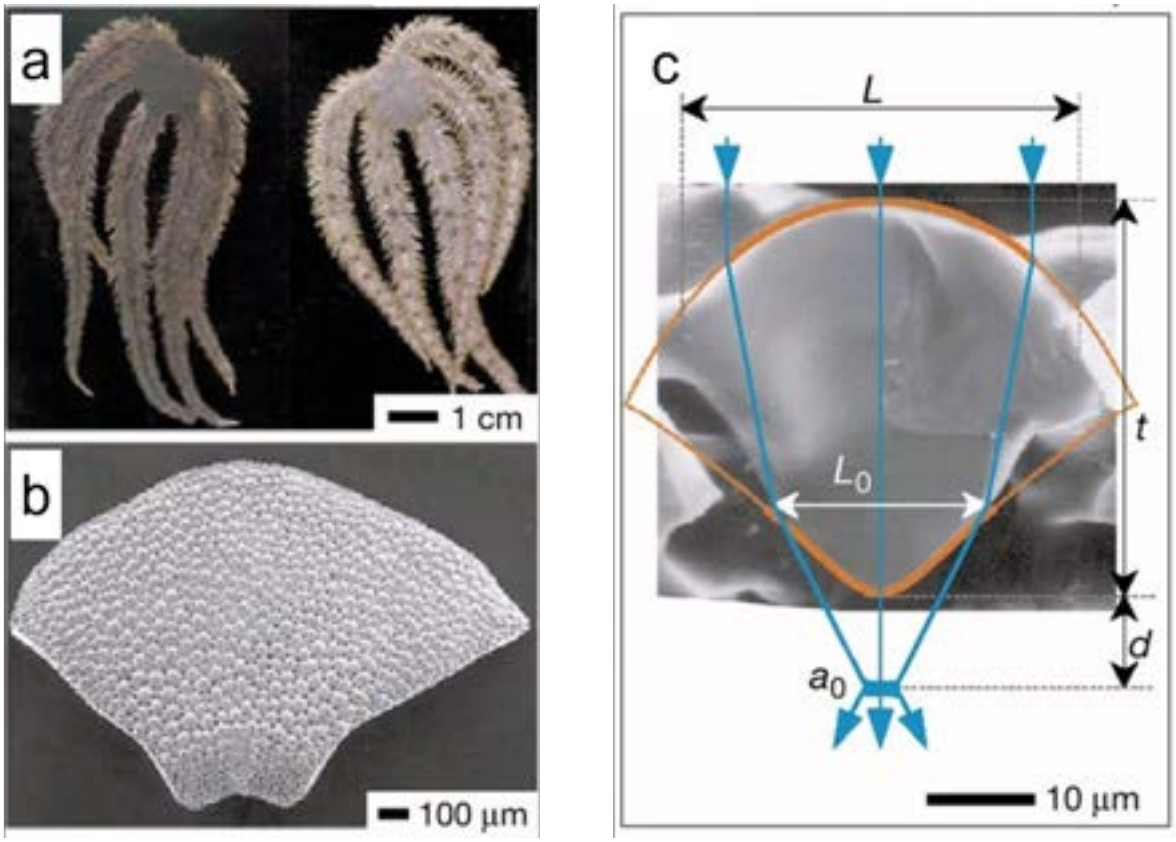

FIGURE 1.3. Members of the brittlestar family (Ophiocomids) contain calcitic inclusions in their arm ossicles which may act as microlenses as part of a photoreceptor system. **a)** The brittlestar *Ophiocoma wendtii* changes colour from day to night (left to right). **b)** Scanning electron micrograph (SEM) of a section of the dorsal arm plate, showing the calcitic inclusions thought to act as lenses. **c)** Cross-sectional image taken using SEM of an individual lens in *Ophiocoma wendtii*. Red lines represent the profile of an aspheric lens which accounts for spherical aberration. Blue lines show the path of light rays passing though a lens with the profile shown in red. Figure adapted from [47].

Many animal species use guanine crystals or chitin to create multilayer reflectors, the protein reflectin is used by some squid species [48] and the silica-based frustule in the centric diatom, *Coscinodiscus granii*, has been shown to achieve a 2D photonic crystal with optical resonances in the visible spectrum [49].

Sometimes the saturated colour, high reflectivity or iridescent colouration can draw unwanted attention. Indeed, chitin is so successful at creating coherent scattering that in the shells of many crustaceans, thick opaque layers form on the outside. This is thought to hide the inevitable iridescence seen internally which would otherwise draw unwanted attention [50]. Polycrystalline structures refer to photonic structures with small, ordered domains which are randomly orientated with respect to each other. These can introduce long range disorder to achieve angle *independent* structural colouration, as in the dull, green beetle, *Calloodes grayanus* [51]. Similarly the diffuse blue colouration in the dermis of some mammals and avian species is due to quasi-ordered 2D photonic crystal structure in collagen fibre arrays [33, 52]. This was initially thought to be due to incoherent scattering effects and was mislabelled as Tyndall scattering due to its lack of iridescence [53].

Whilst structural colour is widely utilised in animals for mating signalling, warning signalling, species recognition, camouflage and mimicry, there are a limited number of cases where the use of photonic structure serves some purpose other than visual signalling. Regular arrays of small calcite crystals act as photonic microlenses in the arm ossicles of one photosensitive brittlestar [47]. The surface shape and orientation of the calcite crystal structure helps to reduce spherical aberration which would otherwise reduce the amount of collected light. Photosensitive nerve bundles are common in brittlestar species and help with detection of shadows cast by predators. In the *Tridacnidae* (giant clam) family, highly ordered multilayer organelles called iridocytes act to enhance the forward scattering of photosynthetically useful wavelengths towards the photosymbiotic microalgae that grows in the mantle [54, 55]. Finally, there is growing evidence that the 2D photonic crystal formed in the frustule of the diatom, *Coscinodiscus granii*, is used as a waveguide to couple light to chloroplasts distant from the illumination area to enhance photosynthetic efficiency across the whole diatom [56]. These examples are far fewer in number in the literature and commonly involve photosynthetic processes.

1.3.2 Photonic structures in plants and algae

Plants also display a wide range of photonic structures, usually in tandem with the densely pigmented flowers to stand out to potential pollinators. However structural colouration has also been identified in fruits and in the foliage of some species.

Many flowers use brightly pigmented flowers and fruit to attract pollinators and seed dispersers,

and whilst pigmentation has been studied extensively [57], the contribution of structural colour to bright attractive displays has only gained attention in the past few decades [58]. Whilst not strictly considered a photonic structure, the surface shape of cells in petals an have a significant effect on the way light is reflected or transmitted. Flat geometry can lead to a glossy look, with more specular reflection. In *Ranunculus repens* (common Buttercup) the flat cell surface is aided by a thin film of air enhancing the reflectivity of the bright yellow petals. This reflectance is highly directional possibly increasing visibility to a moving pollinator through perceived flashes of reflected light [58]. Conical shaped surface cells in petals are common and in general create a diffuse reflectance with minimal gloss. Some studies have shown that conical cell surface geometry can enhance the colour signal of pigments contained within [59, 60]. However, it is noted that in terms of pollinator attraction there are many other features the cell shape affects such as wettability, pollinator grip and more [61]. Finally many petals have parallel surface striations on the micron scale. In the case of *Hibiscus trionum* has been demonstrated as visibly and measurably iridescent, adding a 'blue halo' to the otherwise darkly pigmented inner region of the flower [62] which can enhance bee foraging efficiency [63]. The striations act as diffraction gratings and using artificial petal targets, both pigmented and iridescent, it has been shown that the presence of iridescence can increase object detection for bumblebees without impairing object identity [64]. There are some suggestions that this form of iridescence may not be visible in natural lighting conditions [65], which is an important point to keep in mind in general. However, whilst the iridescence may be slight, the blue reflectance can clearly be seen in *Hibiscus trionum* [62].

In addition to attracting pollinators, some plants aim to attract seed dispersers with brightly coloured fruit, promising highly nutritious flesh. The fruits of *Viburnum tinus* have metallic-blue colour produced by a multilayer configuration of globular lipids [66]. This established signal is hijacked by some fruit which produce bright blue reflectance using multilayer structures which endure long after the fruit has dried out and lost its nutritional value [67–70]. In the case of *Polia condensata*, the multilayer in the helicoidal stack gives rise to circularly polarised light and the highest reflectivity of any biological photonic structure [67].

Structural colour is found in marine macroalgae, predominantly in species native to shallow coastal waters or intertidal regions [71]. Examples are found in both Phaeophyceae (brown algae) and Rhodophyta (red algae). Many show multilayers in the cell wall [72, 73] and otherwise structural colour comes from regions initially termed 'iridescent bodies' [71]. These are small regions in the epidermal cells which each appear to contribute their own, distinct colouration, usually appearing blue or green under reflectance. TEM imaging shows that these are likely to be quasi-ordered opal structures and therefore are not likely to be iridescent. The general purpose of structural colouration in marine macroalgae is still rather murky. There are suggestions that

it may act as a mechanism of anti-herbivory by disrupting species recognition. Some species have well documented examples of chemical synthesis of metabolytes for this very purpose, and highly iridescent striping may play a secondary, back-up role [71]. In many species with opal-like structures, the blue-green colouration is only seen at the growing tips of the fronds, which supports the idea that their purpose may be in photoprotection. In shallow coastal waters the amount of UV and photosynthetically active radiation (PAR) can easily exceed the amount needed for photosynthesis [71]. For species living in intertidal zones such as *Ericaria selaginoides* (previously *Cystoseira tamariscifolia*), light attenuation or absorption may be equally important as they deal with changes in the water column above between $0.4-3m$ [74]. Recent research showed that the opal-like photonic crystal (OPC) can reversibly transition between a highly ordered, blue reflecting state in low light, to a disordered, low reflectance state in high light [74] and suggested this may work to scatter more light towards the chloroplasts in low light.

Photonic structures would be particularly useful for photoprotection in environments where specific wavebands need to be attenuated. This is the case in underwater environments, where the longer wavelengths can be rapidly attenuated compared to shorter, blue wavelengths, leading to a light spectrum enriched in the shorter wavelengths. A similar situation arises at high altitudes, where irradiance levels of UV light can be significantly higher than at sea level. The edelweiss plant (*Leontopodium nivale*) is found in alpine environments up to 3400m altitude and the bracts are known to have cell walls that are particularly absorptive of UV wavelengths [75] and therefore may be more susceptible to damage. The bracts of the edelweiss flower are covered in a photonic crystal fibre structure which has exceptional absorption of UV-A wavelengths ($320-400nm$) [76]. The structure acts as a web of optical fibres; as light couples into the fibres as guided modes its optical path length dramatically increases allowing much more absorption to take place. Epicuticular wax found most famously on the needles of Blue Spruce (*Picea pungens*) may have a similar role in photoprotection as it is found to be highly reflective in the UV-B to blue wavelengths ($220-450nm$) due to incoherent scattering [77]. This species and closely related Spruce species are found at high altitudes in the Rocky Mountains ($1800-3500m$) in the USA, where levels of UV radiation can be up to 17.5% higher than at sea level [77].

Another prominent form of structural colouration in foliage is via multilayers in the cell wall cuticle. This was first identified in the leaves of deep shade Selaginella species, *S. wildenowii* and *S. uncinata* using reflectance measurements and electron microscopy [78], these can be seen in figure 1.4c-f. The same blue reflectance was found in many more tropical understorey plants, which thrive in deep shade conditions [79–81]. The purpose of this category of structural colouration is not well understood, as it is not clear that reflecting away PAR light that is not causing photo-inhibition or photodamage is beneficial for photosynthesis. Similarly this is a light environment where excess UV light is not a problem, in general the light reaching the tropical

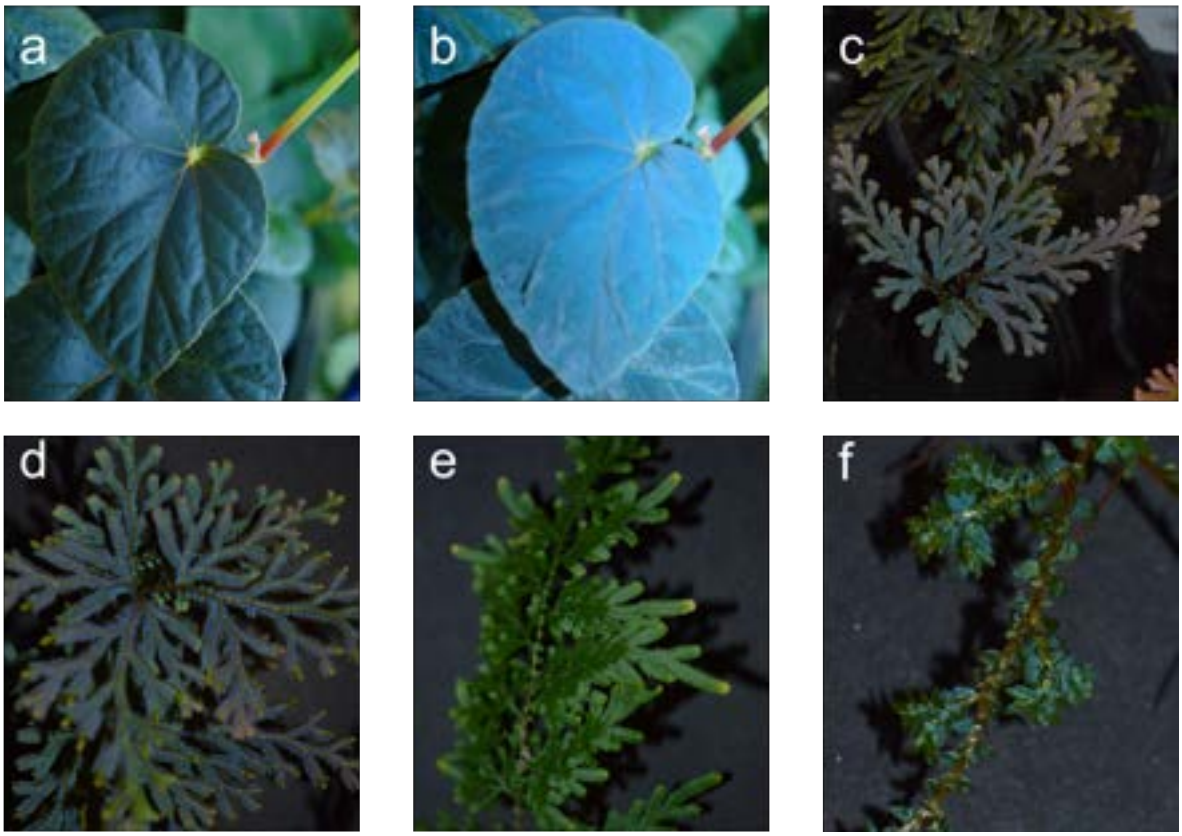

FIGURE 1.4. Photographs of Begonia and Selaginella spp. with some examples of blue reflectance. From top left going clock-wise:**a, b)** *B. grandis x pavonina* under (a) no-flash photography (b) flash photography. The blue reflectance can be seen much more prominently in the flash photograph. **c, d, e, f)** *Selaginella siamensis* (c, d) , *wildenowii* (e) and *uncinata* (e). Blue structural colour from cell wall multilayers can be seen on the edges of many of the fronds in (c, d, f). The specimen in (e) is not showing any blue reflectance.

understorey can be as little as 1% of the irradiance at the canopy and is typically thought to be enriched in the green wavelengths (around $550nm$) [82]. Photoprotection may be important for species in this environment due to sunflecks, transient shafts of full sun caused by the movement of branches in the canopy [83]. Some have suggested that the blue colouration may be a mechanism of anti-herbivory [84]. A recent study showed that iridescence does impair object recognition for Bees [85], and whilst this was not tested with naturally iridescent plant specimens it is a striking result.

1.4 Plastids and iridoplasts

1.4.1 Introduction to plastids

The presence of plastids is characteristic of photosynthetic eukaryotes. They are the result of an endosymbiotic event in which a host protoeukaryotic cell took in a cyanobacterium cell. This event happened multiple times between 1.5 and 1.6 billion years ago [86]. The host benefitted from the energy produced by the cyanobacteria through photosynthesis whilst the symbiont gained a safe and nutritional environment to function. The plastids present in modern day eukaryotes are no longer considered cyanobacteria largely due to the fact that their genome was transferred over evolutionary timescale to the host nucleus. Plastids do still contain a genome, vital to their function [87].

During the evolution of algae and land plants, plastids have diversified and taken on differentiated forms, to fulfil a number of roles. Most of these differentiated plastids do not have roles in light capture, such as chromoplasts, amylioplasts, elaioplasts and etioplasts Chromoplasts contain carotenoids, a group of yellow-orange pigment molecules, but these are not considered to be photosynthetic in any way. They are generally thought to contribute to the attraction of pollinators and seed dispersers since they are found in flowers, fruit and leaves and they are densely pigmented [86]. The next two can be grouped by their role as storage organelles, known collectively as leucoplasts. They are differentiated by the types of molecule they are used to store. Amylioplasts are used for the storage of starch, large grains of which usually take up the entire internal structure. Elaioplasts are used for the storage of lipids, and have a structure more similar to chromoplasts, containing lipid droplets [86].

Etioplasts can be thought of as an intermediary stage of a developing plastid. In the absence of light etioplasts build up, and can be triggered to develop into chloroplasts in the presence of light. These plastids have semi-crystalline arrays of membranes called prolamellar bodies, which allow the rapid development of the membrane structure needed in chloroplasts. However these plastids do not contain any significant amounts of light absorbing pigments and so are not considered to play a role in light capture or photosynthesis [87].

Due to the common ancestry of plastids, some are interconvertible, a process relevant to the senescing of plant leaves associated with autumn. However, despite this plasticity, none of these plastids share an internal membranous structure characteristic of chloroplasts.

Chloroplasts are the most well studied of the different types of plastid, and they are the only category of plastid relevant to this thesis.

Chloroplasts are the site of photosynthesis, and have a densely interconnected and hierarchical internal structure of membranes, in which are contained the protein-pigment complexes responsible for light capture and the transduction of light energy into biocompatible chemical energy. Thylakoid membranes are the site where the photosynthetic architecture is found, these are appressed into discoidal stacks known as grana, which are interconnected by membranous bridges known as stroma lamellae. The stroma is the aqueous medium surrounding the thylakoids, and there is another aqueous medium known as the lumen, internal to the grana structure.

The plasticity seen in etioplasts and plastids in general is shared by chloroplasts. Chloroplast function and structure is strongly associated with light spectral quality, intensity and both the spatial and temporal distributions of photon flux density. These are all characteristics of a natural light environment which will dictate the amount of useable photon flux. For example shading by foliage can lead to light depleted in photosynthetically useful wavelengths, shading by clouds can vary drastically in its temporal distribution, or shade can be highly spatially localised. All of these changes to the incident flux on a plant can be accounted for in different ways by the plasticity of chloroplast membrane structure and biochemistry. This is discussed in further detail in chapter four in section 4.1.2.

1.5 Iridoplasts in Begonia

A set of deep shade plants with iridescent bodies *within* the epidermal cells have gained a much more compelling argument as to one possible purpose of the photonic structure. First identified in 1996 by Gould and Lee [79], two species of plant were found to have modified plastids in the adaxial epidermis, termed “iridoplasts”, which were proposed to be the cause of bright blue reflectance (figure 1.4a, b).

Iridoplasts appear in the adaxial epidermal cells and are made up of the same building blocks as regular mesophyll chloroplasts. It is not common for plants to have photosynthesising plastids in their epidermal cells. They have groups of two to three thylakoid membranes, called grana, where the photosynthetic architecture is contained, separated by stromal layers which are considered mostly aqueous with low concentrations of proteins. Each thylakoid sub-unit is a pair of lipid bilayers, surrounding the lumen, which is also considered mostly aqueous with low concentrations of proteins. A diagram can be seen in figure 1.5.

Typical chloroplasts contain many tall stacks of thylakoid sub-units called grana. The thylakoid sub-units are disk-like, have a radius roughly ten times smaller than the chloroplast itself, and most importantly, are not separated by a stromal layer. The thylakoid stacks are interconnected by stroma lamellae and do not follow any strict shared orientation.

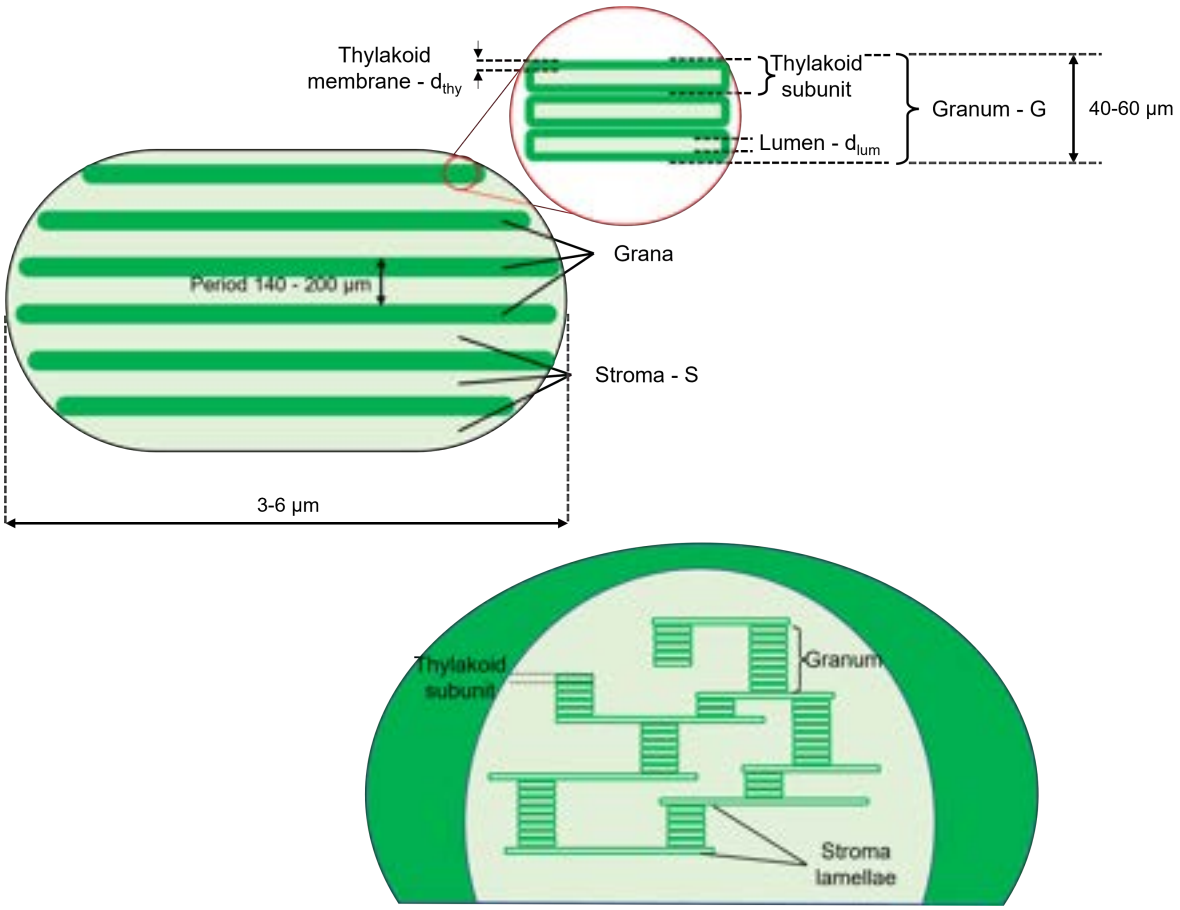

FIGURE 1.5. Diagram of internal structure of chloroplast and iridoplast **TOP** Iridoplast structure showing grana-stroma multilayer. Inset shows the finer structure of the grana made up from thylakoid subunits: a thylakoid membrane enclosing the lumen. **BOTTOM** Internal membrane structure of the typical mesophyll chloroplast, showing grana stacks made from short, discoidal thylakoid subunits, connected by stroma lamellae. Other components of the organelle are ignored here for simplicity.

In contrast, the grana in iridoplasts are extended over the entire length of the body, which is flat and lenticular in shape. The thylakoids making up the grana make a total thickness of roughly $50nm$, and are separated by the stromal medium, which has a thickness of roughly $120nm$, giving rise to a periodicity of around $170 \pm 20nm$ [88]. Iridoplasts usually have 8-12 grana. They are found appressed to the bottom cell wall of the adaxial epidermal cells such that they are flattened out, and the granal layers are parallel to the leaf surface.

Iridoplasts have recently been subject to a thorough optical characterisation with optical modelling to elucidate the mechanism of their reflectance [88]. The research found that the multilayered structure gives rise to photonic effects, like striking blue reflectance which has iridescence under microscopic measurement. Electron microscopy (see methods section 2.2) was used to image and extract dimensions of the iridoplast structure, which was fed in to optical modelling. Transfer matrix modelling (see methods section 2.3) was used to confirm the mechanism of blue reflectance and iridescence, and indicated that a strong absorption band, present on the long wavelength edge of the reflectance band was primarily due to the photonic structure. Finite-difference time-domain modelling was used to show that the absorption band was likely due to a 'slow light' effect, whereby absorption can be enhanced at the edges of a stop-band (reflectance band) due to a reduction in the group velocity. This can also be thought of as an increase in the mean path length of certain wavelengths due to constructive interference of forward and backward propagating waves.

Measurements of chlorophyll fluorescence using pulsed amplitude modulation (PAM) fluorometry showed that iridoplasts have an increased photosynthetic yield compared to mesophyll chloroplasts, in low light conditions. This use of photonic structure in a photosynthetic body is the first instance of its kind, but multi-layered modified chloroplasts are present in a number of other species, some extremely phylogenetically distant from Begonia.

Phyllagathis rotundafolia is a deep shade angiosperm with large, blue reflecting iridoplasts. The fern *Trichomanes elegans* is often grouped with iridoplast containing species but has distinctly different epidermal plastids with many more layers than iridoplasts. These multilayered bodies are still believed to be the source of blue-green iridescence [80, 84]. Large, dimorphic chloroplasts are found in many Selaginella species [89]. These 'bizonoplasts' have a region of well ordered, multilayered thylakoid membranes, next to a less ordered region with structure similar to regular mesophyll chloroplasts [90]. The bizonoplast in *Selaginella erythropus* was found to have blue iridescent reflectance, when individual bodies were measured microscopically, reminiscent of Begonia iridoplasts [91]. This is contrary to the conclusions of some recent studies [90, 92], however, both are studies which did not use reflectance microscopy. This is likely due to the chloroplast-based nature of its structural colour, meaning it is much less visually striking

and less visibly iridescent than examples of cell wall multilayer iridescence.

Selaginella (spikemoss) are one of the three orders in the class of lycophytes, phylogenetically distinct from the fern, Trichomanes, and the angiosperms Begonia and Phyllagathis which are all in different phylogenetic classes. The fact that multilayered, blue-reflecting modified chloroplasts evolved in these deep-shade, but phylogenetically diverse species is an example of convergent evolution and indicates that it is a beneficial trait in those environments.

1.6 Aims

This research aims to better understand the photonic structure properties of iridoplasts over the wide range of structures observed and how they might change or be limited in the context of light capture and photoprotection. This involves identifying and measuring the optical properties of interesting iridoplast structures using reflectance microscopy and electron microscopy, and characterising the photonic structure and its influence using optical modelling.

Chapter 2 is a discussion of the experimental methods and techniques used.

Chapter 3 looks at the occurrence of the novel green-reflecting iridoplasts. The measured optical characteristics will be compared to more common blue-reflecting iridoplasts and mesophyll chloroplasts. Optical modelling will be used to explore a structure-based explanation for the optical characteristics of green iridoplasts. The implications of their occurrence and the difficulties of observing these bodies will be discussed.

Chapter 4 primarily aims to test the plasticity of the optical properties of iridoplasts in an acclimation-type response to monochromatic light of different wavelengths in order to better understand their function. This chapter will also include an assessment of a newly measured species as a potential model species. Finally this work will include an analysis of the impact of natural disorder present in iridoplast structures on the photonic structure and optical properties using measured structural data.

Some further points of discussion and future prospects for research are raised in chapter 5 which are relevant to the research topic but not covered in chapters 3 or 4.

CHAPTER 2

METHODS

2.1 Plant materials and growth conditions

Begonia plants were all grown in the Bristol Life sciences facilities, by Alanna Kelly. The species *B. sutherlandii* (chapter 3), *grandis x pavonina*, *maurandiae* (chapter 4) were all grown in climate controlled growth rooms by RefTech using growth conditions with no natural light at 85% humidity, with a day-night cycle of 16:8 hours, with temperatures of $25°C$ and $20°C$, respectively. General "white" light was provided using a 7:3 ratio of cool:warm white fluorescent tube lights (FL TUBE LIGHTS) attenuated with neutral density optical filter (Lee Filters 209 0.3ND/ 211 0.9ND) to achieve photosynthetic photon flux density (PPFD) of $10 \pm 3 \mu mol m^{-2} s^{-1}$. PPFD measurements were made with a LICOR LI-250A light meter using a cosine corrected quantum sensor suited for ambient light. Plants were clonally propagated as leaf cuttings from mother plants which them selves have been clonally propagated as leaf, stem or rhizome cuttings eventually leading back to plants that were acquired from from Dibleys CN and RBGE suppliers. An exhaustive list of where individual species were acquired from can be found in table 2.1 in the thesis of O-Phart Phrathep [93]. Leaf cuttings were planted in a mixture of three parts Sinclair all purpose growth medium (at the time this product was a mix of peat and sand in an unspecified ratio and has since changed due to regulations on the use of peat),and one part 50:50 medium grade Sinclair pro vermiculite and Sinclair standard 2-5mm perlite. Plants were watered from the bottom by hand weekly using reverse osmosis water. Fertiliser used was Maxicrop Original with seaweed extract, applied fortnightly. All plants used for experimental measurements were grown for at least 4-6 weeks, at which point leaves were harvested for measurement. To standardise the developmental age, leaves chosen were always 2-3 internodes away from the new sprouting leaf tip such that the leaf chosen was fully expanded, but not so old that the chloroplasts could have been adversely affected by leaf maturation. A single leaf was taken from 4-6 individual plants within a growth

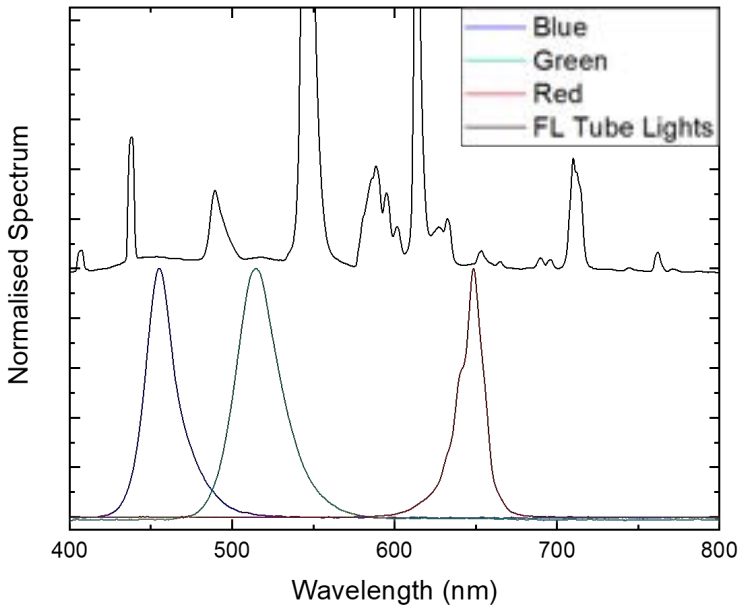

FIGURE 2.1. Measured light spectra for LED lights (blue/green/red) and fluorescent tube lighting (FL) used in climate controlled growth rooms. The LED lights were only used in work presented in chapter 4. The fluorescent tube lights were the standard lighting in the controlled growth rooms. The spectra was measured from a 7:3 ratio of cool:warm white fluorescent tube lights. All spectra were measured between $40-60cm$ away from the lights, representative of the plant-bulb separation. Spectra shown are normalised. The FL tube light spectrum is offset from the LED spectra by 1, on the normalised intensity scale.

condition group, and 6-10 individual iridoplasts from that leaf were measured. In the results chapters, "n" or "N" will always refer to individual iridoplasts, and unless stated otherwise will have been collected from single leaves from different individual plants as described above.

A small number of Begonia species presented in chapter three were grown only in glasshouses, with humidity at $70-80\%$, and a temperature maintained at $20\pm5°C$. Natural sunlight was attenuated with Rokolene 73% shade netting to achieve deep shade light levels between $5-15\mu mol m^{-2}s^{-1}$. In the winter months this was supplemented with compact fluorescent bulbs (Plug and Grow 125W, 6400K).

In chapter four, some plants were grown under monochromatic light from LEDs, which was attenuated to PPFD levels of $10\pm3\mu mol m^{-2}s^{-1}$ using neutral density filter (Lee Filters 209 0.3ND/ 211 0.9ND). All plants used in these experiments were propagated as leaf or stem cuttings and are therefore clones of the specimens maintained at either Old Park Hill glasshouses or in

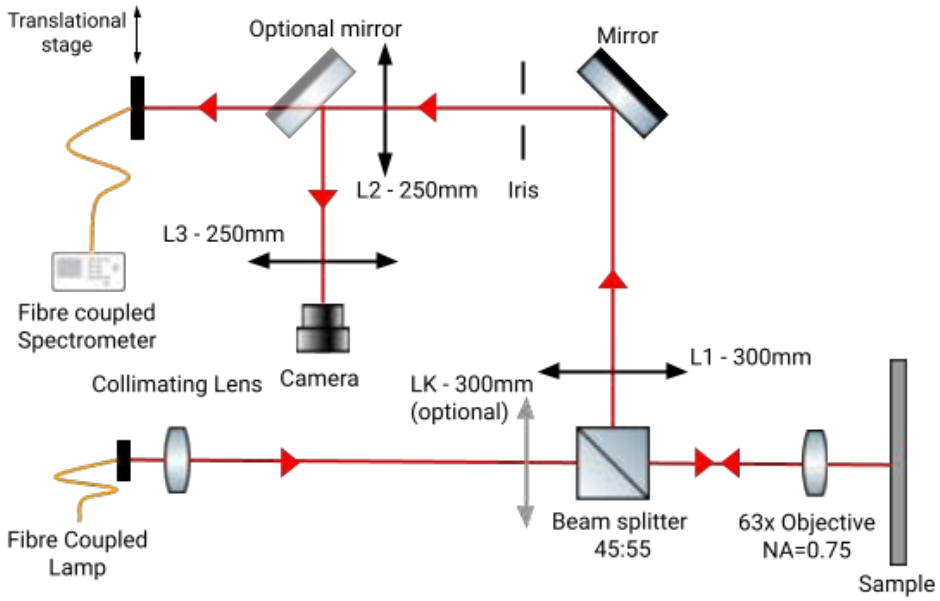

FIGURE 2.2. Schematic of optical epi-illumination reflectance spectroscopy set up used to image iridoplasts in magnification and take spectral measurements using a fibre coupled spectrometer. Objective Lens - Zeiss LD "Plan-Neofluar" 63x/0.75 Corr M27. Collimating Lens - Reversed 4X Olympus Plan Achromat Objective, L_1,L_K - 300mm doublet, L_2,L_3 - 250mm doublet. The objective lens and the lenses L_1 and L_2 form a 4F configuration shown in figure 2.4. Mirrors used were silvered mirrors. Pellicle beam splitter 45:55. Lamp fibre - 600μm multimode fibre. Spectrometer fibre - 200μm multimode fibre. Spctrometer - OceanOptics USB2000 VIS-NIR-ES. Illumination lamp - THORLABS OSL2, 3200K. Camera - THORLABS CMOS Camera, 1280 x 1024, colour sensor. Iris - Max diameter 8mm, circular 12 bladed iris

the Life Sciences building. The light spectra for each LED treatment and the fluorescent tube lights used is shown in figure 2.1.

2.2 Microscopy techniques

2.2.1 Epi-illumination microspectrometry

To investigate the optical properties of the photonic structure present in iridoplasts an epi-illumination Fourier imaging spectroscopic microscope has been used. The schematic of this set up can be seen in figure 2.2. Microscopic measurements are necessary to measure individual iridoplasts and by using an epi-illumination set up, one where the subject is illuminated from the same side as the light is collected, reflected light can be measured. Both imaging and spectroscopy are necessary for finding and measuring individual iridoplasts.

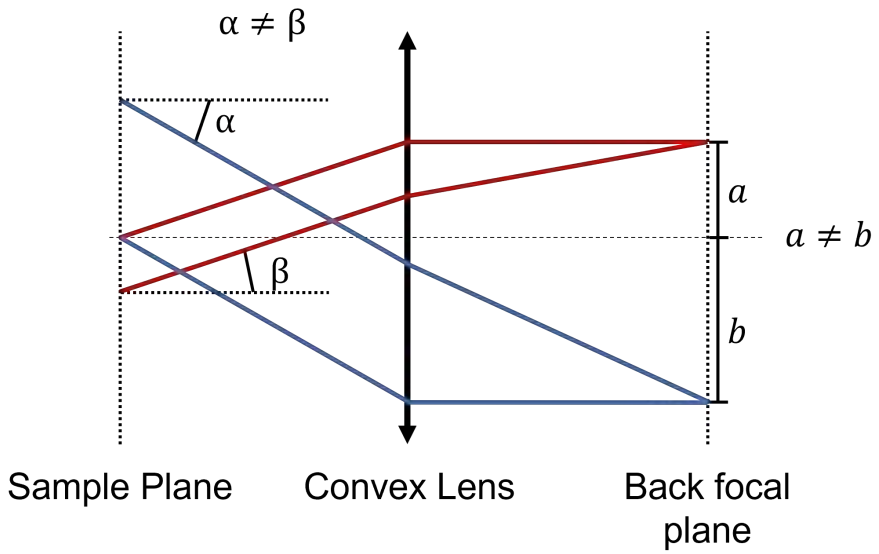

FIGURE 2.3. Optical ray diagram showing the spatial transformation made by a convex lens. The coloured rays are parallel but entering the lens at different angles: α, β. The convex lens performs the spatial Fourier transform on incoming rays such that parallel rays entering at angles α, β are focused at points a, b on the back focal plane, respectively

The photonic structure in iridoplasts reflects light in the visible wavelengths, usually between $440 - 500nm$, therefore it is necessary to illuminate the sample with at least these wavelengths of light. In practice white light is used, coupled from a halogen bulb source (THORLABS OSL2, 3200K) using a multimode fibre with diameter of $600\mu m$. The larger the illumination fibre diameter is, the more light it will collect from the white light source. However, this is a trade off between the intensity of light and how well the light can be collimated. Perfect collimation can only occur from a point source of light, and the larger the fibre diameter is, the more diverging the collimated beam will be. White light is also subject to chromatic aberration, whereby the wavelength-dependence of the refractive index of glass or other transparent materials causes light of different wavelengths to have different focal lengths for a lens. This can be significantly reduced by the use of an achromatic lens as the collimating lens, in this case a reversed objective was used (4X Olympus Plan Achromat Objective, 0.10 NA). Critical to investigating the photonic structure is measuring the change of the reflectance spectrum over wide angles. To achieve this microscopically it is useful to look at the back focal plane (BFP). As shown in figure 2.3, all light coming from the front focal plane of a convex lens at the same angle will be superposed to a single point on the BFP, such that light coming from the object at different angles will appear at different positions in the BFP. Mathematically the amplitude of the light in the BFP is proportional to the Fourier transform of the amplitude of light in the front focal plane, hence why it is sometimes referred to as the Fourier plane, or Fourier spectroscopy. To ensure that

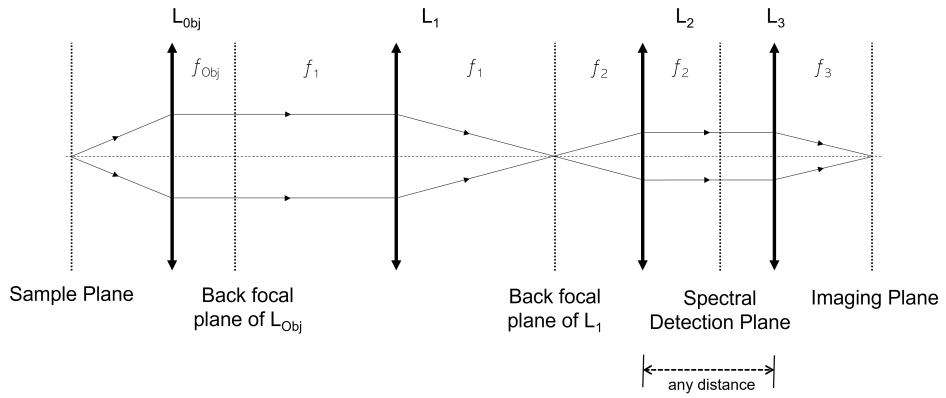

FIGURE 2.4. Optical ray diagram showing the 4F system of lenses. The light at the back focal plane of the objective is projected out to the detection plane optimally using this configuration. The image of the sample is focused at the imaging plane. Whilst the detection plane is fixed at a distance f_2 away from L_2, the distance between L_2 and L_3 is not fixed. In figure 2.2 these two optical paths are split by an optional mirror, allowing the choice between spectral measurement in the Fourier plane or real space imaging.

reflected light can be collected from a wide angular range, the sample must be illuminated from the same range. The angular illumination (and collection) range is fundamentally dictated by the numerical aperture of the objective lens, and is given by the expression:

$$NA = nsin(\theta),$$

where NA is the numerical aperture, n is the refractive index of the medium (in this case air) and θ is the angle between the beam axis and the edge of the focussed beam. An objective with $NA = 0.75$ gives an angular range of 48.5° when the medium between the objective and the sample is air. Illuminating the sample from the full angular range of the objective is known as critical illumination and results in a small, focussed illumination spot. If another lens is added at L_K, such that its focal length is positioned at the BFP of the objective, the illumination spot will consist of collimated light with a much larger area. This is known as Kohler illumination and can be used for scanning a larger area, however since the sample is theoretically only illuminated at normal incidence, this can not be used to measure the full angular range of the reflectance spectrum. To measure the back focal plane, it is necessary to project it out away from the objective as the natural position is usually inside the body of the objective. This is done using a 4F system of lenses, as detailed in figure 2.4. The 4F system requires a lens, L_1, to be placed with its focal length at the back focal plane of the objective. Another lens, L_2 is placed at a distance of the combined focal lengths of L_1 and L_2 from L_1, such that an image plane is formed between them. An iris is placed at the back focal plane of L_1 as a spatial filter. The detection plane for the BFP of the objective occurs at the focal length of L_2, as this is where the image of the BFP is formed.

This is where the spectrometer fibre is positioned in figure 2.2. An optional mirror between L_2 and L_3 diverts the beam away from the spectral detection plane where a final lens, L_3, is used to reform the sample image which is collected by a CCD camera (DCC1645C-HQ CMOS, Colour sensor). This is used to search the sample and choose an individual iridoplast as a subject.

At the detection plane a fibre is used to collect the light for a spectrometer (OceanOptics USB2000 VIS-NIR-ES). The fibre is mounted on a translational stage with fine movement in one dimension: perpendicular to the beam axis and parallel to the plane of the optical bench. The diameter of the fibre determines how much light is collected, as well as the sampling resolution. The translation of the fibre allows us to collect the full width of the beam in linear steps, which can be converted to angular steps using a calibration. This is much more manageable than trying to measure the full angular range of the spectrum using a rotational translation (which would naturally have steps made in angular increments) and is the preferred method for microscopic measurements. The translational position of the fibre is calibrated to an angle, θ_{out}, using the well defined angular reflectance spectrum of a diffraction grating with period, Λ, an example of which can be seen in figure 2.5. The inner edge of the reflectance band for either side of normal incidence was extracted and its plot fitted with two linear equations. The coefficients of these fits were used with the calibration equation to calculate the angle of collected light corresponding to the perpendicular position at the collection plane. The calibration equation used was

$$\theta_{out} = sin^{-1}\Big(\frac{NA}{n_{med}} - \frac{\lambda}{\Lambda}\Big),$$

where NA is the numerical aperture of the objective, n_{med} is the refractive index of the medium between the sample and the objective (in this case air) and λ is the wavelength of light in the spectrum. In the normal measurement of iridoplasts, all reflectance spectra were calculated as the percentage of reflectance compared to a silvered mirror reference spectrum.

2.2.2 Confocal laser scanning microscopy (CLSM)

Confocal laser scanning microscopy was used to image iridoplasts in Begonia species *in vivo* to evaluate any changes in cell size, spatial distribution and spatial number density. It was particularly suited for this use when observing auto-fluorescence of the photosynthetic pigments contained in iridoplasts. Small leaf lamina, cut from the leaf using a razor blade were illuminated with a $488nm$ excitation laser, and chloroplast auto-fluorescence emission was collected between $600-750nm$. Confocal imaging is used to exclude all unfocused light, outside of a thin depth of focus. For this reason it was necessary to take multiple z-stacks to include light from the whole iridoplast, which were combined in a maximum intensity projection using the image analysis software, ImageJ. Images were generally taken at a lower magnification than for reflectance microscopy so that many iridoplasts could be imaged in each frame. Measurements were made using a Leica TCS SP5 confocal laser scanning microscope using either 20x or 40x objective.

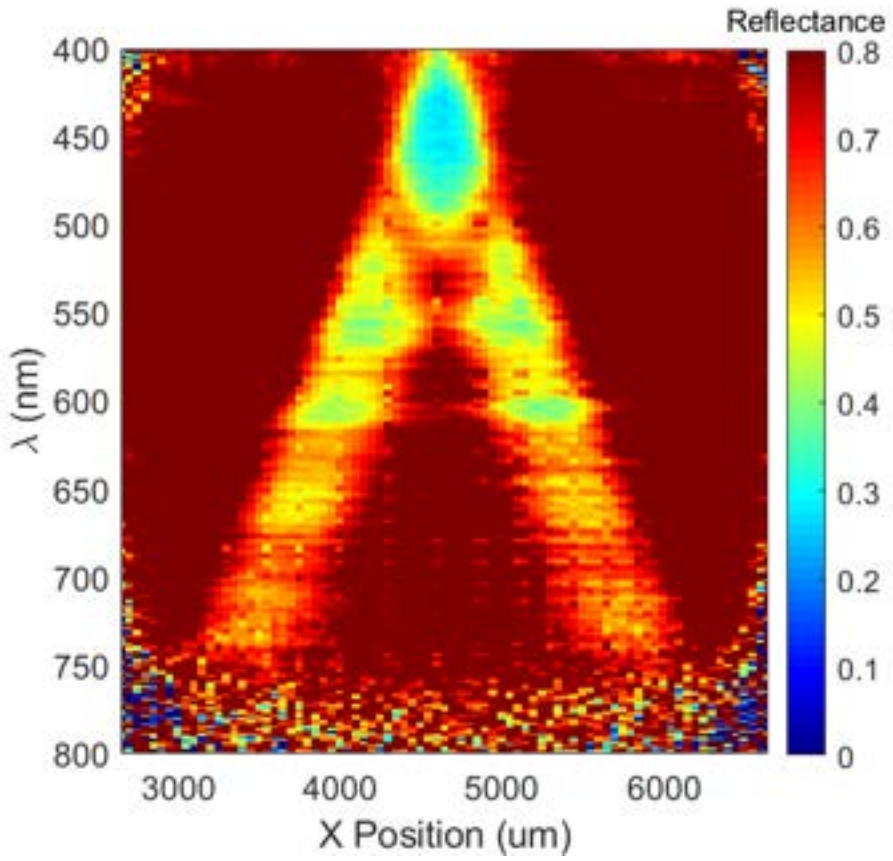

FIGURE 2.5. Reflectance from a grating measured at the back focal plane using the epi-illumination microspectrometry set up described in this chapter. The full angular range of the objective was measured using a fibre coupled spectrometer in the projected back focal plane of the objective using a 4f microscope. The fibre was translated in the collection plane perpendicular to the beam axis, an spectra were plotted together. The inner edge of the reflection bands were used for the calibration from linear position to angle if incident light.

2.2.3 Transmission electron microscopy (TEM)

Electron microscopy allowed a detailed look at the ultrastructure of iridoplasts, in cross-sectional view. Transmission electron microscopy provides the magnification and resolution needed to examine the fine layer structure in iridoplasts. A standard protocol was used, adapted from Jacobs *et al* [88] and the Wolfson Bioimaging suite facility. A fully expanded leaf, no further than 3 internodes from the emerging leaf bud was chosen to exclude any leaves which were still developing and any that had matured. Small leaf lamina were excised with a fine razor and dark adapted in ample moisture for 30 minutes. Samples were submerged in fixative (2.7% glutaraldehyde solution in 0.1M sodium cacodyLate buffer pH 7.2) at room temperature for 2-24 hours, then post-fixed in 1% Osmium tetroxide in 0.1M sodium cacodylate buffer at room

temperature for 1.5 hours. A dehydration series using ethanol (20%, 30%, 50%, 70%, 90%, absolute) was done in ten minute steps, before transferring first to a 1:1 ratio of absolute ethanol to LR White resin for 1.5 hours, and then to pure LR White resin at $4°C$ for 24 hours. Samples were embedded in fresh resin and polymerised at $60°C$ for 24 hours. Seventy nanometer slices were cut from resin blocks using an ultramicrotome knife, which were then stained using 3% uranyl acetate (10 minutes) and 2.6% lead citrate (10 minutes), separated by washes using de-ionised water (5 minutes). Images were captured using a FEI Technai T12 electron microscope.

2.3 Transfer matrix modelling

Transfer matrix modelling (TMM) is a technique suited for calculating propagation of light in one dimensional photonic crystals. The multilayer structure in Begonia iridoplasts is considered one dimensional as the stacked discoidal layers are considered uniform in the radial direction, and periodic in the vertical direction. The transfer matrix method treats the propagation of light waves through each layer and at each interface as propagation and interface matrices, respectively. These take input of the layer thickness and complex refractive index. The matrices associated with each layer and each interface are multiplied together, in order, to produce the transfer matrix which can be used to calculate the reflectance, transmission and therefore the absorption of the photonic crystal, both at normal incidence and over an angular range. The calculation was implemented in MATLAB (MathWorks, USA), based on the method described by *Yeh et al* [28], written originally by Martin Lopez-Garcia and adapted by myself.

This method of optical modelling has been widely used in the study of Begonia iridoplasts [88, 94] and the similarly structured bizonoplasts in *Selaginella erythropus* [91]. These studies have built up a representative structure based on the average layer thicknesses and layer configurations measured from numerous TEM images, which is shown in figure 1.5. Stromal layers separate the grana which are made up of a triplet of thylakoid subunits which in turn are made up of two thylakoid membranes surrounding a lumen layer. The lumen and stroma are both considered aqueous with low concentrations of proteins, so have a non-dispersive refractive index of $n_{l,s} = 1.35$. The complex refractive index for thylakoid membranes (n_{thy}) was taken from the literature [95], and can be found in appendix A.1. Most importantly it is wavelength-dependent and has some non-zero extinction coefficient which is associated with the absorption of the layer due to the presence of chlorophyll, other absorptive pigments and the whole photosynthetic architecture.

In some cases measuring the layer thickness of individual thylakoid membranes and lumen is inaccurate as their size ($3-7nm$) is close to the resolution of TEM. To reduce this error measurements of the entire grana layer thickness can be made, and the resulting structure used in the

TMM is one that contains alternating grana and stroma layers. To account for the presence of lumen in the grana layers an effective refractive index is calculated for the whole grana layer as

$$n_{eff} = \sqrt{f n_{thy}^2 + (1-f) n_l^2},$$

where $f = 0.55$ and is the proportion, by thickness, of thylakoid membrane in one granum. This type of structure was used in chapter 4. Theoretically this should have minimal impact on the light propagation calculated in the TMM because the fine layer structure in the grana have dimensions much smaller than the wavelengths of light used. This was confirmed by calculations of both types of structure, shown in appendix A.2.

CHAPTER 3

IDENTIFICATION OF NOVEL GREEN-REFLECTING IRIDOPLASTS IN MULTIPLE BEGONIA SPECIES

3.1 Introduction

Iridoplasts were first found and identified in *Begonia pavonina* (pictured in figure 3.2c) and *Phyllagathis rotundafolia* by Gould and Lee [79] when investigating the blue iridescent leaves of four different deep shade species. Blue iridescence had been noted as a common adaptation for understorey tropical rainforest plants [97]. The number of Begonia species with iridoplasts increased to 9 with the work of Jacobs *et al* [88], and a further 23 were identified by the work of Pao *et al* [98]. In that study, out of the 23 taxa with iridoplasts visible in the adaxial epidermis under TEM, only 3 were identified as visibly iridescent. The difficulty of properly identifying these structures is discussed later.

Of the Begonia iridoplasts that have been previously measured in reflectance microscopy, all have been shown to have peak reflectance wavelengths between $440-500nm$, and have only been described as having blue or blue-cyan iridescence. In this work iridoplasts have been found with peak reflectance wavelengths between $500-526nm$, a significant shift to greener wavelengths compared to the range previously reported.

In this data, the *Begonia* species *sutherlandii* and *plebeja* have both been found to contain iridoplasts with peak reflectance in this range. Seven other Begonia species known to contain iridoplasts were examined for this work and are presented in figure 3.8 but the main focus of this chapter was *B. sutherlandii* as it showed iridoplasts with peak reflectance exclusively in this range and most reliably. *Begonia plebeja* belongs to the neotropical clade-2, in which many

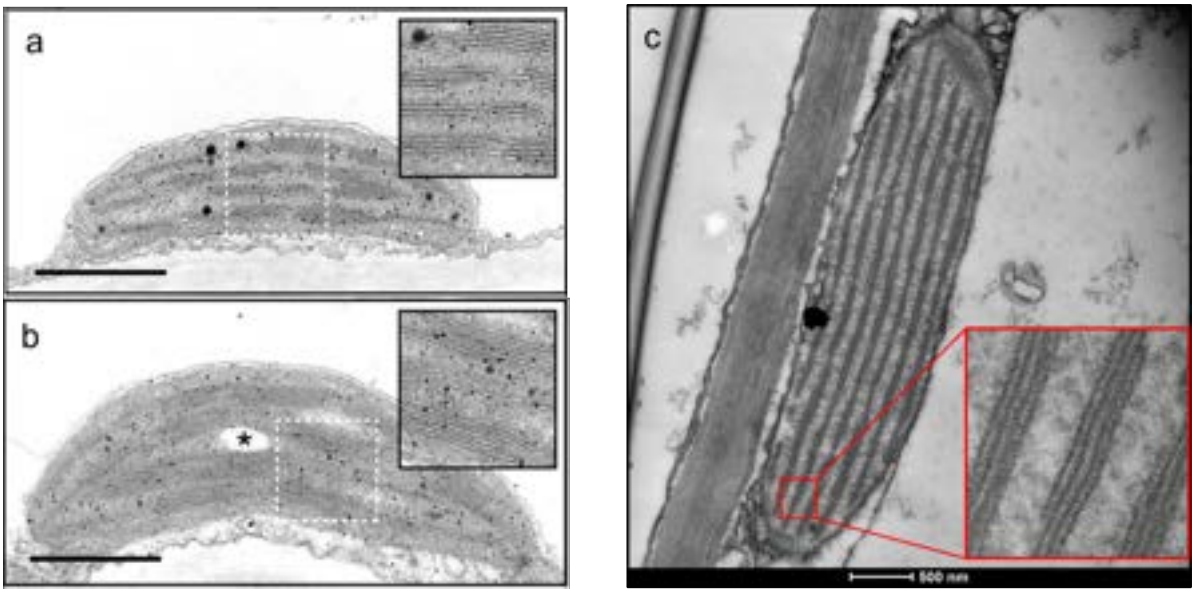

FIGURE 3.1. Epidermal chloroplast in *Arabidopsis thaliana* compared to iridoplast in *Begonia grandis x pavonina* seen in TEM. **a, b)** TEM images of chloroplasts found in the epidermal pavement cells of *Arabidopsis thaliana*. They are of similar size to iridoplasts ($5\mu m$ length) but the grana are clearly not extended over the full length of the body. There are no extended multilayers made up of grana/stroma. The thylakoid membranes making up the grana can be seen an in general there are many more thylakoids per grana than in iridoplasts. Figures converted from [96]. **c)** Iridoplast in the adaxial epidermis in *B. grandis x pavonina* showing the common features in iridoplasts: long extended grana, ordered multilayer structure between the grana/stroma, each grana has similar thickness indicating that they are made up of a similar number of thylakoid membranes. Inset shows 3 individual thylakoid sub-units in each grana.

of the other species contain iridoplasts [93]. It is found across South and Central America in Mexico, El Salvador, Brazil, Honduras, Nicaragua, Panama, often found in moist shaded areas [99]. *Begonia sutherlandii* belongs to the seasonally dry adapted African clade (SDAA-1), amongst many species which don't contain iridoplasts [93]. It is found in shaded, steep slopes of forests, particularly near rivers or waterfalls in South Africa [100].

In the leaf, iridoplasts are only found within the adaxial epidermal cells, appressed to the lower cell wall such that the multilayer stack is parallel to the leaf surface. They have thylakoid membranes bundled in groups of two or three called grana, which are extended over the full length of the body (figure 3.2d, e). The grana are separated vertically by stromal layers, forming ordered periodic stacks of around 8-10 grana. The grana bundles in normal mesophyll chloroplasts usually comprise of shorter, discoidal, stacks of thylakoids with no significant separation,

connected by single layer stroma lamellae. These can be seen in figure 3.2f as darker rectangular bodies.

Epidermal chloroplasts have been found in *Arabidopsis thaliana* [101–103] and a number of tobacco species [104], which are not likely to be iridescent as TEM micrographs show no significant multilayer structure. A comparison can be seen in figure 3.1 between chloroplasts in the epidermal pavement cells in *Arabidopsis thaliana* and an iridoplast in *Begonia grandis x pavonina*. In the epidermal chloroplasts the grana lamellae appear as short stacks connected by stroma lamellae, more similar to normal mesophyll chloroplasts. Therefore it is important to establish a distinction between iridoplasts with green structural colour and other non-photonic epidermal chloroplasts. These non-photonic epidermal chloroplasts would likely also reflect green wavelengths due to chlorophyll content, albeit without the strong reflectance and iridescence of the iridoplast structure.

Dynamic changes (over short time scales) to the thickness of thylakoid, lumen and stromal layers have been reported for mesophyll chloroplasts [105] in response to high and low light. The lumen, a mostly aqueous space separating adjacent thylakoid membranes, was found to expand under exposure to high light over the course of a few minutes. It was suggested that this would inhibit protein diffusion [105] and cyclic electron transfer [106] as a means to provide photoprotection, in a reversible photosynthetic state transition [107]. A recent theoretical study by Castillo *et al* [94] used data from the literature to model how these dynamic changes to the dimensions of the thylakoid, lumen and stroma could affect the optical characteristics of iridoplasts and bizonoplasts. They found a stark shift in the reflectance peak of an iridoplast structure from blue (450nm) to green (550nm) between the low and high light states, respectively. The implications of that study on this work are discussed in this chapter (see section 3.3.1).

Reflectance spectroscopy has been shown to be an effective tool in the study of iridoplasts and other multilayer photonic structures. In particular the full angular range of the reflectance spectrum can demonstrate whether a bodies' reflectance is iridescent or not. Iridescence can act as a smoking-gun indication that the reflected light from a body is impacted by photonic structure. It is possible to have photonic multilayer structure without iridescence, but in the case of ordered iridoplast structures measured so far, iridescence is always present. It is important to make these measurements *in vivo* as the periodic, ordered structure may be disturbed without the presence of supporting structures and the natural pressure inside the protoplast [108].

This study aims to make clear the distinction between a mesophyll chloroplast which reflects green wavelengths due to pigmentation and iridoplasts that have peak reflectance wavelength greater than 500nm. *In vivo* reflectance measurements will be made of both plastids over a wide

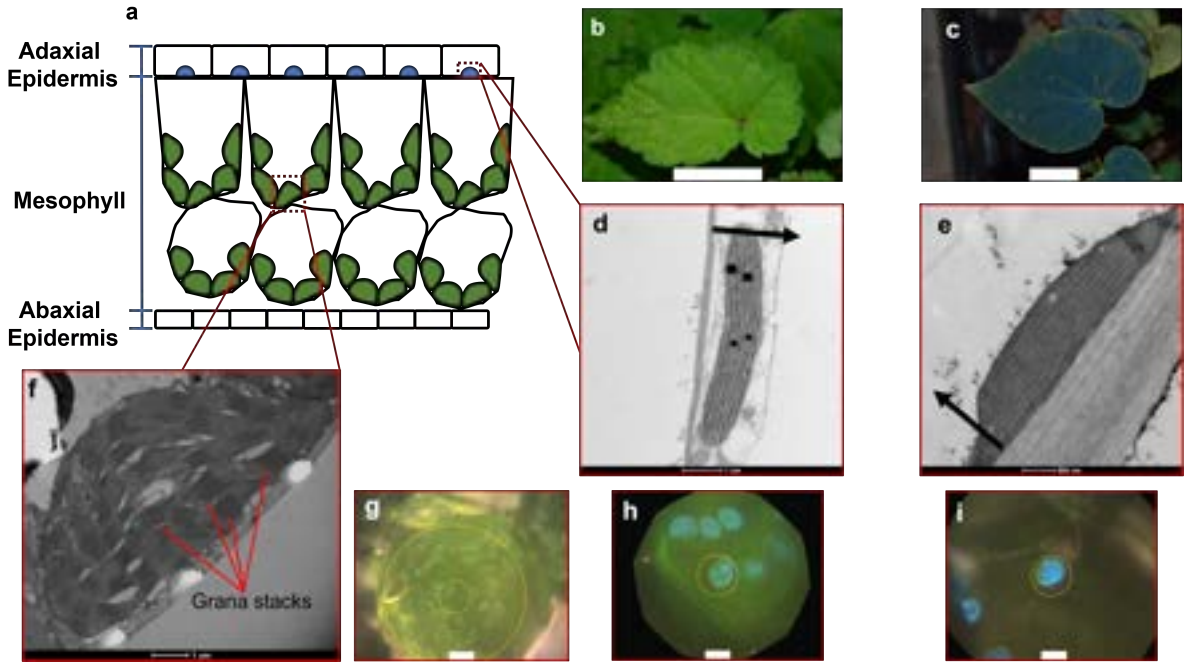

FIGURE 3.2. Iridoplasts and chloroplasts in a Begonia species leaf **a)** Cross section of a leaf showing the location of iridoplasts and chloroplasts (Adapted from [93]). **b,c)** Normal incidence flash photographs of a leaf in *Begonia sutherlandii* (b) and *grandis x pavonina* (c). Scale bar $2cm$. Typically these species have shown exclusively green or blue reflecting iridoplasts, respectively. Scale bar $1cm$. **d,e)** TEM images of iridoplasts in *B. sutherlandii* (d) and *B. grandis x pavonina* (e). Black arrows indicate the direction of the adaxial epidermal surface. **f)** TEM image of a mesophyll chloroplast . Scale bar (d,f) $1\mu m$ and (e) $500\mu m$. **g, h, i)** Epi-illumination reflectance microscopy images of an exposed mesophyll chloroplast (g) a green reflecting iridoplast (h) and a blue reflecting iridoplast (i) with peak reflectance at 550, 515 and $470nm$, respectively. Scale bar $5\mu m$. All iridoplasts were from leaves harvested from plants as described in section 2.1.

angular range to confirm the presence of structural colour in these iridoplasts. Transfer matrix modelling will be used to probe the optical characteristics of an iridoplast structure which reflects at this waveband to compare its functions to blue reflecting iridoplasts. These structures are already difficult to identify, and the existence of iridoplasts which may not have a strong colour contrast to its surroundings may mean that these structures have been mis-identified in the past, leading to the possibility that such structures are more prevalent than previously thought.

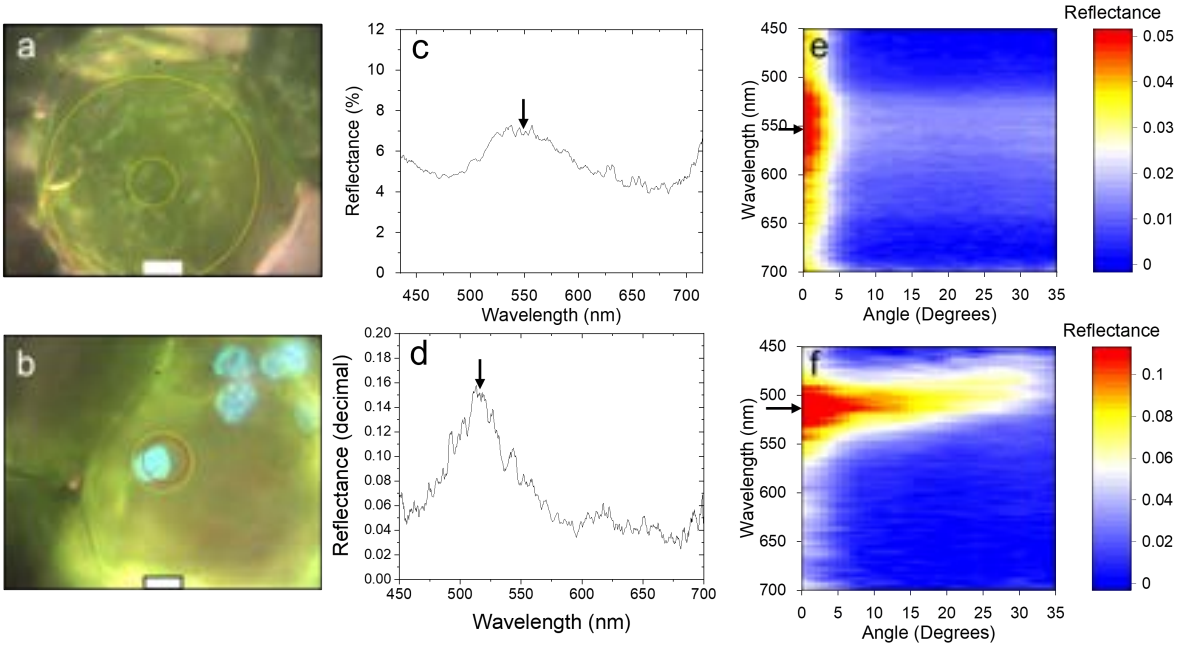

FIGURE 3.3. Reflectance microscopy images (a, b) and spectra, at normal incidence (c, d) and over a wide angular range (e, f), for mesophyll chloroplasts (a, c, e) and green-reflecting iridoplasts (b, d, f). **a, b)** Microscopy images taken on a custom-built reflectance microscope, the yellow and red circles are used as a guide to the eye during measurement to keep the aperture size consistent. Scale bar $5\mu m$. **c, d)** Normal incidence reflectance spectra of the corresponding plastid in (a, b), the aperture was reduced down to the large yellow circle in (a, c) and the small red circle in (b, d) so as to only accept light from an individual plastid in each case. **e, f)** Wide angle reflectance spectra of a mesophyll chloroplast (e) and a green-reflecting iridoplast (f). The vertical arrow in (c, d) marks the centre of the peak and corresponds to the peak centre marked by the horizontal arrows in (e, f) as a guide to the eye. All iridoplasts were from leaves harvested from plants as described in section 2.1.

3.2 Results

3.2.1 Optical microscopy of iridoplasts and mesophyll chloroplasts

Epi-illumination (reflectance) microscopy was used to image and measure the spectra of green reflecting iridoplasts. Green reflecting iridoplasts are already distinct from mesophyll chloroplasts since they are only found in the adaxial epidermis. To test whether they reflect green light due to their photonic structure, reflectance spectra were measured over a wide angular range to determine if there is red or blueshift out to wide angles. Change in reflected wavelength with changing viewing angle is known as iridescence and is an indicator of photonic structure. The

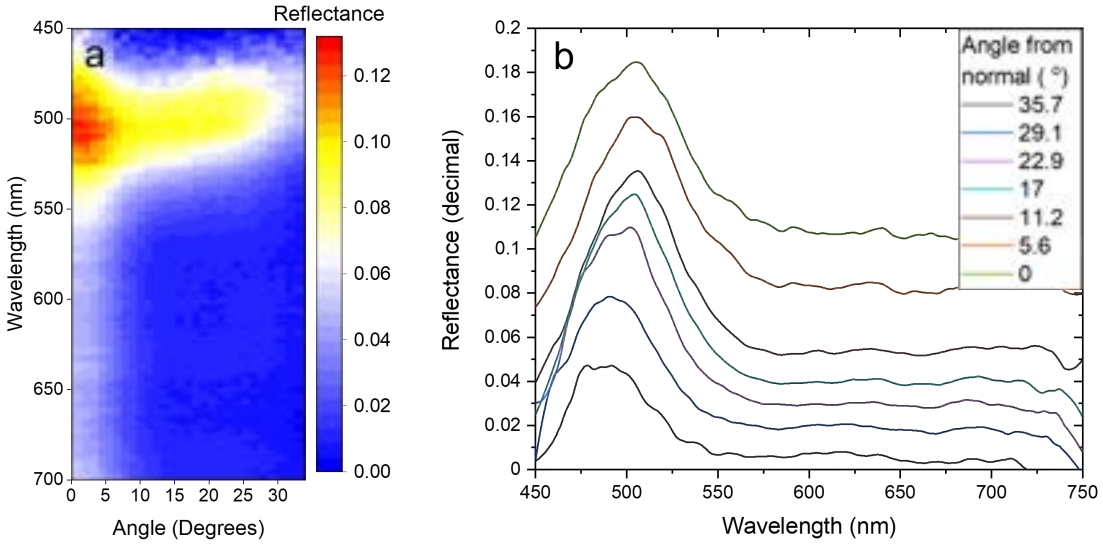

FIGURE 3.4. Reflectance spectrum over angular range (a) with Y-Offset plot of single angle spectra (b). **a)** Reflectance spectrum for iridoplast with normal incidence peak reflectance wavelength of $505nm$, showing blue-shift with increasing angle. **b)** Single angle spectra extracted from (a) with a constant Y-Offset value of 0.01. The peak reflectance wavelength at 35.7° is $485nm$.

full angular spectra of iridoplasts have previously been confirmed by measurement and optical modelling as showing blueshift with increasing angle from the normal [88], but their research only found iridoplasts with peak reflectance wavelengths at normal incidence between 450-500nm.

Figure 3.3 shows microscopy images, normal incidence spectra and angular spectra for a green reflecting iridoplast and a mesophyll chloroplast. The colour representation in the microscopy images is not a good indicator of the true colour of the features as the colour balance on the sensor is not calibrated, or necessarily fixed between images. Since these measurements are done *in vivo*, the microscope is only able to resolve features in the first cell layer. Moving the focal plane down through the leaf, past the epidermal cell layer results in too much scattering and extinction from the cell boundaries and epidermal cells making imaging or collecting reflectance spectra for mesophyll chloroplasts impossible in this way.

To expose the mesophyll chloroplasts to reflectance measurement, a paradermal grazing-angle cut was made with a fine razor. The edge regions of the cut were searched until mesophyll chloroplasts were found which could be reasonably resolved. This allowed for the direct comparison of spectra between green reflecting iridoplasts and mesophyll chloroplasts from the same leaf. The larger

diameter, but weaker reflectance of chloroplasts required a larger aperture to be used for spectral measurements (marked by the yellow circles in figure 3.3a, b), likely accounting for the higher signal to noise ratio of the chloroplast spectrum compared to the iridoplast, shown in figure 3.3c, d.

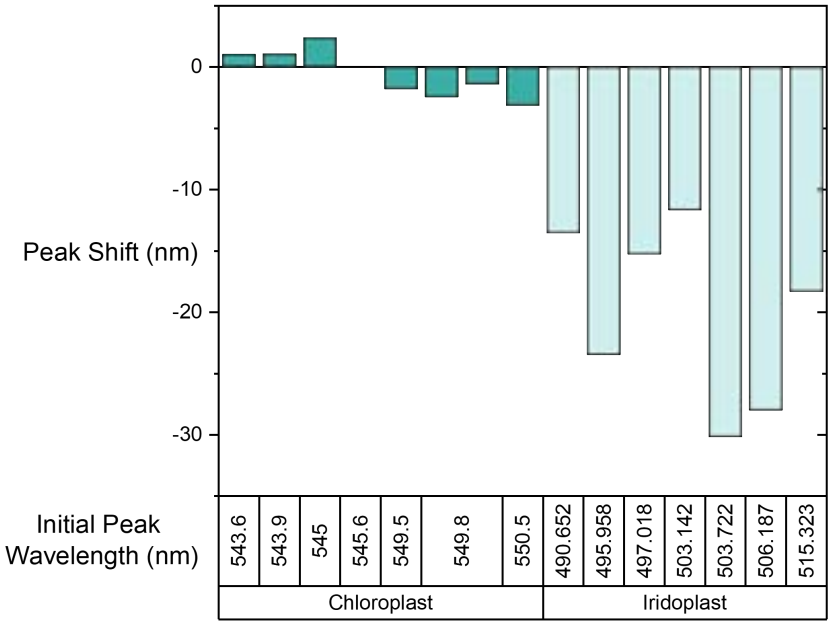

FIGURE 3.5. Amount of change of the central peak reflectance wavelength between normal incidence and wide angle (0-24 degrees), for individual mesophyll chloroplasts and iridoplasts. Positive values mean redshift and negative values mean blueshift at 24 degrees. The initial peak wavelength is taken at normal incidence.

2.1.

At normal incidence the mean peak reflectance of a chloroplast measured here was $545 \pm 6nm$ with two minima at $480 \pm 6nm$ and $674 \pm 6nm$ (n=13), whereas iridoplasts show a single high reflectance peak with peak reflectance wavelengths in this sample between 490–515nm (n=7), "n" here refers to the number of individual iridoplasts. In this case one iridoplast corresponds to a leaf from an individual plant. The full angular spectra for iridoplasts and chloroplasts are also very distinguishable, as shown in figure 3.3. In mesophyll chloroplasts, the reflectance peak is observed with strong intensity at zero degrees (marked by a horizontal arrow in figure 1.2e), but at angles greater than 5 degrees the reflectance intensity is dramatically decreased. It is normal to see greater absolute reflectance over the whole visible spectrum between ±5 degrees due to the build up of partial backreflection across all the transparent elements in the beamline. However, the reduction in absolute reflectance at wider angles is much smaller in iridoplast spectra (figure 3.3f).

The reflectance band for the chloroplast is still visible at wider angles, but does not change

in shape or wavelength appreciably, whereas in the case of the iridoplast clear blueshift of the peak is visible. This can be seen for an individual iridoplast reflectance spectrum over an angular range of 34° in figure 3.4a, b. In figure 3.4b, showing single angle spectra across the whole angular range, the blue-shift in reflectance can be seen. When accounting for the constant Y-offset value of 0.01 between these spectra, the gradual reduction in maximum reflectance can be seen. The extent in the shift in peak wavelength between normal incidence and wide angle ($0-24$ degrees) was measured for eight chloroplasts and seven iridoplasts and is shown in figure 3.2.1. In the case of chloroplasts both positive (redshift) and negative (blueshift) values are seen and all values are between -3 and $+2nm$, well within the error associated with estimating the peak centre of chloroplast spectra, $\pm 6nm$. In the case of iridoplasts measured here, all showed blueshift, with wavelength shifts varying between $11-30nm$. It is worth noting here that the error associated with with estimating the peak centre of iridoplasts is smaller ($\pm 3nm$) than for mesophyll chloroplast spectra above ($\pm 6nm$), due to the sharper curvature of their peaks.

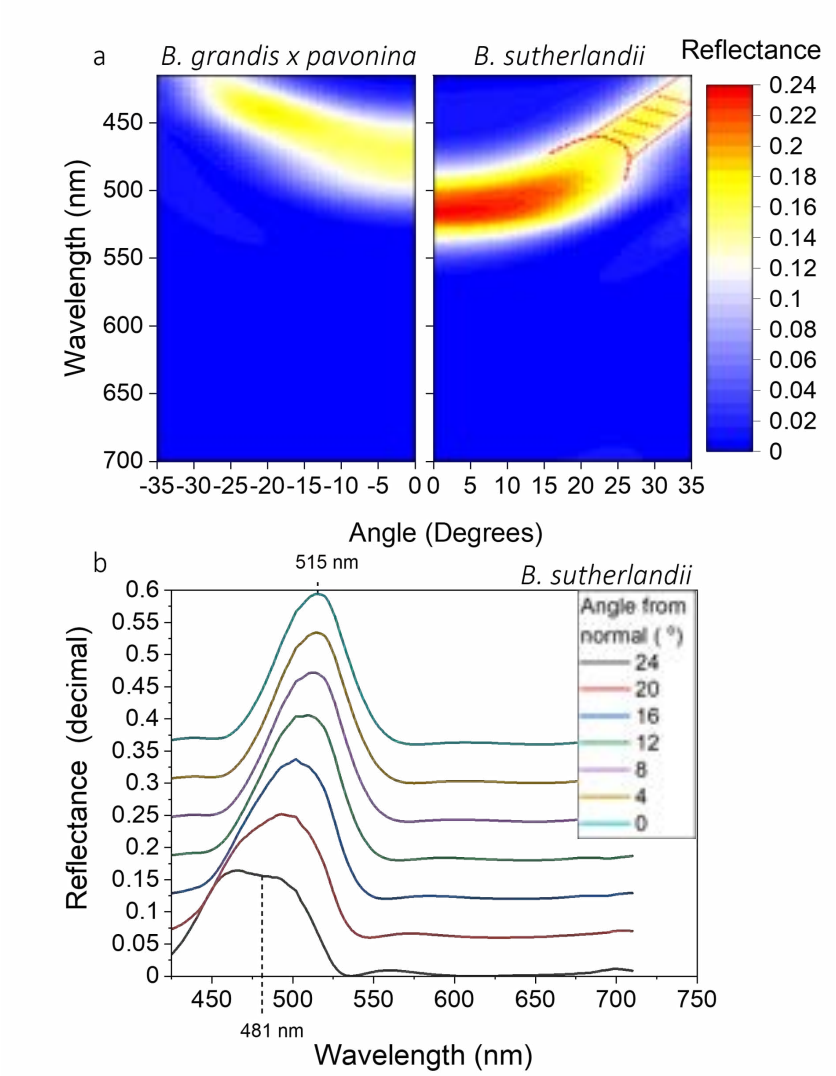

FIGURE 3.6. Reflectance spectra over half-angle range of blue-reflecting and green-reflecting iridoplast structures calculated using the transfer matrix model (TMM). **a)** Each spectrum uses an iridoplast structure with peak reflectance at normal incidence of 475nm (LEFT) and 515nm (RIGHT), using structural dimensions based on *B. grandis x pavonina* from the literature [88] and structural data for *B. sutherlandii* collected by O-Phart Phrathep [93], respectively. The region marked with red dashed lines is likely to be an artefact at large angles from the transfer matrix method. **b)** Single angle spectra extracted from (a, RIGHT) with a constant Y-offset value of 0.06. The peak reflectance wavelength for the spectrum at 24° is taken from the peak shape on the long wavelength side of the peak, as the short wavelength side is likely affected by an artefact of the calculation. Discussed in section 3.2.2.

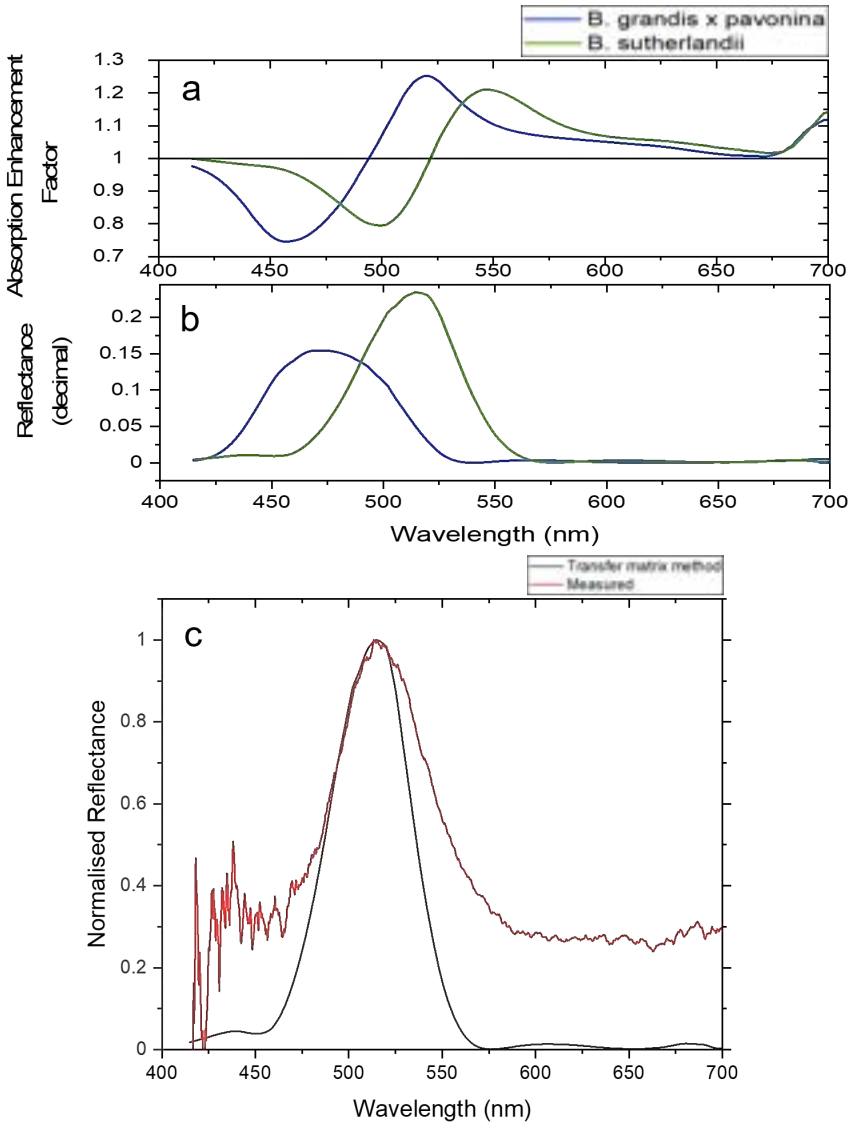

FIGURE 3.7. **a)** Absorption enhancement factor and **b)** reflectance calculated using the transfer matrix method for blue-reflecting and green-reflecting iridoplast structures. The blue- and green-reflecting iridoplast structures are based on structural dimensions for *B. grandis x pavonina* from the literature [88] (blue) and *B. sutherlandii* from data collected by O-Phart Phrathep using the same methods [93] (green). The peak reflectance wavelength of each spectrum is $475nm$ (blue) and $515nm$ (green). **c)** Comparison of the calculated reflectance shown in **(b)** to a measured reflectance spectrum of an individual iridoplast in *B. sutherlandii* at normal incidence showing a peak reflectance wavelength of $515 \pm 3nm$.

3.2.2 Optical modelling of green iridoplasts

To investigate how the optical characteristics are different between a blue-reflecting iridoplast and a green-reflecting iridoplast, structural dimension data was fed into a transfer matrix model and used to calculate the full angular reflectance spectrum and absorption characteristics. The dimension data used to generate a green-reflecting iridoplast structure with peak reflectance at $515nm$ was from TEM images of iridoplasts in *B. sutherlandii* as this species has shown iridoplasts with peak reflectance exclusively between $500-526nm$. This data was collected by O-Phart Phrathep during his Ph.D research. The structure had grana and stroma widths of $83.5nm$ and $99.2nm$ after scaling to calibrate against a peak reflectance of $515nm$. The structure of a blue-reflecting iridoplast was taken as the structure reported in [88], with grana and stroma widths of $47nm$ and $125nm$ and had a peak reflectance of 475nm (shown in figure 3.7b).

Figure 3.6a shows predicted reflectance spectra over a wide angular range for the same blue and green-reflecting iridoplast structures. The two modelled sets of spectra are of different absolute reflectance, shown in figure 3.7b. Otherwise the spectral shape and angular dependence is consistent between both structures, and is consistent with measured spectra (shown in figure 3.3). The peak wavelength shift between $0:24^\circ$ for the *B. sutherlandii* structure is $35\pm5nm$ (figure 3.6 b). This is slightly larger than the largest value seen in measured spectra ($30\pm3nm$, figure 3.2.1). The peak reflectance wavelength at 24° was chosen using the peak shape on the long-wavelength side of the reflectance peak, as the short-wavelength side shows an extra peak. This extra peak is part of the marked region in figure 3.6a, RIGHT which is likely to be an artefact of the transfer matrix method calculation. The TMM calculation treats the iridoplast structure as a stack of layers of defined thickness, but infinite width. This assumption of infinite planes is built in to the mathematics of the calculation and introduces artefacts at larger angles.

The absorption enhancement factor (γ) for each structure was calculated, which is defined as

$$\gamma = A_{irid}(\lambda) / A_{chloro}(\lambda)$$

where $A_{irid}(\lambda)$ is the absorption spectrum for the iridoplast structure and $A_{chloro}(\lambda)$ is the absorption spectrum for the same amount of absorptive layers but a stromal spacing of zero, hence no photonic structure is present. This ratio is a good indicator of the enhancement/reduction ($\gamma > 1$ / $\gamma < 1$) of absorption due to the presence of the periodic structure. The absorption enhancement factor for a green-reflecting iridoplast structure shows almost identical shape to the blue-reflecting iridoplast structure. The peaks in γ for the green-reflecting structure show smaller magnitude, compared with the blue-reflecting structure, this is likely due to the higher reflectance of the green-reflecting structure.

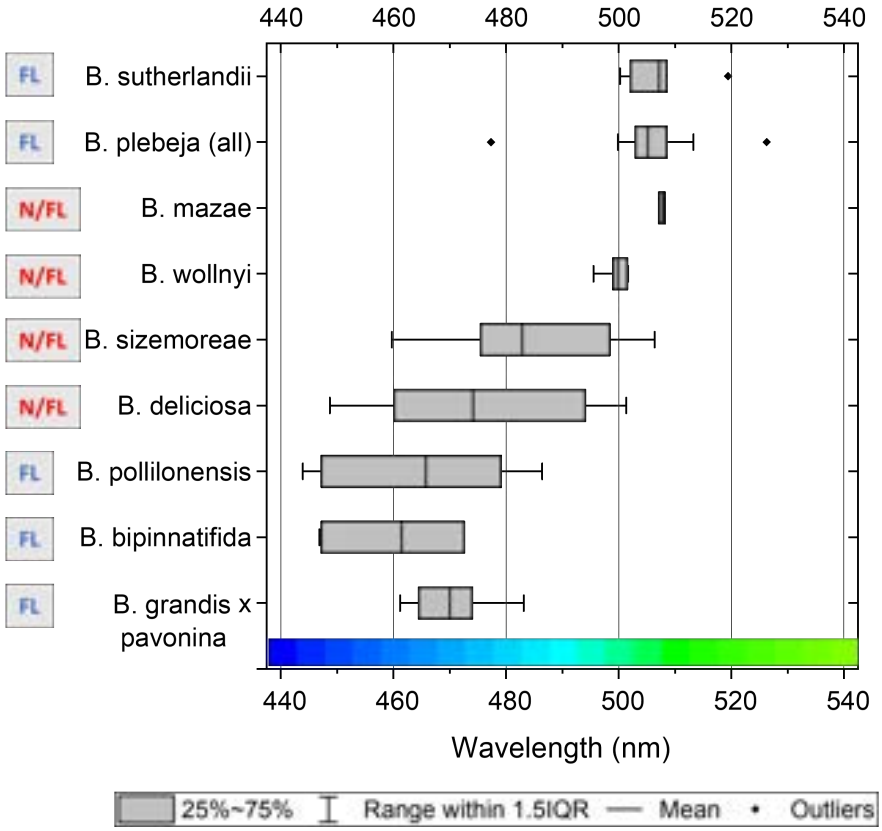

FIGURE 3.8. Box plots showing the normal incidence peak reflectance wavelength for iridoplasts in nine Begonia species, grown in shade conditions (10-15umol m-2s-1 PAR). Some species were grown in glasshouses under shade netting and received natural light with supplementary fluorescent lighting (N/FL) and others in growth cabinets under fluorescent bulbs with shade netting (FL).

3.2.3 Range of iridoplast spectra

Measurements made in this work of iridoplasts in a number of Begonia species show that peak reflectance wavelengths from $443nm$ (deep blue) to $526nm$ (green) are present (shown in figure 3.8). From 96 iridoplast measurements across nine species, 68% lie between $443:499nm$ and 32% between $500:526nm$, showing that green reflecting iridoplasts are not uncommon. Green iridoplast reflectance is found across five of the nine species. All iridoplasts were from leaves harvested from plants as described in section 2.1. Further, whilst some species (*B. sutherlandii, mazae*) appear to contain only green reflecting iridoplasts, other species (*B. sizemoreae*) show blue, cyan and blue-green reflecting bodies are present in the same leaf. All species received light levels of $10-15\mu molm^{-2}s^{-1}$ of photosynthetically active radiation (PAR) by the use of shade netting. The different light sources for plant growth (fig 3.8 N/FL, FL) does not appear to have

any correlation with the peak reflected wavelength of iridoplasts measured here.

3.3 Discussion

3.3.1 Green iridoplasts are distinct from mesophyll chloroplasts

Iridoplasts have been found in some Begonia species which have the same shape, location and ordered multilayer structure, and comparable reflectance characteristics to previously studied iridoplasts in *Begonia grandis x pavonina*. However, in this study, some iridoplasts have been found with peak reflectance wavelengths between 500-526 nm, which is significantly red-shifted compared to the the wavelengths measured previously [88], and much closer to the green part of the visible spectrum than the blue.

It is important to note that it can be misleading to assign a colour to photonic structures since there can be a number of optical phenomena relevant to what wavelengths of light will be scattered, and how they will be scattered. For example, the angle-dependence of an iridescent object would have significantly different considerations to a photonic structure which allowed propagation/reflection of certain wavebands in one direction, and different wavebands in an orthogonal direction. The absorption, reflectance and transmission of a material can be all be simultaneously altered when photonic order is introduced. The directionality of light sometimes present in photonic structures further obscures a simple description of the colour of a body, since it may only be visible from certain viewing angles, or with the right wavelengths of illuminating light. Additionally the different epistemic understandings of colour and dependence on observer visual system is not insignificant when considering the natural world.

Here to differentiate between the current findings and the previously studied bodies the iridoplasts are indexed by their normal incidence peak reflectance wavelength. This is either categorised as green-reflecting or blue-reflecting, which in this case is referring to either $500-526nm$ or $440-500nm$ respectively. It can be seen in figure 3.3b, d that the reflectance peak for the iridoplast with peak reflectance at $515nm$ at normal incidence drops to half of the peak maximum at $490nm$ and reaches a background level around $470nm$, on the short wavelength side. This means a broad range of blue wavelengths are still reflected, even in an iridoplast which is categorised as green-reflecting. The distinction made here is based on the fact that previously iridoplasts had only been seen with peak reflectance wavelength between 440–$500nm$, it is not a distinction made on macroscopic visible colour as observed by humans.

The iridoplasts found here are similar in size, morphology and location to iridoplasts described previously [88] and therefore are distinct from regular mesophyll chloroplasts. Figure 3.3 shows that the reflectance spectra for the novel iridoplasts have a single, high reflectance peak which

undergoes blue-shift at wider angles, with a similar amount of peak-shift as iridoplasts with peak reflectance less than 500nm (as can be seen in figure 3.2.1). Mesophyll chloroplasts have negligible shift of the reflectance peak at wider angles. This shows definitively that the reflectance in the novel iridoplasts is due to the underlying photonic structure, whereas the colouration in mesophyll chloroplasts is likely to only be due to pigmentation.

There has been some theoretical work investigating whether photonic effects may be significant in the stacked thylakoid bundles in normal mesophyll chloroplasts (these can be seen in figure 3.2f as the many dark grey rectangular regions). It was found that nanophotonic effects may be significant, allowing the system a morphological transition between high and low absorbing states [109]. However, due to the near-zero separation of the thylakoid layers the reflectance is not enhanced as it is in the structure of iridoplasts. Also the relative orientation of grana bundles is much less uniform and not co-planar to the plant leaf surface meaning that an iridescent reflective signal would not be present.

The possibility of iridoplast structures with peak reflectance wavelengths up to 575nm was predicted, using transfer matrix modelling, by Jacobs *et al* [88]. They took their iridoplast structure (constructed from dimensional data measured from multiple TEM images of iridoplasts) and varied the thickness of the stroma layer, effectively varying the periodicity of the multilayer. In the work presented in this thesis an iridoplast structure was generated using dimension data from TEM images collected by O-Phart Phrathep during his PhD research, which was calibrated to have a peak reflectance wavelength of 515nm. This was done as a way to counteract the unknown amount of shrinkage that occurs during the chemical fixation process for TEM [110]. Compared to the blue-reflecting iridoplast structure, which used the same structure used by Jacobs *et al* and had a peak reflectance wavelength of $475nm$ [88], the green-reflecting iridoplast structure has an absorption enhancement factor (γ) that is redshifted and compressed, with a reduced trough-peak separation of $48nm$ compared to $63nm$.

The predicted angle-dependent spectral shift for both blue- and green-reflecting structures is shown in figure 3.6 and shows comparable blue-shift at wide angles, as long as the large angle artefact peak is ignored (see section 3.2.2). This strongly suggests that green iridoplast structures could represent an extension to the range of periodicities of the multilayer structure found in iridoplasts. However this does not rule out the possibility that the change in reflectance seen *in vivo* is due to a change in the refractive indices in iridoplasts, which would be concurrent with a change in the relative levels of pigment molecules in the thylakoid membranes [111, 112]. The refractive index for thylakoid membranes is extremely difficult to measure *in vivo*, and whilst measurements of pigment concentrations are routine [113] and even measurements of the refractive index of extracted thylakoid membranes have been demonstrated in the past [95],

extracting iridoplasts in isolation from regular mesophyll chloroplasts has proven difficult in previous research [108].

Castillo *et al* [94] calculated the optical characteristics of iridoplast structures based on data from the literature for the dynamic changes in thylakoid and stromal ultrastructure in response to low or high light levels, for chloroplasts [105] and iridoplasts [98]. They found a strong red-shift in predicted reflectance for the high-light acclimated structure compared to the low-light acclimated structure, with peak reflectance wavelengths at normal incidence of $450nm$ (low light acclimation, blue reflectance) and $550nm$ (high light acclimation, green reflectance). In the data presented here, iridoplast reflectance was always measured after 30 minutes of dark treatment, to establish the brightest reflectance [88, 91]. This means that iridoplasts in this study should be in their shortest reflectance wavelength state. It may be possible, even likely, that the structures observed here, if illuminated in high light for a short time may follow the same morphological state transition as seen in the literature [98, 105], and show a redshift in their reflectance spectrum at normal incidence. It is important to note that the iridoplasts found here had peak reflectance at normal incidence between $500 - 526nm$, but no iridoplasts have been measured to have peak reflectance as high as $550nm$.

3.3.2 Macroscopic and microscopic measurements

In the Begonia species confirmed to have iridoplasts or iridoplast-like bodies it is noted that most do not look strongly iridescent or brightly coloured to the eye [98]. Pao *et al* conducted a study of 40 Begonia species and using TEM found that 23 contained iridoplast-like bodies (which they termed lamelloplasts) in the adaxial epidermal cells but only 3 species looked visibly blue-green iridescent to the unaided eye.

Interestingly, out of 11 different lamelloplast-containing species which were examined in that study under TEM, the three that were identified as visibly blue or blue-green iridescent had the smallest stromal layer thickness – with means between $67.53 - 77.91nm$. Lamelloplasts in the other 8 taxa had greater stromal layer thicknesses – between $90.56 - 148.78nm$. As the granal layer thickness stayed constant between all taxa, this amount of increase could be consistent with a shift from blue reflectance to cyan or green reflectance, as the period is increased.

In the case of blue reflecting iridoplasts it is sometimes possible to identify a metallic blue sheen 'by eye' using flash photography or a high intensity light source (see figure 1.4a, b). This is classified as a macroscopic observation. This can be difficult to observe and appears to be linked to iridoplast size as species with abnormally large iridoplasts were identified to be strongly iridescent to the 'unaided eye' [98]. The factors that can obscure visual identification are numerous and varied. The illuminating light needs to contain the wavelengths of light which can be reflected

by a photonic body. The direction of illuminating light, viewing angle and leaf surface angle all need to fit the conditions of strong reflectance, and visual perception may rely on adequate colour, or brightness, contrast between a leaf and its surroundings. On top of this, a photonically green-reflecting iridoplast would be near-impossible to distinguish macroscopically from the chlorophyll pigment-green colouration in the leaf.

Furthermore visual perception of the unaided eye can be dramatically affected by other factors such as surface reflection or translucency. Waxy surfaces can have a glossy or matte look to them, depending on the surface structure of the wax. High gloss, whilst possibly increasing overall visibility to pollinators [114], may desaturate any narrow-band colour signals [115]. Plants with highly convex or conical epidermal cells can take on a velvety look which, in the case of flower petals has been shown to enhance the visibility of strong colouration from pigmentation [116]. Iridoplast size and number will both affect how strong a reflective signal is when viewed on the macro scale, which have been shown to be highly variable, both between species [93] and within species for plants grown in different light environments (see section 4.2.1.2).

It is only under reflectance microscopy that iridoplasts can be consistently seen and identified, and if they are not close to the leaf surface this becomes much more difficult. Bright colouration and reflectivity do not necessarily mean photonic structure. Iridescence, the continuous change of reflected wavelength with changing viewing angle is a clear indication of photonic structure and is usually produced in ordered multilayer structures, although there are examples of chirped or chaotic multilayer reflectors with less angular dependency [51]. In the case of *Selaginella erythropus*, blue iridescence from both cell wall multilayers and highly ordered regions of the bizonoplasts [91] (modified chloroplasts with multilayer structure resembling iridoplasts) are visible under reflectance microscopy and look strikingly similar. Masters *et al* showed a clear example of this [91]. Examination of the ultrastructure under electron microscopy is vital to distinguishing between such cases.

It is clear that iridoplasts with peak reflectance wavelengths greater than 500nm are prevalent, as can be seen in figure 3.8. Thirty-one out of 96 iridoplasts measured over nine species of Begonia showed iridoplasts with peak reflectance in this range. Iridoplasts of all types may be difficult to identify without the use of microspectrometry as the visible reflective signal can be obscured due to 1) the low number or small size of iridoplasts 2) obfuscating surface reflections, or 3) the iridoplasts may predominantly reflect greener wavelengths, thus competing with the pigment-green colouration from chlorophyll. It should be noted that even under reflectance microscopy, identification of iridoplasts is not always straightforward, as other reflective areas may be observed from a number of well documented photonic effects: from the cell wall [78, 117], cuticle [118] or cellulose helicoidal structure [80, 81], and further structural imaging may be

necessary.

Blue reflecting iridoplasts were shown [88] to have an increased photosynthetic yield in low light conditions compared to mesophyll chloroplasts, and the optics of novel green-reflecting iridoplasts here appear to show comparable phenomena to previously studied iridoplasts. Since a number of the species containing green-reflecting iridoplasts are shade dwelling species there should be some evolutionary bias to produce iridoplast structures, although in the case of green-reflecting iridoplasts the phenomena is not visibly reflective, iridescent or brightly coloured, unless viewed microscopically.

3.4 Conclusion

Since the first reports of iridoplasts in *Begonia pavonina* [79], many Begonia species have been identified as having iridoplasts, all of which have been found to have blue-cyan structural colour with peak reflectance wavelengths between $440-500nm$. Here, 31 out of 96 iridoplasts, over 9 species, have been found with peak reflectance between $500-526nm$, significantly closer to the green part of the visible spectrum than previously reported. Using microspectrometry the reflectance spectra was measured over a wide angular range showing blue-shift iridescence characteristic of iridoplasts in the literature [88]. These were also compared to exposed mesophyll chloroplasts, which showed no iridescence, and much weaker reflectance for incident angle $> \pm 5^{\circ}$. Optical modelling using the transfer matrix method suggests that differences in period alone can easily account for the longer wavelength peak reflectance, but does not rule out possible differences in pigment content as a cause for the different colouration. The difficulties in identifying these bodies is already apparent: macroscopic measurements and even some microscopic measurements can still end in ambiguity due to the diversity of structures that can produce blue structural colour. Additionally, the green reflectance wavelengths suggests that these structures may have been mis-reported already [98], and may be much more prevalent than previously thought. The advantage of these structures over the previously described blue-reflecting iridoplast structure is not well understood, further investigation of the differences in photosynthetic yield could provide a clearer picture.

CHAPTER 4

RESPONSE OF IRIDOPLAST ULTRASTRUCTURE TO AVAILABLE LIGHT

4.1 Introduction

4.1.1 *Begonia maurandiae*: a new model species?

Previous characterisation of the photonic structure in iridoplasts has been done on a lab grown hybrid, *Begonia grandis x pavonina*. This hybrid was developed to allow experimental work on iridoplasts year round. It is common among the neo-tropical or iridoplast-containing Begonia species to be extremely seasonal, which is true in the case of *B. grandis*. *B. pavonina* can be grown year round, but the cross breed benefits from the robust and fast growth of *B. grandis*.

This hybrid has many benefits aside from being easy to propagate and grow year round. It has a relatively high number of iridoplasts compared to other species, which are generally of consistent size and reflectance. *Begonia pavonina* was first described by Gould and Lee [119] who suggested the striking blue colouration was due to novel plastids they named iridoplasts in the adaxial epidermis. Now iridoplasts (sometimes termed lamelloplasts) have been found in many Begonia species [93], both visibly iridescent and not [98] as discussed in the previous chapter.

Begonia maurandiae is native to Colombia, primarily found at higher altitudes ($1700-2300m$) and is a creeper style plant, commonly found trailing from trees in shaded tropical forests [120]. It has smaller but more numerous leaves compared to *Begonia grandis x pavonina* and is much faster growing. This macrophysiology coupled with the fast growth is very desirable for experiments under controlled conditions where novel light environments are needed. The plant being a low-growing creeper means that the majority of leaves will exist at the same height even as the plant continues to grow many more leaves. In most iridoplast containing species the plants will

grow to increasing height as more leaves are produced, putting the new leaves closer to a typical light source. This has the potential to drastically change the photon flux density (PFD) arriving at a particular leaf. It has been shown for a few Begonia species that growth under high/low PFD has a considerable effect on the morphology of iridoplasts [93], and application of shade netting directly to leaves of Begonia plants which are visibly iridescent causes visibly stronger colouration [98, 108].

This work aims to determine whether *Begonia maurandiae* shows consistent and numerous iridoplasts, as in *B. grandis x pavonina*, so it can be used as a potential new model species for studying iridoplasts.

4.1.2 Range and plasticity of iridoplast ultrastructures

Iridoplasts have been found with a range of reflectance wavelengths between $450-500nm$ [88, 108]. In the case of *Begonia sutherlandii* some iridoplasts have been found with reflectance wavelengths between $500-526nm$, significantly greener than the $450-500nm$ (blue-cyan) range. The range of iridoplast reflectances could be due to a corresponding range in the periodicity of the multilayer structure as this has a strong influence on the reflected wavelengths. A recent characterisation and optical modelling of the iridoplast predicted structures with strong reflectance from $440-575nm$, by effectively varying the multilayer period [88]. The presence of photonic structure in iridoplasts has been shown to be closely related to enhanced absorption for certain wavelengths, possibly through the action of a slow light effect.

A slow light effect in photonics refers to the reduction of the group velocity of light for wavelengths at the edges of a photonic band gap (a wavelength range where light propagation through a structure is not allowed, usually associated with strong reflectance). The reflectance peak of iridoplasts can be thought of as a soft band gap (soft, since the reflectance is only in the range of $10:20\%$). The reduction of the group velocity occurs because of the presence of an optical resonance, where energy is transferred between two or more modes of electromagnetic radiation [121]. In the case of a 1D multilayer reflector the different modes, in the simplest terms, could be forward and backward propagating waves. These forward and backward propagating waves will lead to standing waves in the stratified medium for certain frequencies of light, dictated by the period of the multilayer and the refractive indices of the layers. Traditionally absorption may be enhanced at both edges of a photonic band gap [122], but in the case of iridoplasts, only enhancement at the longer-wavelength edge is seen [88]. The reason for this is that the standing waves at the longer-wavelength edge ($520nm$) have their anti-nodes aligned with the absorbing grana layers and those at the shorter-wavelength edge ($440nm$) have their anti-nodes aligned with the non-absorbing stroma layers. This particular use of structural slow light for enhanced absorption at one band edge has been demonstrated in non-biological man-made structures

before as a way to enhance solar cells [123], and has been proposed as a strong candidate for lab-on-a-chip biosensing [124].

It was noted that enhanced absorption at the long-wavelength reflectance band edge could be an adaptation to the light environment of the neo-tropical understory – one which is depleted in red and blue wavelengths (and thus enriched in green wavelengths relative to the light incident at the canopy) due to the absorption of leaves in the canopy [82]. In the iridoplast structure, it is the slow-light-like effect that allows for the unique absorption properties. As the range in periodicities allows for a range in reflectance peak wavelengths, it also introduces the tunability of the absorption peak wavelength.

Macrophysiological differences are widely seen in many species when grown under light with varying spectral quality. In general, plants grown under green and red light frequently show physiological changes characterised as shade avoidance or shade stress [125, 126] – larger stem, increased inter-node length and expanded leaves. Similarly, changes to the physiology and chemistry of mesophyll chloroplasts due to light spectral quality has been widely reported. Dramatic changes to the stacking of thylakoid membranes in grana are reported under low or blue light [127, 128], whilst green and red light have been reported to decrease chloroplast size and shape uniformity [129]. Light intensity and spectral quality is known to affect the ratios of chlorophyll a/b and photosystems I / II [130, 131] because of reorganisation of the thylakoid architecture [132, 133].

The case for iridoplasts to enact structural changes to adapt to the most abundant wavelengths seems much stronger than for mesophyll chloroplasts since the iridoplast may have to only slightly change its periodicity, possibly a much less disruptive change to the membrane structure than the changes observed in mesophyll chloroplasts. This work aims to explore whether iridoplasts show a change to their ultrastructure and optical characteristics in response to different monochromatic light environments.

4.1.3 Disorder in iridoplast structures

The effect of disorder on biological photonic structures is well studied in relation to visual cues in insects, birds and other animals [134, 135]. The structure of periodically spaced surface striations on petals, subject to natural disorder was characterised and replicated without pigment. Optical measurements of the replicas showed a photonic blue 'halo' which was found to improve identification by pollinators [136]. Some work focuses on quasi-ordered and completely disordered structures, which, one two cases, are shown to have striking benefits for brilliant white reflectance [137] or strong angle-*independent* reflectance [138]. These systems are notable since equivalent man-made photonic structures would need to be much thicker or require materials with extreme

refractive index contrast, respectively, to achieve the same properties [137, 138].

However, since this work is focused on fundamentally ordered photonic structures, the disorder that will be considered here is the variance of the period and layer dimensions of the ordered structure, not uncommon in bio-photonic systems.

It has been noted that in mesophyll chloroplasts individual thylakoids in a granal stack vary in thickness and lateral displacement [139]. A recent theoretical study [109] examined only the effects of lateral displacement disorder of the thylakoids in granal stacks in mesophyll chloroplasts and found that for small displacements, absorption efficiency was minimally affected but at larger displacements a noticeable decrease in absorption efficiency was found and the scattering efficiency was increased. However, variance to the vertical layer thickness, and therefore multilayer periodicity of such thylakoid stacks, would not have significant impact on their absorption or scattering efficiencies, since the stromal gap between thylakoid subunits is orders of magnitude smaller than in the case of iridoplasts. In this case no multilayer interference is possible in the visible light wavelengths, as the separation of the thylakoid subunits is negligible. This means that slow-light effects which are likely prevalent in iridoplast structures would be insignificant in the granal stacks of mesophyll chloroplasts.

4.1.3.1 Correlated and uncorrelated disorder

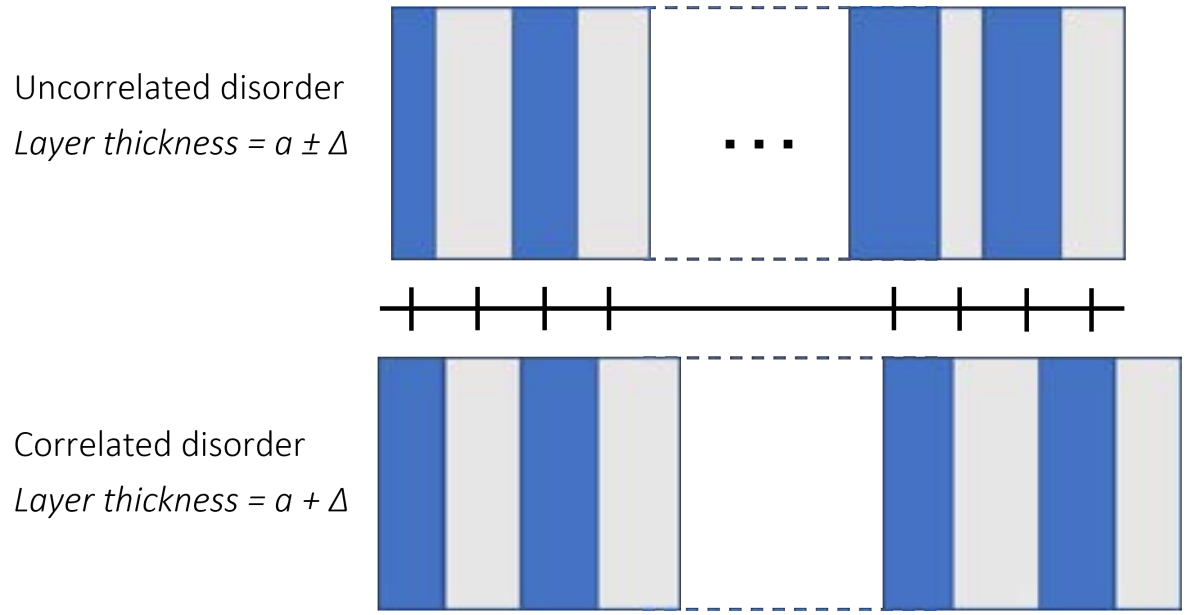

FIGURE 4.1. Schematic showing a fundamental differece between correlated and uncorrelated disorder. Here the layer thickness is determined by a base thickness, a, modulated by a variable, Δ which is a random number normally distributed between $\pm\delta$, the variance of layer thickness. In the uncorrelated structure, layer thickness can be disordered but over many layers, the fundamental periodicity dictated by a is not significantly different from the periodicity of the disordered structure. In the correlated disorder structure, period of the disordered structure is significantly different from the fundamental period given by a after many layers. In this sense the long range order has been destroyed.

A theoretical study by Liew and Cao [140] explored the effects of disorder on 1D photonic crystals with Bragg reflector structures. That is, biphasic multilayer structures with a repeating subunit of alternate layers. They used layers with a low refractive index contrast ($|n_1 - n_2| = 0.05$), as is common in iridoplasts and other biophotonic structures. They calculated the effects of layer position and layer thickness disorder, both correlated and uncorrelated, on the optical properties of those structures.

A correlated layer-position disorder occurs when small displacements to the layer position contribute constructively in one dimension over the course of a periodic structure. Lots of small deviations to layer-position in the same direction would act as larger distortions after many periods as they would have an additive effect. Eventually this may destroy the long range order and thus would have a significant impact on a photonic band gap (shown as a reflectance band in biological systems). An uncorrelated layer-position disorder would consist of displacements

to the layer positions which are evenly distributed around zero over the total number periods. In this case we would expect that with subsequent layers the displacements do not drift away from the expected position by more than the standard deviation of the period. A schematic of this can be seen in figure 4.1. For 1D Bragg reflector structures Liew and Cao showed that correlated and uncorrelated disorders can have very different impacts on the optical properties [140]. For modelled structures with only correlated layer-position disorder there is a reduction to the depth of the transmission peak associated with the photonic band gap (PBG), and the full-width at half maximum (FWHM) is drastically increased. The depth of the transmission peak is relatively unchanged for uncorrelated disorders and also for correlated layer thickness disorder. The FWHM for the same transmission peak shows a small increase under correlated thickness disorder, but reductions for both types of uncorrelated disorder.

Another theoretical study [94] simulated iridoplast structures with varying levels of disorder, based on measurement uncertainty and standard deviation over many samples reported in the literature, and analysed the changes to the optical characteristics. Their results suggested that up to reported levels of uncertainty in layer thickness, reflectance peaks are reduced in height and broadened but the peak wavelength was minimally affected. They concluded that there were clear signs of correlated layer-position disorder in the effects on optical properties and in the logic of how the structures were generated, however the magnitude of the effect was not as large as in the study by Liew and Cao [140]. They conclude that this indicated there is likely a combination of correlated layer-position disorder and uncorrelated layer-thickness disorder present. It is important to note that the structure-generation method in this study may have introduced artefacts which would not be present in real iridoplasts (discussed further in section 4.2.3.3).

This work aims to characterise the amount of disorder present in iridoplast structures using dimensions from TEM imaging. Additionally this work will calculate the effects of disorder on the optical characteristics of measured iridoplast structures with natural disorder and compare with ordered iridoplast structures. It may be possible to determine if there are characteristics of correlated or uncorrelated disorder present.

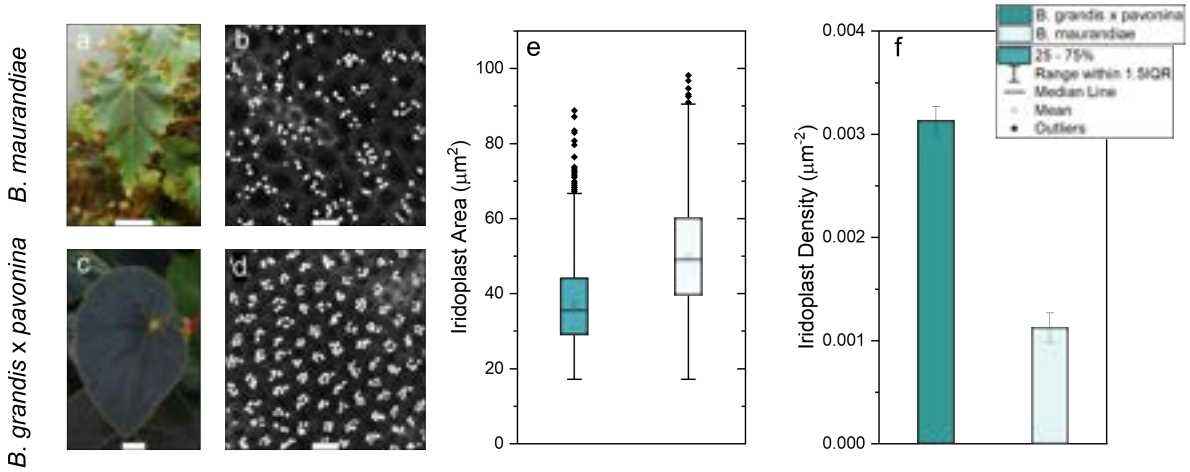

FIGURE 4.2. Confocal laser scanning microscopy (CLSM) with fluorescence showing the iridoplasts in *B. grandis x pavonina* (c,d) and *B. maurandiae* (a,b) used to find the number density (f) and area (e) of plastids. **a, c)** Photographs of a single leaf of each species with scale bar $1cm$. **b, d)** Confocal fluorescence images of iridoplasts (for details on excitation/collection wavelengths see section 2.2.2. Scale bar $50\mu m$. **e, f)** Area and number density of individual iridoplasts calculated using a cell counting procedure in ImageJ. Total of 3389/2116 iridoplasts counted in *B. grandis x pavonina* / *maurandiae*, respectively.

4.2 Results

4.2.1 Characterisation of iridoplasts in *B. maurandiae*

4.2.1.1 Iridoplast number and size

Confocal laser scanning microscopy (CLSM) was used with fluorescence to image the iridoplasts in each species (figure 4.2 b,d). The focal plane was incrementally shifted in the z-axis to capture vertical stacks of images, which were then compiled as a maximum intensity projection. This accounts for the full height of each iridoplast and any curvature of the plane at which the iridoplasts are present. The faint rings and cell-like shapes visible in the background are the top layer of the mesophyll cells and do not correspond to the cells in which the iridoplasts occur. These images were processed in image processing software, ImageJ, and a particle counting process produced information on the number, area and largest diameter of each iridoplast.

The iridoplasts in *B. grandis x pavonina* show distinct groupings of 4-6 iridoplasts, this is in accordance with the literature [88, 108], with each group likely occurring in a single epidermal cell. There is no obvious grouping in *B. maurandiae*.

The iridoplasts in *B. maurandiae* were, on average, larger than for *B. grandis x pavonina* (figure 4.2e) with median areas of $49 \pm 15\mu m^2$ and $35 \pm 10\mu m^2$ (median ± standard deviation, N=2116, 3389) respectively, and whilst there is a lot of overlap between the two groups, each range identifier is consistently higher for *B. maurandiae*, except for the minimum values. However, the minimum value for each group is fixed at $17\mu m^2$ as this is an artefact of the particle counting process.

The number density (figure 4.2f) showed that *B. maurandiae* had almost a third of the number of iridoplasts per square micron when compared to *B. grandis x pavonina*. Measurements of the epidermal cell area show average values of $630 \pm 13\mu m^2$ and $600 \pm 10\mu m^2$ ($n = 29, 27$ mean±SE) for *B. maurandiae* and *B. grandis x pavonina* respectively. When examining TEM sections, the low number density of iridoplasts in *B. maurandiae* lead to many sections with zero iridoplasts to image, making collecting enough images to make a representative dataset too expensive.

4.2.1.2 Iridoplast reflectance

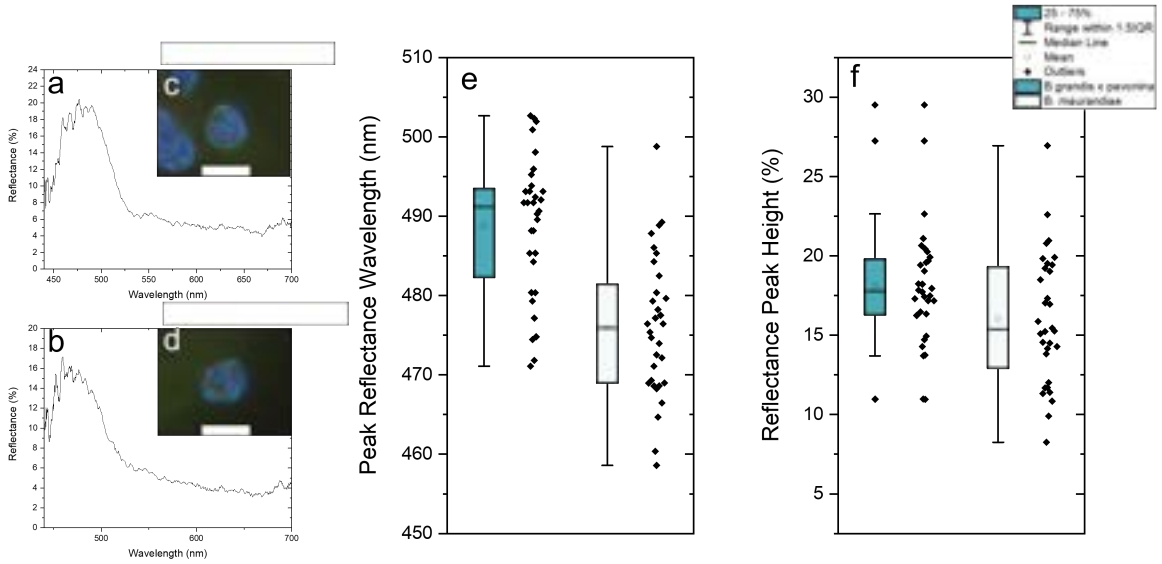

FIGURE 4.3. Reflectance spectra and reflectance microscopy images of individual iridoplasts in *B. grandis x pavonina* (a, c) and *B. maurandiae* (b, d); the central wavelength (e) and maximum reflectance (f) were collected for each spectrum and compiled into box plots. The red circles (c, d) are a marker used to maintain a consistent aperture size when taking spectral measurements. Scale bar $5\mu m$. All iridoplasts were from leaves harvested from plants as described in section 2.1.

Reflectance microscopy with spectroscopy was used to both image and measure the spectra of individual iridoplasts. These measurements were made using a home made epi-illumination microscope (see section 2.2.1 for details). An aperture was used during spectroscopic measurements to isolate an individual iridoplast from its surroundings, seen as the red/yellow circle present in microscopy images (figure 4.3 c,d), this was necessary to achieve the same aperture size for each measurement.

Peak values from each spectrum were found by applying a smoothing function and finding a local maximum. The set of peak wavelength and peak height for each species can eb seen in figure 4.3. The iridoplasts in *B. maurandiae* showed a range of peak wavelengths between $459 - 499nm$, in agreement with the range that has been reported previously for *B. grandis x pavonina* [88]. Here *B. grandis x pavonina* showed a range between 471–$503nm$ with a median at $490nm$. The median for *B. maurandiae* is blue-shifted compared to the *B. grandis x pavonina* grown here at $476nm$. Although there is some offset between the peak reflectance wavelengths here, the *B. maurandiae* is in a range considered most common for iridoplast-containing Begonia species.

The peak heights have a similar median value but the iridoplasts in *B. maurandiae* have more examples of lower reflectance. This is dependent on iridoplast size, degree of order, number of layers and anything causing extinction in the optical path between the iridoplast and the leaf surface.

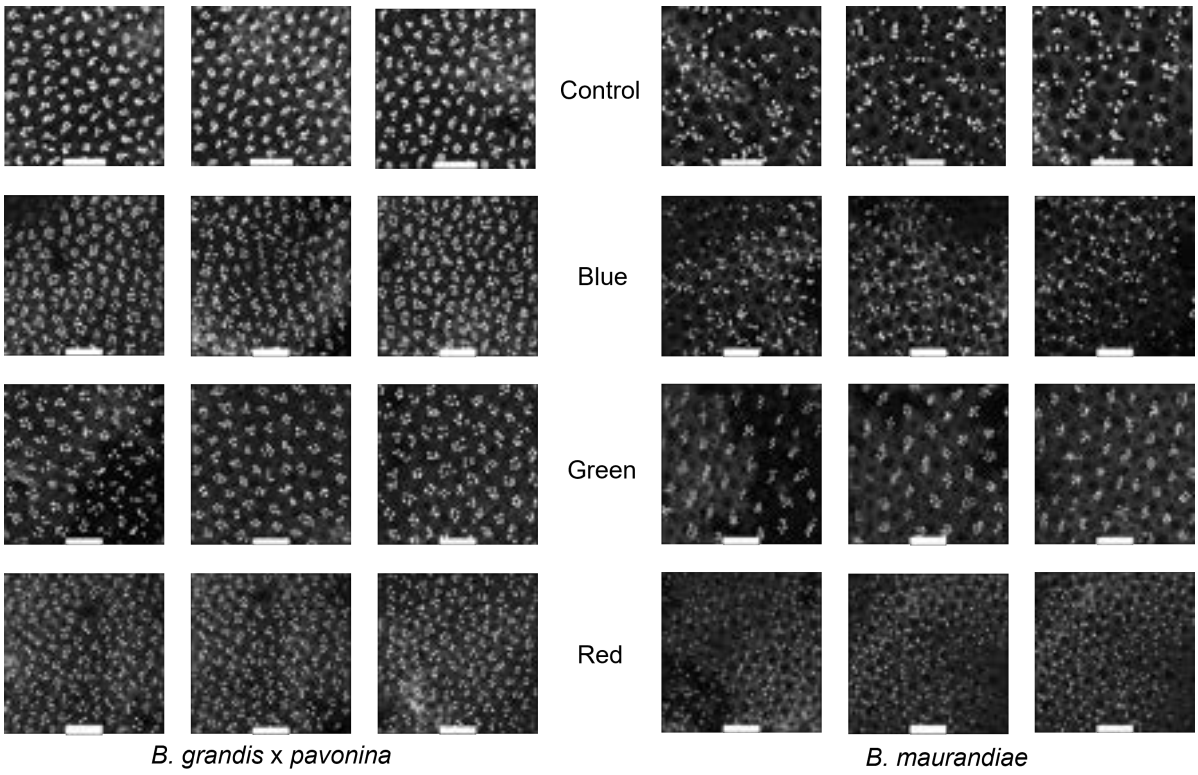

FIGURE 4.4. Confocal fluorescence microscopy of iridoplasts in *B. grandix x pavonina* and *B. maurandiae* plants grown under three different monochromatic low-light environments and a control. Scale bar 100μm.

4.2.2 Iridoplasts grown in monochromatic light environments

4.2.2.1 Iridoplast number and size

Here plants of each species were grown under monochromatic light of three colours (see section 2.1 for spectra) and characteristics of the iridoplasts were compared to a control group, which was grown under standard lighting used in the controlled growth rooms: fluorescent tube light bulbs.

In figure 4.4, iridoplasts in plants grown under different wavelengths of light show some differences in their spatial distribution. For *B. grandis x pavonina* iridoplasts are grouped for all light environments but the green light-grown plants appear to show a larger spacing between groups, shown in figure 4.4. In *B. maurandiae* the iridoplasts in the blue and red-grown plants are more randomly arranged, in accordance with the control group, which were grown under the fluorescence tube lighting. In contrast, those grown under green light showed a strong grouping, similar to the iridoplasts in *B. grandis x pavonina*.

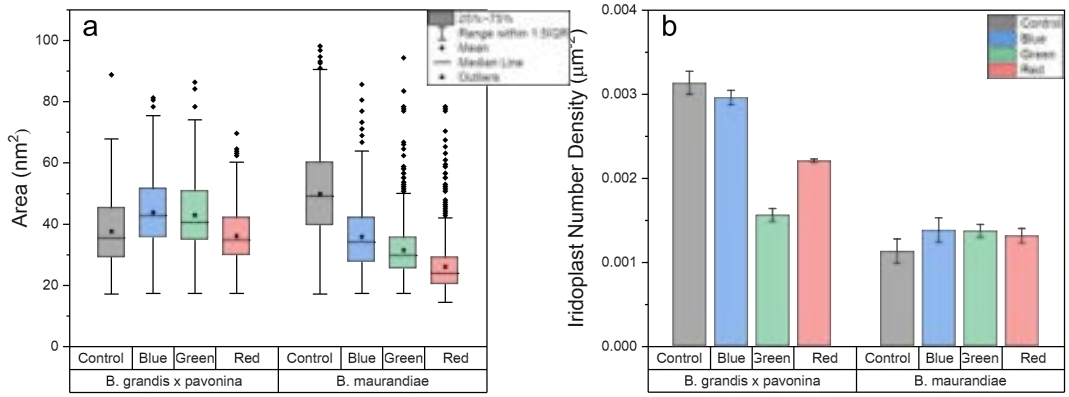

FIGURE 4.5. Iridoplast area (a) and number density (b) for plants grown under different monochromatic low-light conditions. Calculated from confocal microscopy images in figure 4.4 via a cell counting procedure on image analysis software, ImageJ.

In *B. grandis x pavonina* the variations in spatial distribution are somewhat consistent with the values for number density (figure 4.5), between the blue light group and the control group there is no significant change but there is a reduction of around 50% and 33% for the green and red light group respectively. The iridoplast area is not significantly changed for any group compared to the control.

In contrast, the number density (fig 4.5) of iridoplasts in *B. maurandiae* does not significantly change from the control group. The number density value for each coloured light group value is within 1.5 times their uncertainty of the control group. This is especially interesting for the green light-grown plants, which showed a clear, consistent difference in the spatial grouping of their iridoplasts (figure 4.4). The area of iridoplasts are reduced in all monochromatic light-grown plants, and whilst some show lower mean values than in *B. grandis x pavonina*, there is still significant overlap.

4.2.2.2 Iridoplast reflectance

Figure 4.6a shows that measurements of the reflectance spectra show that iridoplasts in *B. grandis x pavonina* showed a significant change to the peak reflected wavelength from the control group when grown under both blue and red light ($p<0.05$), and whilst the statistical significance test for the green light group indicated no significant change, there is a visible grouping of irido-

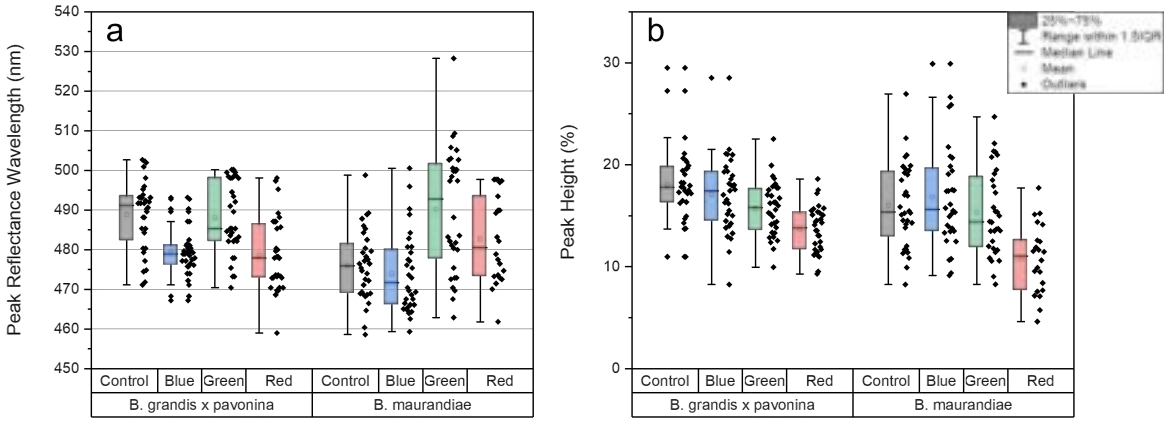

FIGURE 4.6. Peak reflectance wavelength (a) and maximum reflectance (b) for individual iridoplasts in plants grown under weak monochromatic light. Measured using reflectance spectroscopy at normal incidence. All iridoplasts were from leaves harvested from plants as described in section 2.1.

plasts with peak reflectance around $500nm$. The statistical significance tests used throughout this chapter were two sample t-tests comparing a coloured light group to the control group, and the significance level used was 0.05.

The blue light group presented a very tight grouping around $479nm$, with the smallest interquartile range of $4.8nm$. The average peak height showed small decreases of 1.5% and 4.5% for plants grown under green and red light respectively, and both showed significant change from the control group when tested using a two sample significance test ($p<0.05$).

For *B. maurandiae*, only iridoplasts in plants grown under green light showed a significant change ($p<0.05$) in peak reflectance compared to the control group (figure 4.6). The average value and entire interquartile range for the green light group was redshifted with respect to the control group. The range of peak wavelengths was large compared with almost all other groups, and whilst the mean value of 490nm would be considered blue-cyan, 41% have peak values between $497-510nm$ which is closer to the green part of the visible spectrum. The peak height remains unchanged for all groups apart from the red light group which showed a stark reduction in all statistical range identifiers.

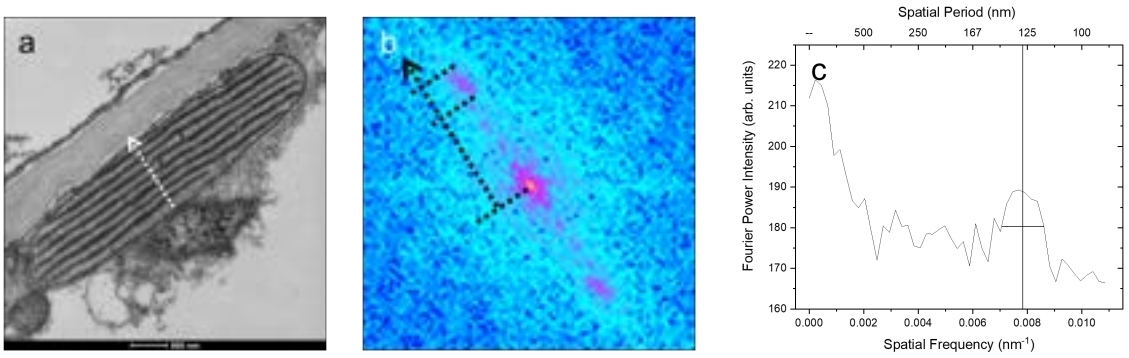

FIGURE 4.7. Extracting period from TEM images using 2DFFT. **a)** TEM image of an iridoplast, white dashed line shows the direction of the periodicity Dark bands are grana and light bands are stroma layers. Scale bar $500nm$. **b)** Central region of the 2DFFT of (a) showing the symmetrical peaks either side of the centre corresponding to the grana/stroma periodicity in (a), black dashed line as a guide to the eye shows the same angle as the white dashed line in (a). **c)** Plot of the line profile taken from the 2DFFT image centre through the top left peak indicated in (b). Vertical and horizontal lines at the feature in (c) show the central value and FWHM used as the period and variation of the period, respectively.

4.2.2.3 Ultrastructure and optical modelling of TEM data

The structural dimensions of iridoplasts can be used as input to a transfer matrix model, used to calculate the optical characteristics of a 1D photonic crystal. TEM imaging offers the magnification and resolution necessary to measure the grana and stroma, but measuring individual thylakoid membranes is more difficult. Thylakoid membrane layers may be well resolved for some regions of an iridoplast and impossible to resolve in others – likely due to distortions of the sample during the chemical fixation process or ultramicrotome slicing.

To apply these dimensions to the optical model, here we make the assumption that the refractive index of the different layers remains constant (discussed further in section 4.3.2.1). The refractive index of thylakoid membranes used here was taken from the literature [95]. With the assumption that the refractive indices are constant, the reflectance peak is dictated entirely by the periodicity of the grana-stroma layering. As long as the proportion of absorbing media (thylakoid membrane) is conserved, the arrangements of the individual thylakoid membrane and lumen layers have little impact on the reflected light as they have periodicities two orders of magnitude smaller than the wavelengths of visible light. Therefore we would expect the distribution of periodicities from TEM images to correspond to the distributions of peak reflectance wavelength from individual iridoplasts measured under reflectance spectroscopy.

To find the grana-stroma period from TEM images, the most complete view is given by performing a 2D fast Fourier transform (2DFFT) on the image of an iridoplast. This transforms a real space image (figure 4.7a) to a 2D power density distribution in spatial frequency space (Fourier space) of the periodicities present in the image (figure 4.7b). The direction and prominence of periodic features in a real space image will correspond to the angular position (relative to the centre) and intensity of peak in Fourier-space, respectively. This means that any variations in the grana-stroma period, over the whole iridoplast, are accounted for in the spread of its corresponding peak in Fourier-space.

Periodicities for the grana-stroma layering were found by performing a 2DFFT on TEM images, a line profile was taken from the FFT centre out to the peak and plotted as shown in figures 4.7b and c respectively. The period and range of grana-stroma spacings were taken as the peak centre and full-width at half maximum, respectively. Figure 4.8a shows the distributions of grana-stroma period which appear to have no correlation with the distributions of the measured peak reflectance wavelength in figure 4.6a. The sample size for TEM images was $6-10$ individual iridoplasts per group compared to 32 per group for the reflectance spectra. A minimum of eight iridoplast images was aimed for but for the green light group only six were found, likely due to the reduced number density. As well as the small sample size, any TEM sample would be highly variable due to varying amounts of shrinkage during the fixation process for each sample. The amount of shrinkage has been reported as a 20% dimension difference in bizonoplasts when comparing between chemically fixed TEM samples and cryo-fixed samples for cryo-SEM [91]. Cryogenic fixation methods are much less likely to impart any shrinkage of the sample when performed correctly (see section 2.2.3).

The width of the peak in the line profile of the FFT image is associated with the range of grana-stroma spacings present in the TEM of the whole iridoplast structure. The width of the peak must be taken, in the radial direction of that peak. This direction is normal to the layers in the multilayer structure in the initial TEM image, and can be seen in figure 4.7. This can inform us on how much grana-stroma spacing variation is present. This should be more reliable than the absolute period measurements from the TEM images because the range of spacings should not be adversely affected by the shrinkage that happens during the chemical fixation process if we assume that the structure is uniformly dehydrated on this scale [88, 98, 141]. Therefore we can treat the range of spacings as a measure of how disordered an individual iridoplast is.

In figure 4.8a it can be seen that compared to the control group, the blue and green light groups show significantly different mean values and ranges for the period variation. The red light group shows no significant change from the control group. This is in contrast with what might be expected from looking at the measured reflectance peak height in figure 4.6b, as we

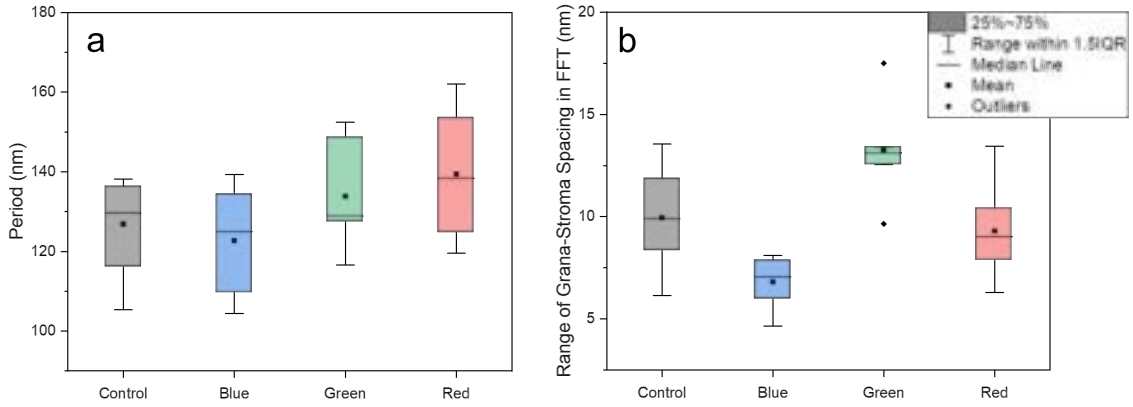

FIGURE 4.8. Period (a) and range of grana-stroma spacing (b) extracted from TEM images of iridoplasts in plants from all light groups using the 2DFFT of TEM images method (detailed in figure 4.7). The range of grana-stroma spacing is determined by the width of the peak in the 2DFFT of the TEM of an individual iridoplast. This can be seen in figure 4.7. All data here is for individual iridoplasts in *B. grandis x pavonina*.

would expect highly disordered structures to have lower maximum reflectance. The relationship between disorder and the reflectance peak will be investigated in section 4.2.3 and discussed in section 4.3.4.

In this case the distributions of measured peak reflectance wavelength (figure 4.6a) are likely to provide a less distorted view of the iridoplasts ultrastructure than the measurements from TEM images due to the smaller sample size of TEM images, and more generally due to the unknown amount of shrinkage present for each sample.

The shrinkage will always have to be accounted for when plugging dimensions into an optical model. In general a shrinkage factor is chosen such that the reflectance peak outputted by the transfer matrix model matches the mean value of measured reflectance peak wavelengths (since it is not possible to measure the same iridoplast under reflectance and TEM). In this case those values are Control – 489, Blue – 479, Green – 488, Red – 478 and Green500 – $499nm$, where the Green500 refers to the cluster of values around 500nm in the green light group (seen in figure 4.6a). These values fall into three groups: Control and Green, Blue and Red, and the Green500 cluster. These peak reflectance values were used to calibrate the shrinkage factor for each structure and the TMM was used to calculate reflectance, transmission and absorption.

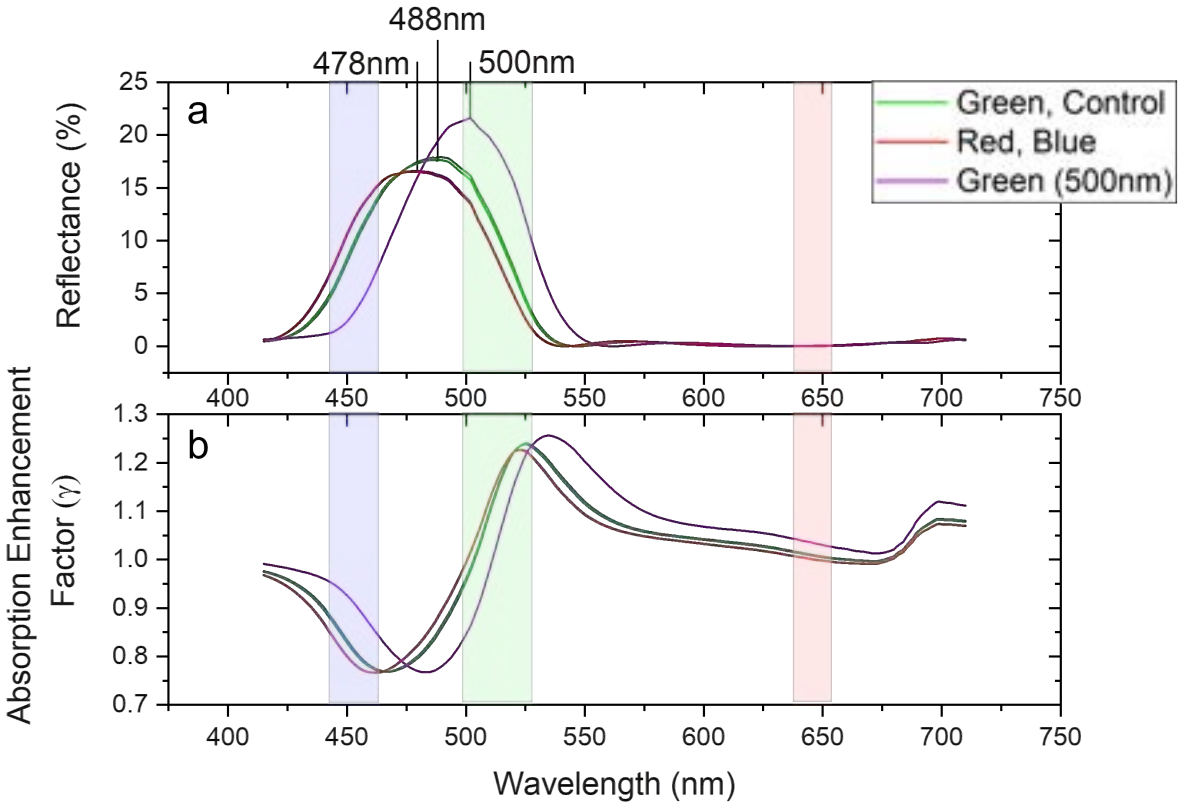

FIGURE 4.9. Reflectance (a) and absorption enhancement factor (b) calculated using TMM for iridoplast structures for each light group (control, blue green, red, and green500nm - [see section 4.2.2.3]). Mean values for the period of iridoplast ultrastructures were calibrated to mean central wavelength values from *in vivo* reflectance measurements, shown in figure 4.6, to generate structures used in TMM calculations.

Therefore, in figure 4.9 there are three distinct curves in both the reflectance and absorption enhancement factor. The groups have peak reflectance wavelengths at $478-9$, $488-9$ and $499nm$. The reflectance peaks' maxima show an increase by 1.2% between the 479 and 489 curves and a much larger increase of 3.75% between the 489 and $499nm$ curves. The full width at half maximum decreases from 68 to 66 to $58nm$ for the 479, 489 and 499 curves respectively. The absorption enhancement factor curves fall into the same three groupings as the reflectance peaks and will be referred to according to the reflectance peak wavelength that they correspond to. Between the 479 and $489nm$ curves there is only a small redshift of the absorption enhancement factor of $2-3nm$. There is a larger redshift for the $499nm$ curve with minimum and maximum redshifting by $9.5nm$. There is an accompanying increase in the positive values which is upheld over the longer wavelengths until the end. For the absorption enhancement factor, the mathematical area after integrating increases from $295nm$ to $297nm$ to $302nm$ for

the 479, 489 and 499nm groups respectively. To clarify, this integration is of the absorption enhancement factor, a unitless ratio over the entire wavelength range, in nanometers. This gives the integration area units, confusingly, as nm.

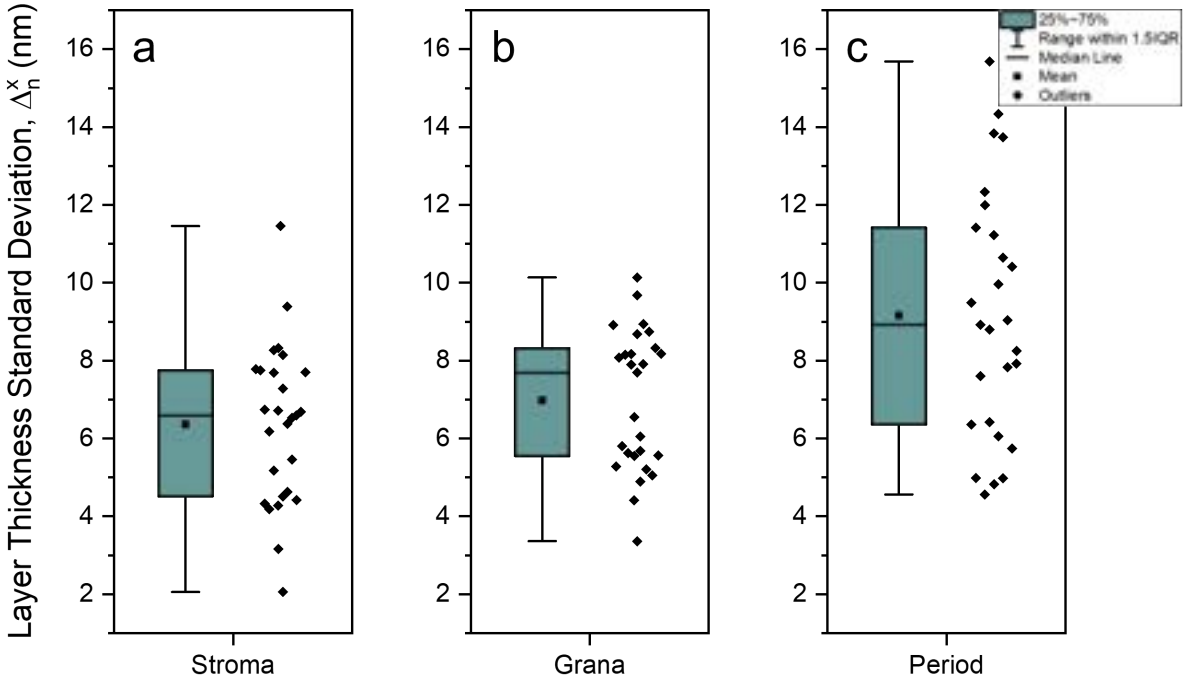

FIGURE 4.10. Standard deviation values for stroma (a) and grana (b) layer thickness for individual iridoplast structures such that each data point corresponds to one iridoplast TEM image. This gives a measure of how disordered each individual iridoplast appears when imaged with TEM.

4.2.3 Impacts of disorder in the iridoplast ultrastructure based on measured data

4.2.3.1 Amount of disorder present

To get a measure for how much disorder is present in individual iridoplasts, layer dimensions were measured from TEM images of individual iridoplasts. This was the same TEM image data used in section 4.2.2.3. Initially the layer thicknesses for whole grana and stroma layers were measured, layer by layer. The accuracy of measuring the thickness of whole grana is much higher than when trying to measure the thickness of individual thylakoid membranes and lumen, as they are much thinner and in many cases close in size to the resolution of the TEM images. The standard deviation of layer thicknesses within a single iridoplast was calculated for each iridoplast as a measure of how disordered each structure was. This is shown in figure 4.10. The mean standard deviation for layer thicknesses were $6.4nm$ and $7.0nm$ for stroma and grana,

respectively, measured over 27 iridoplasts. Jacobs *et al* reported standard deviations of $16nm$ and $7.6nm$ for stroma and grana, respectively [88]. However, this was measured from TEM images of many different iridoplasts so a larger variance is expected, especially in the stroma thickness, due to the different periodicities of different individuals. The standard deviation in the period, Δ_n^P, for an individual iridoplast was also calculated and is used as the measure of how disordered an individual structure is. The index, $n = 1, 2...$, is used here to denote different individual iridoplast structures.

4.2.3.2 Effects of disorder on optical characteristics

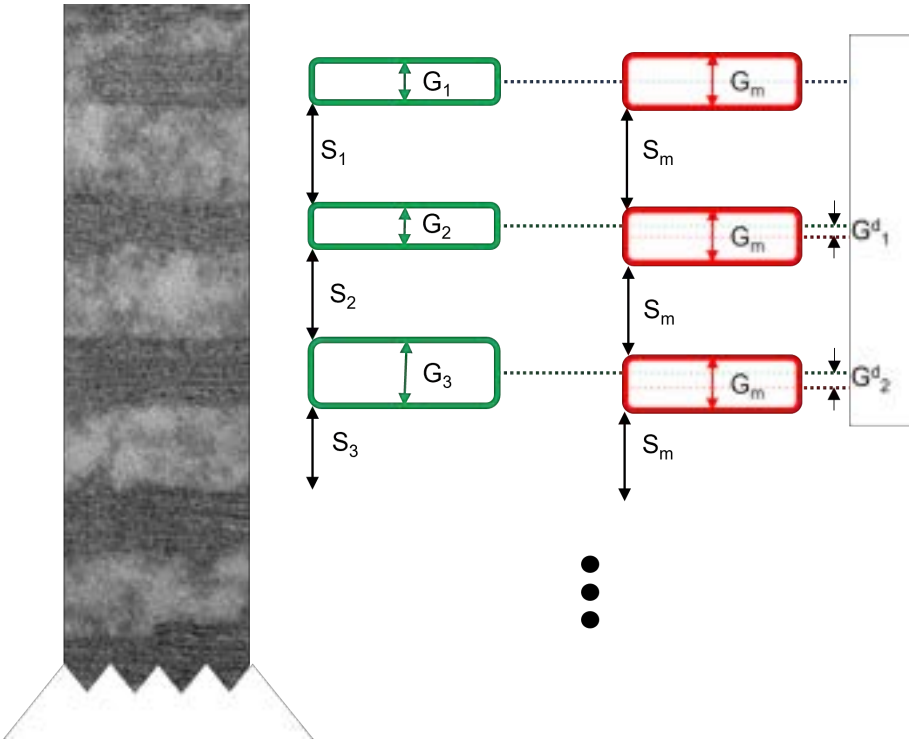

FIGURE 4.11. Diagram showing how layer thickness and layer displacement measurements for TEM images of iridoplasts were made. Left hand side shows vertical rectangular excerpt from a TEM image of an iridoplast. G_i/S_i denotes the thickness of layer $i = 1, 2, 3...$, used to build up the raw data iridoplast structure. G_m/S_m are the mean layer thicknesses for that iridoplast, used to build an ordered iridoplast structure. G_i^d is the displacement of the central position of each layer in the raw data structure from its corresponding layer in the ordered structure.

To explore the effect of disorder on the optical characteristics of iridoplasts the structures with the largest standard deviation in period were examined. Each consecutive layer thickness was

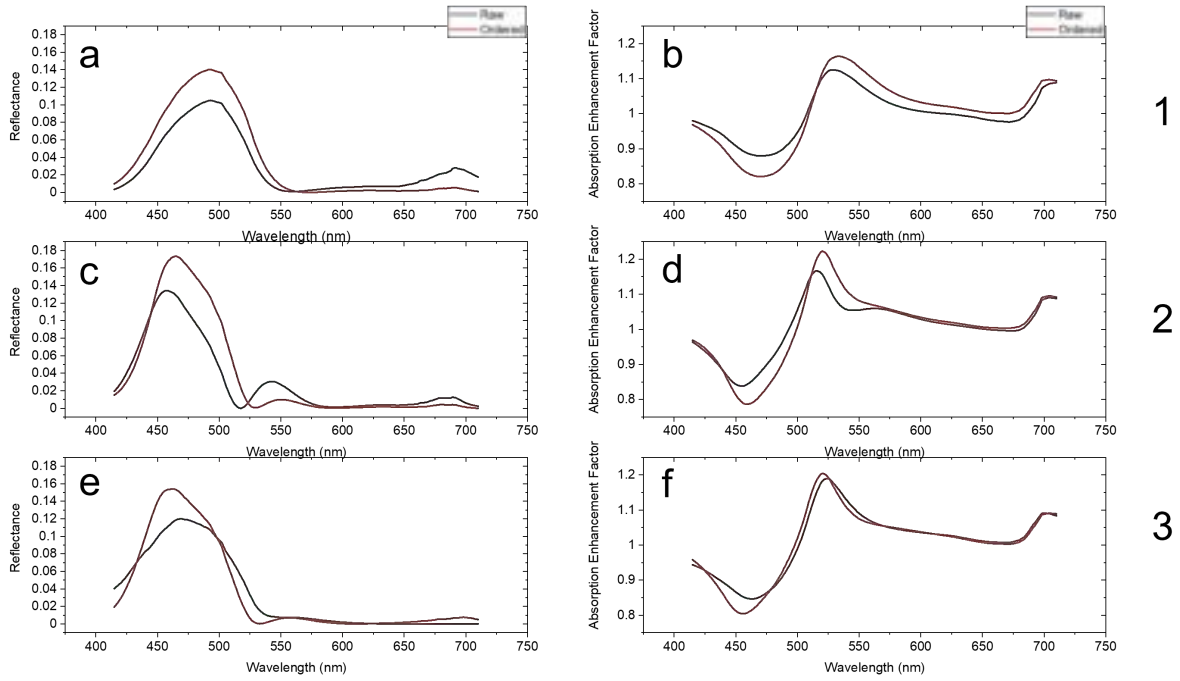

FIGURE 4.12. Predicted reflectance (a, c, e) and absorption enhancement factor (b, d, f) for raw iridoplast structures (red lines) and the corresponding ordered structures (black lines), calculated using TMM. Iridoplast 1, 2 , 3 had standard deviations in their period, $\Delta_n^P = 11.4, 12.3$ and $7.9nm$, respectively, which are all near the top of the range. This is a good indicator that these are some of the most disordered individuals in this data set.

input to the structure and the transfer matrix method was used to calculate the reflectance across the angular range and absorption enhancement factor. The transmission was also calculated and can be seen in appendix A.3. The changes seen were minimal.

Dimensions were measured from TEM images of iridoplasts as in figure 4.11. The thickness of each granum ($G_{i=1,2...}$) and stroma ($S_{i=1,2...}$) layer was measured and used as the raw data structure for that iridoplast, where i is an integer number denoting the layer number. The means of each set of layer thicknesses (G_m, S_m) were used as layer thickness to generate a perfectly ordered structure for each iridoplast, before both were used as input to the transfer matrix model.

In figure 4.12 it can be seen that the reflectance curves for the raw data structures show a 0.03-0.04 reduction in absolute maximum reflectance compared to the ordered structures. For

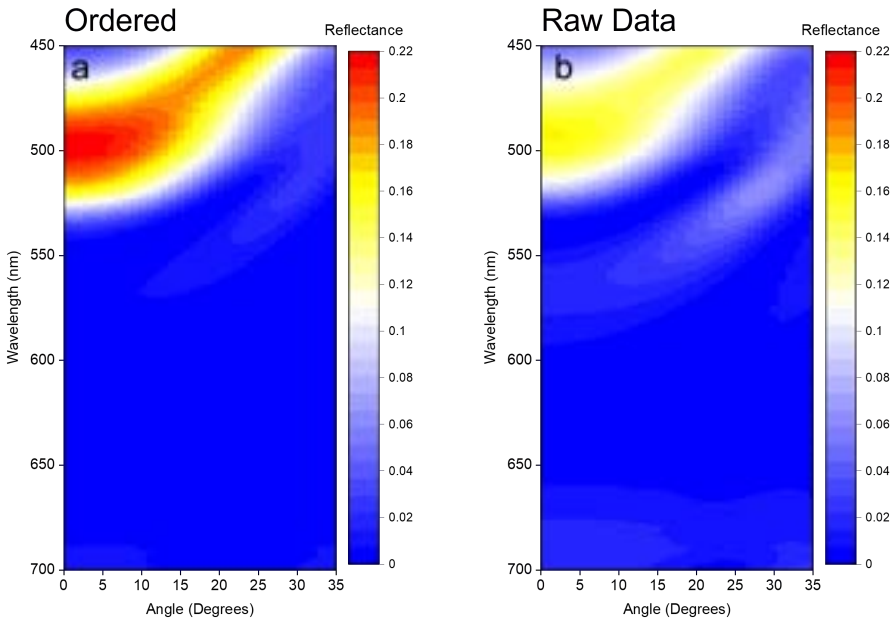

FIGURE 4.13. Predicted reflectance spectrum over angular range for a raw (b) iridoplast structure and corresponding ordered structure (a), calculated using TMM. The iridoplast used has a standard deviation in the period $\Delta_n^P = 12.3nm$, one of the highest values in the data set.

example, a reduction from 0.18 to 0.14 is seen in iridoplast 2. When comparing the reflectance peak between the ordered and disordered structures, only one shows a wavelength shift in the peak, going from $464nm$ to $457nm$ for the ordered and raw data structures, respectively. With the decrease in overall reflectance, there is a corresponding decrease in magnitude of the absorption enhancement factor, except in the case of iridoplast 3 in figure 4.12e, f. For iridoplast 2 (figures 4.12c, d) , there is an enhancement of the peak at $550nm$, which is mirrored as a dip in the absorption enhancement factor at the same wavelength.

Figure 4.13 shows the full angular reflectance spectrum for iridoplast 2, the same structure from figure 4.12c,d. The reduced reflectance and reduced FWHM is the same as is seen in the normal incidence spectrum and is present along the whole angular range. The blue-shift at wide angles is conserved between the ordered and raw structures. The longer wavelength minor peak is preserved and grows in reflectance out to wide angles in the raw structure where more disorder is present.

4.2.3.3 Correlated or uncorrelated disorder

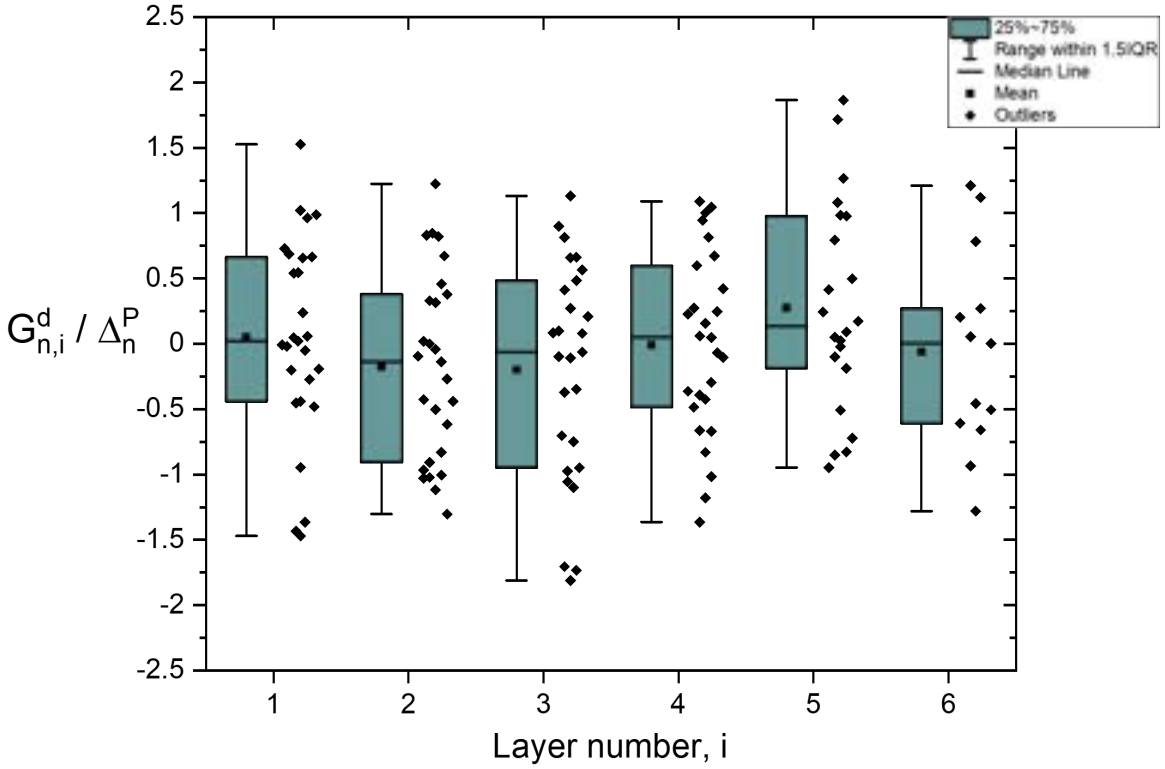

FIGURE 4.14. Normalised layer position displacements, $G^d_{n,i}/\Delta^P_n$ for all iridoplasts ($n = 1,2...$) as a function of layer number ($i = 1,2...$) to show if there is significant drift from the average periodicity after many layers. The displacements for an iridoplast, n, are normalised with the standard deviation of the period, Δ^P_n, in that individual. There are fewer data points after layer number 4 as some structures only had 5 measurable layers, and each structure was considered to start at layer zero with a displacement of zero.

Disorder can be categorised by whether it is correlated or uncorrelated throughout the structure [140] (see section 4.1.3.1). Different types of disorder will affect the optical characteristics in different ways (as described in section 4.1.3). Correlated layer-position disorder will affect the reflectance most significantly as it will affect the long range order. In the case of correlated layer-position disorder, after many layers the layer position would be displaced away from the expected position by more than the standard deviation.

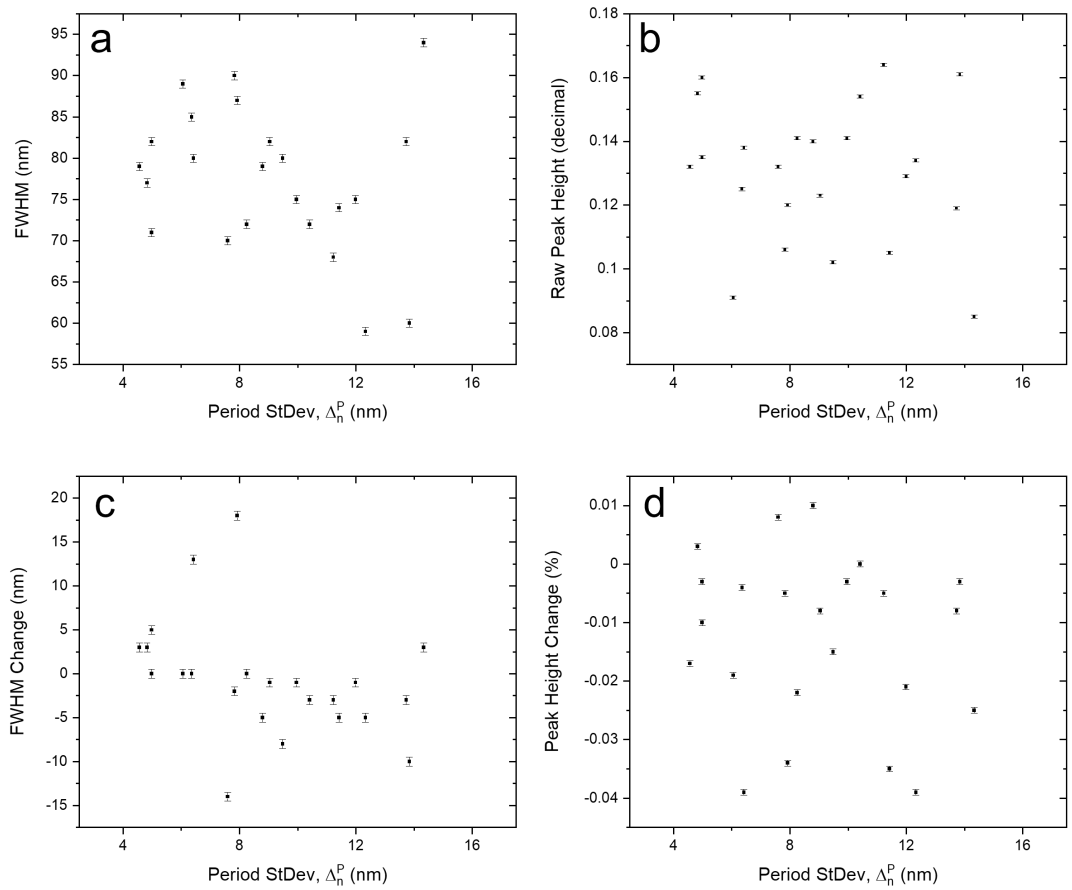

FIGURE 4.15. FWHM (a) and maximum peak reflectance (b) for reflectance spectra of raw iridoplast structures calculated using TMM, plotted against the combined % uncertainty for stroma and grana layer thicknesses (as calculated for figure 4.10) to investigate whether there is correlation.

To test for deviation from the long range order, the displacements between the layer positions in the raw data structures and the ordered data structures ($G^d_{i=1,2...}$, as seen in figure 4.11) were normalised and averaged out over all iridoplasts , per layer. The displacements for each iridoplast, n, were normalised using the standard deviation of the period for that individual, Δ^P_n. This allows for a comparison between each iridoplast. The normalised displacements at each layer, i, ($G^d_{n,i}/\Delta^P_n$) were plotted for every iridoplast, so as to determine whether there were any trends of increasing displacement with increasing layer number. This can be seen in figure 4.14. Whilst the mean value at each layer does vary around zero between $-0.2 : 0.27$, there is no drift away from zero with increasing layer number, indicating that there is not a strong presence of correlated layer-position disorder.

It has been reported that for simple Bragg reflectors, in structures with only correlated layer position disorder there is a predicted increase in the full width at half maximum, whereas structures with only uncorrelated layer thickness disorder there is no significant change [140]. This is likely due to correlated layer-position disorder having an effect on the long range order, and increasing the contribution of a wider range of spacings to the overall reflectance of the structure. This has subsequently been shown for iridoplast structures in a theoretical study by Castillo *et al* [94] using dimension data for thylakoid, lumen and stroma taken from the literature [88, 98, 142]. To investigate if there are such changes in the data presented here, the full width at half maximum of the predicted reflectance spectra for individual iridoplasts was plotted against the standard deviation of the period, Δ_n^P, as a proxy for the varying amount of disorder. This can be seen in figure 4.15a where there is no discernible correlation. Castillo *et al* found that with increasing disorder, the reflectance peak height diminished. Here the spread of peak heights (figure 4.15b) looks largely uncorrelated with the amount of disorder present. Each value here represents an individual structure so the wide range of values is not unexpected. To account for this, the change in FWHM and maximum peak height between the ordered and raw data structure was plotted against Δ_n^P. No correlation was seen in these cases. All of these results indicate that there is no significant presence of correlated layer-position disorder in the structures quantified here.

4.3 Discussion

4.3.1 Viability of *Begonia maurandiae* for study of iridoplasts

Plants of *Begonia maurandiae* were grown alongside the hybrid *B. grandis x pavonina* to assess how viable it is for experiments needing optical and structural characterisations of iridoplasts. It has a much faster propagation time and growth rate and a large scale physiology much more desirable for running experiments with novel light environments (see section 4.1.1 for further discussion). It appears that plants can be propagated and grown (under artificial conditions) from summer to winter months, which is noteworthy compared to some iridescent *Begonia* species. This has only been shown over a period of 5-6 months.

The iridoplasts show reflectance peaks and iridoplast sizes comparable to *B grandis x pavonina* (figures 4.2, 4.3), making *in vivo* optical measurements viable when using either confocal to assess the cell size and distribution or reflectance microscopy to measure reflectance spectra. In this set of measurements there are more iridoplasts with maximum reflectance values lower than for *B. grandis x pavonina*. This can be influenced by iridoplast area, degree of order, number of layers and anything causing extinction in the optical path between the iridoplast and the leaf surface. However, the iridoplasts with the lowest maximum reflection here still have spectra with which relevant features can be identified.

The number density of iridoplasts is significantly lower for *B. maurandiae* than for *B. grandis x pavonina* which does not affect *in vivo* microscopy (CLSM, reflectance spectroscopy), since the area of leaf that is examined in both cases is sufficiently large to display enough iridoplasts. However samples prepared for TEM use a much smaller area meaning that it was not uncommon to find only one or zero iridoplasts on a particular slice. Obtaining a comparable number of iridoplasts to *B. grandis x pavonina* would be possible but would take many more slices and a much longer imaging time. The number density of iridoplasts in *B maurandiae* was a third of the value found in *B. grandis x pavonina*, and the spatial distribution is much less regular which could have compounded the issue. In reality this made it obstructively expensive to collect enough images in TEM for *B. maurandiae* so all analysis of TEM images of iridoplasts is only done for *B. grandis x pavonina*.

4.3.2 Ultrastructural changes due to monochromatic light

To assess the ultrastructural response in iridoplasts to each light environment, both direct and indirect methods have been used here. Electron microscopy (see methods section 2.2.3) was used as a direct method to image iridoplast structures. Dimensions of the iridoplast ultrastructure can be measured by hand, for each layer, or by the use of 2DFFT, which encompasses the periodicity of the structure over the whole image (see section 4.2.2.3).

The indirect method used here is the measurement of the reflectance spectra of individual iridoplasts, shown in figure 4.6. By reducing each reflectance spectrum down to its peak reflectance wavelength, one can create a set of wavelength values for a number of individual iridoplasts, over a number of individual plants. This can be used as an indication of the periodicities of iridoplast structures, if we assume that the refractive index remains constant between individuals and over time.

4.3.2.1 Impact of refractive index on reflectance spectra

In the simplest terms, the assumption that the refractive index remains constant would depend on the relative levels of pigments present in the thylakoid membranes remaining roughly constant between individual iridoplasts and plants.

In a simplified test of how much a change in refractive index would affect the optics [94], Castillo *et al* applied a uniform scale factor to the whole wavelength range of the refractive index of a thylakoid membrane. They used the same data from the literature for the dispersive and complex refractive index for thylakoid membranes as used in this work [95], shown in appendix A.1. Changes between the expected refractive index and the extremes of the scale factor used ($\pm 10\%$) amounted to peak wavelength shifts of around $\pm 7nm$. This value is not much larger than

the error of estimating the peak wavelength of measured reflectance spectra ($\pm 3nm$) due to their asymmetry. Furthermore this range is much smaller than the range of peak wavelengths associated with (i) ranges in membrane widths and (ii) the range in periodicities directly measured here (which can account for peak wavelength shifts of up to 80nm).

This does not take into account the change in wavelength dependence of the refractive index if the relative levels of certain pigment molecules were to change. However, this change is obstructively difficult to measure or calculate due to a range of factors. The iridoplasts are difficult to isolate without isolating chloroplasts from the same leaf as well [108]. And whilst it is widely agreed upon that the relative level of pigments in a thylakoid membrane would affect the refractive index, calculating exactly their impact is made complex when considering that the formation of different complexes at the molecular level would likely have an impact on their interaction with light.

The refractive index values used in this thesis and in previous research on iridoplasts [88, 93, 94, 108] are one of the only measurements in the literature for thylakoid membranes [95]. It was measured for thylakoid membranes extracted from mesophyll chloroplasts in spinach which is phylogenetically distant from the Begonia genus. So whilst this may not be completely representative of iridoplasts in Begonia it is consistent with previous research efforts.

4.3.2.2 Observed changes to peak reflectance under monochromatic light

Due to both of these factors this work makes the assumption that the refractive index remains constant between iridoplasts, making ultrastructural periodicity the most significant contributor to peak reflected wavelength. From figure 4.6a, it can be seen that for *B. grandis x pavonina* there is a statistically significant change in peak reflectance wavelength when plants are grown under blue or red light, however, only when grown under blue light did the iridoplasts show a tight grouping – in this case around $479nm$. For *B. maurandiae* there was only a significant change for plants grown under green light, and in this case there was far less consistency in the peak reflected wavelength, with the largest interquartile range of any group.

4.3.2.3 Observed changes to ultrastructural periodicity of iridoplasts from TEM images

Direct methods of measuring the changes in ultrastructure all used TEM images as this imaging technique provides the magnification and resolution required to observe the individual layers. It is well known [110, 143, 144] that the chemical fixation process can introduce an unknown amount of shrinkage and distortion to the sample. In previous studies, dimension data from

TEM images has been supplemented with cryo-fixation imaging techniques such as cryo-SEM [74, 88]. There is strong consensus that a cryogenic fixation process such as flash freezing in liquid ethene or nitrogen should not introduce any change in the structural dimensions [145]. However, to expose the multilayer structure of an iridoplast for cryo-SEM a freeze fracture technique is used whereby the leaf lamina is fixed vertically in a vice, flash frozen and the protruding section of frozen leaf is sharply struck to horizontally fracture the leaf to expose an internal cross section. In practise the chance that an iridoplast has been exposed in a given fracture is low. It is apparent in data here and in previous studies [88, 93, 98] that iridoplasts with a range of reflected wavelengths or ultrastructural dimensions are found, even within the same leaf. So to properly supplement a set of ultrastructural dimensions from TEM images a comparably large number of cryo-SEM images would be necessary.

To best allocate the funding in this work, collecting the largest set of TEM images of iridoplasts was prioritised in the hope that natural variation in iridoplast ultrastructures and shrinkage factors would not be the dominant factors. To measure the periodicity of individual iridoplasts, images were converted to spatial frequency representations using a 2DFFT (shown in figure 4.7). This has the benefit of including the grana-stroma spacing seen across the whole iridoplast body, accounting for any variation across the body.

The set of periodicities measured using the TEM - 2DFFT method can be seen in figure 4.8a. The TEM image data is only for *B. grandis x pavonina* as collecting TEM images for *B. maurandiae* was made obstructively expensive by the extremely low number density of iridoplasts. In this case only the green and red light-grown groups are significantly different from the control group ($p < 0.05$), which is not in good agreement with the measured peak reflectance wavelengths (figure 4.6). Again, the statistical significance tests used throughout this chapter were two-sample t-tests, comparing one of the coloured light groups to the control group, with a significance level of 0.05. It is likely that the sample size for TEM images here was still too small, therefore the most reliable characterisation of the iridoplast ultrastructure here was from the measured peak reflectance values.

On the whole, the reflectance data (figure 4.6) is the most accurate measure of ultrastructural changes in the iridoplasts grown under monochromatic light. The TEM periodicity data (figure 4.8) is not reliable because the relative differences between period for different coloured light groups, measured from TEM by 2DFFT do not agree with the relative differences in the measured reflectance peak wavelengths (figure 4.6). Given that finding, the different wavelengths of light used here did not appear to illicit a strong ultrastructural response from iridoplasts,

except for blue light which lead to a tight grouping of the peak reflectance wavelength around $479nm$. Whilst some iridoplasts in both species did show a tight grouping around $500nm$ when grown under green light, it was not true for the majority of iridoplasts in those groups.

In contrast, changes to chloroplast physiology have been widely reported in many plant species in response to light intensity [127, 146, 147] and spectral light quality [129]. Chloroplasts grown under low light or blue light have shown elongated shape [129], uniform size, greater numbers of grana lamellae [128] or enhanced ratios of stacked thylakoid membranes compared with the un-stacked stroma lamellae[132]. These are accompanied by a host of chemical differences, most notably the chlorophyll a/b and PS1/PS2 ratios [127, 131]. It is important to note that these changes, whilst widely reported, are species dependent [148]. But the significant plasticity of chloroplasts (with respect to acclimation changes) in many species appears to not be strongly reflected in iridoplasts in the species studied here.

This is not what was expected, as it was assumed that the change of periodicity in iridoplasts would be far less energy and resource intensive than the ultrastructural changes that chloroplasts undergo, mentioned above.

4.3.3 Enhanced absorption or photoprotection

Whilst the periods measured from 2DFFTs may be unreliable for the absolute values in this study (section 4.3.2), the width of the peak in the 2DFFT will be given by the range of grana-stroma spacings seen in the TEM image. Effectively this could be seen as a measure of how disordered the iridoplasts are (if we assume that the shrinkage of the sample during dehydration is roughly uniform over length scales as small as the grana/stroma layers). Figure 4.8b suggests that iridoplasts grown under blue light should be significantly more uniform in their multilayer structure than iridoplasts in plants grown under all other conditions, with the greatest disorder seen under green light. It may be expected that this should negatively impact the intensity of reflected light, but a recent study [94] has shown this effect may be quite small (detailed effects of disorder on the optical properties are discussed in section 4.3.4). In this case, the measured reflectance peak heights in figure 4.6b do show some reduction for green and red light groups compared to blue light and the control, but the relative amounts by which they are reduced is not in strong agreement with the relative differences of the range of spacings in figure 4.8b.

To assess the impact of any structural changes present, the measured periodicities were inputted to a transfer matrix model to calculate the changes to the absorption characteristics associated with the differing grana/stroma periods, this is shown in figure 4.9. Here the periodicities of iridoplasts measured from 2DFFTs were scaled to match the peak reflectance wavelength of the *in vivo* reflectance measurements. This was because the reflectance measurements were

deemed to have much less impact from artefacts such as shrinkage and a larger sample size, thus greater reliability than the TEM images (discussed in section 4.3.2.

The means of the measured reflectance peak wavelengths for each light group are either 479nm for blue and red light or 489nm for the control and green light. Structures with those reflectance properties were generated to allow calculation of the aborption enhancement factor, γ. A structure was also generated in the TMM calculation for iridoplasts with a peak reflectance wavelength of 500nm, since there was a significant grouping there for plants grown under green light.

In figure 4.9 the changes in reflectance for the 479 and 489nm groups are largely insignificant since each spectrum has significant overlap with the other. This is less true for the 500nm group likely because the full width at half maximum is smaller and the peak height is increased, however these factors may not be reflected in every iridoplast with this peak wavelength. The absorption enhancement factor shows a similar overlap of the 479 and 489nm groups. The 500nm group shows a more pronounced red-shift of around 9.5nm for the absorption enhancements factor, around 3 times larger than the red-shift between the 479 and 489 groups. Interestingly this leads to a reduction in the absorption enhancement factor (γ) between 475-520nm when compared to the 479/489nm curves. This encompasses most of the range of wavelengths that were supplied by the green light. This would be counter-intuitive if the iridoplasts were tuning their structure to enhance absorption, as they are reflecting away a significant portion of the most abundant wavelength of light.

There are similar findings in this work for the hypothesis that the structures may be tuning their wavelength dependence for photoprotection. The reflected light for iridoplasts (figure 4.6) does not line up with the wavelengths of illumination light supplied for any of the modelled iridoplast structures (spectra shown in section 2.1, figure 2.1). If the iridoplasts were all adapting to exist in a photoprotective state, it would make sense that their reflectance peak was concurrent with the most abundant wavelength of light. This finding is also true for the *in vivo* reflectance measurements, except for a small but significant number of iridoplasts in *B. maurandiae* grown under green light which reflect green light.

Whilst there were drastic changes to the number density and arrangement of iridoplasts for plants grown under green light, the only profound structural changes appear in *B. grandis x pavonina* when grown under blue light, which showed a consistent peak reflectance around 479nm between almost all iridoplasts. Transfer matrix modelling of iridoplast structures suggest that the changes in optical characteristics such as reflectance (exclusion of light) or absorptance are minimal. The evidence found here does not support a hypothesis of structural fine-tuning to wavelengths for enhanced absorption at abundantly available wavelengths or exclusion of the

same for photoprotection. Of course, photoprotection is achieved by plants by varied methods outside of the role of photonic structure.

4.3.4 Disorder in iridoplast structures

The iridoplast structure was modelled as grana and stroma layers (as in figure 4.11), as opposed to more detailed structures used in previous studies [88, 94] which accounted for every thylakoid membrane and lumen as individual layers inside the grana. The thylakoid membrane and lumen layer thickness are around $3-7nm$ and any periodicity of lumen layers is of a similar size. This means that this finer structure inside the grana is effectively inconsequential to the photonic optics since the period is orders of magnitude smaller than the wavelengths of light. It will, of course, affect the effective refractive index of the grana as a whole. A calculation of the difference between reflectance spectrum calculated by TMM using the finer structure of thylakoids and lumen, compared to a structure with only the grana-stroma layers is shown in appendix A.2. The period that does effect the optics strongly is the grana-stroma periodicity which is generally between $140-200nm$.

Treating the grana as a uniform layer with a corrected effective refractive index allows the measurements of the whole grana and stroma thickness, thus reducing the large fractional error introduced by the difficult-to-resolve boundaries between individual membranes. The calculation of the effective refractive index of a granal layer is shown in section 2.3 and depends on the ratio of thylakoid membrane to lumen, which over many grana was found to be a near constant 55:45 ratio, in agreement with previous findings [88].

The results in figure 4.12 show that even for the most disordered iridoplasts in this study, the most distinct impact on the optical characteristics is a reduction of 0.03-0.04 in the reflectance peak height, which is accompanied by a similar reduction in magnitude of the absorption enhancement. The fact that both of these values are reduced implies that the reduction in reflectance compared to an ordered iridoplast does not significantly contribute to the absorbed light.

There is no significant change to the peak reflected wavelength. Figure 4.15c shows that for all raw data structures the FWHM shows either no change or a reduction, compared to the ordered structure. However, there is no correlation between the change in FWHM and the amount of disorder. With respect to the angular dependence of the spectra, peak height is affected almost uniformly over the angular range and the angular dependence of the spectrum is conserved.

In a recent theoretical study based on granal stacks in normal mesophyll chloroplasts [109], Capretti *et al* showed that disordered lateral displacements of the disks in a thylakoid stack led to increased scattering but had a minimal effect on absorption. However, in the data presented

here the absorption enhancement factor and scattering are both reduced, indicating that the absorption in this system is more dependent on the photonic effects than in the case of stacked thylakoids. This is in agreement with the idea that a slow light effect is in action here, since the decreased photonic order would hinder the reduction of the group velocity, and therefore there would be less chance for interaction with the absorbing membranes.

The findings in figure 4.14 show that over the 27 iridoplast structures presented here there is no significant trend of correlated layer-position disorder. This is also confirmed by the data in figures 4.15a, c which show no significant correlation of the FWHM or maximum peak reflectance with respect to increasing disorder. This is in contrast to the findings of Castillo *et al* [94], but this is likely due to the way the disordered structures are generated in that study: layer-by-layer. They take as an assumption that the layer-position disorder is correlated because the position of the nth layer is dependent on the positions of all of the previous layers, which is true if all of the layers are grown sequentially and have fixed thicknesses which can not be changed, like rigid bodies. However, given the findings in this work that there is no significant trend of correlated disorder, this supports the idea that the iridoplast does not grow from the first layer to the nth layer, in agreement with the consensus on plastid formation [149]. Additionally the lumen and stromal layers are considered aqueous with low concentrations of proteins, and have been shown to expand and contract in response to light [105]. There is good evidence that the membranes do not act like rigid bodies but will be subject to some physical change under changes in osmotic pressure [146] or electrostatic interaction between neighbouring membranes [150].

4.4 Conclusion

In this chapter iridoplasts in Begonia plants were grown under shade-equivalent levels of monochromatic light with the aim of determining if there was a plastic response of iridoplast ultrastructre to the available wavelengths of light over time scales associated with acclimation (days/weeks). This work did not set out to measure dynamic changes to light over a scale of seconds or minutes. A previous study [88] into the photonic structure present in iridoplasts found they have unique reflectance and absorption spectra due to the photonic structure, and suggested that its characteristic enhancement in absorption of wavelengths between 500-700nm compared to non-photonic, chloroplast-like structures may be an adaptation to the particular spectral quality found in the neo-tropical understorey: one that is depleted in blue and red wavebands and therefore enhanced in the green compared to light arriving at the canopy [82].

The results here show that there is a striking consistency in the reflectance spectra of iridoplasts grown under blue light in *B. grandis x pavonina*, which indicates a structural response. However, the attempts to confirm this using TEM imaging to examine the ultrastructure highlighted the

problems with chemical fixation: trying to measure absolute periodicities in these structures is made difficult and potentially impossible due to the varying and unknown amounts of shrinkage of the sample. The TEM data did show that there may have been consistently and significantly less disorder in iridoplasts when grown under blue light and more disorder when grown under green light. There is a group of iridoplasts in *B. maurandiae* which appear to show the same type of structural response to green light, as this group shows a grouping of iridoplasts with reflectance peak wavelengths between $497 : 510nm$. However, this only accounts for 41% of the peak wavelengths in this light group and the rest of the iridoplasts in this group are spread over the widest interquartile range and total range of any group. It may also be concluded that for *B. grandis x pavonina* iridoplasts in plants grown under blue light showed the structures with the least disorder of any light group, but this is based on the assumption that the shrinkage that occurs during the chemical fixation process for TEM is uniform over the length scale of the iridoplast.

Ultrastructural analysis of TEM images was used to investigate the magnitude and properties of disorder present in the iridoplast structures, and its effect of the optical properties. It was found that even the most extreme cases of disorder had minimal effect on the reflectance and absorption profiles compared to a perfectly ordered structure, showing that the optical properties are robust against the natural disorder present in biological systems, more than was expected. When investigating the layer-position disorder of 27 measured iridoplast structures no significant trend of correlated disorder was found. This was corroborated by the fact that no significant relation was found between increasing disorder and the FWHM or the maximum reflectance peak height. This means that although disorder is present within iridoplast structures, it is not found to disrupt the long range periodicity. This is likely just one contributing factor to how robust against disorder these structures are.

It is clear that iridoplasts grown under blue light showed a consistent ultrastructural change and appeared to show less disorder compared to all other groups. It is not completely clear what the function of this ordering might be given that the analysis on disorder here showed that the optical properties are very robust against disorder anyway. This is still an open question and future work is needed to investigate the behaviour of the photosynthetic processes under these types of structural changes.

CHAPTER 5

FURTHER DISCUSSION AND FUTURE PROSPECTS

5.1 The iridoplast as a photosynthetic body

It is, of course, obvious to think of iridoplasts as photosynthetic bodies for many reasons: they have largely similar photoluminescence excitation autofluorescence spectra to chloroplasts indicating that they both contain chlorophyll [88], they are often seen in TEM images with large starch grains and osmophilic plastoglobuli indicating they are a site of CO_2 fixation [93], and measurements of photosynthetic yield using micro-PAM fluorometry showed a $5-10\%$ increase in photosynthetic yield compared to mesophyll chloroplasts in low light conditions [88].

However, exactly how much of a contribution they make to overall leaf photosynthesis is not well understood. In terms of light collection, compared to non-photonically ordered structures they may have enhanced absorption due to photonic structure in wavelengths greater than 500nm ($\gamma > 1$, figure 3.7) but they unequivocally have reduced absorption in the blue wavelengths at the same time ($\gamma < 1$). This is true in the data presented in this thesis, and in the literature [88, 94, 108]. And in most cases the peak of their enhancement in absorption is roughly around 550nm, which is the region of minimum absorption for chlorophyll pigment, and also the minimum in the imaginary component of the refractive index for thylakoid membranes, which deals with absorption.

When viewed under confocal fluorescence microscopy iridoplasts only appear to take up, at maximum 12% of the leaf area, compared to almost 100% taken up by the palisade mesophyll chloroplasts (not including areas of the leaf taken up by veins). However, it is important to note that in extreme shade conditions with very little directionality to the illuminating light,

as in the tropical understorey, light will penetrate very weakly to the leaf interior. The levels of PAR irradiance drop off significantly as you travel deeper into the leaf, especially for blue and red wavelengths [151]. The region at which the level of PAR intensity is enough to power photosynthesis may be significantly restricted to the epidermal regions.

In the case of green reflecting iridoplasts, it is still unclear how these compare photosynthetically to previously studied blue reflecting iridoplasts. Measurements that inform on photosynthetic efficiency such as PAM fluorometry and time-correlated single-photon counting (TCSCP) are vital to furthering this understanding. This is also true in the investigation of iridoplast ultrastructure in response to monochromatic light. For example it was shown that there was a consistent ultrastructural response to have blue-reflecting iridoplasts when grown under monochromatic blue light in *B. grandis x pavonina* (section 4.2). Microscopic chlorophyll fluorometry measurements possible with TCSCP could elucidate whether this is coupled with enhanced PSII operating efficiency indicating enhanced photosynthetic efficiency, or not. It could be argued that the research presented in this thesis is only one side to the story: treating the iridoplasts purely as photonic structures and investigating the effects on their optical properties. To really understand in what way iridoplasts contribute to photosynthesis in the plant, measurements of photosynthetic processes are vital.

In a similar vein, the iridoplast response to monochromatic light experiment performed here is only investigating acclimation-type changes to the iridoplast ultrastructure, that is changes that take place over days, weeks, or successive 'generations' of newly formed cells. There have been indications experimentally that under the abnormally bright irradiance of the focused light-spot in an epi-illumination microscope iridoplasts undergo a change in their reflectance [152]. A red-shift of the reflectance peak is seen, along with broadening and a reduction to the maximum reflectance. It is not clear currently what the purpose of this change is, but it may be indicative of a structure which can adapt to an extreme range of absolute PAR irradiance.

5.2 The search for iridoplast-like structures in other species

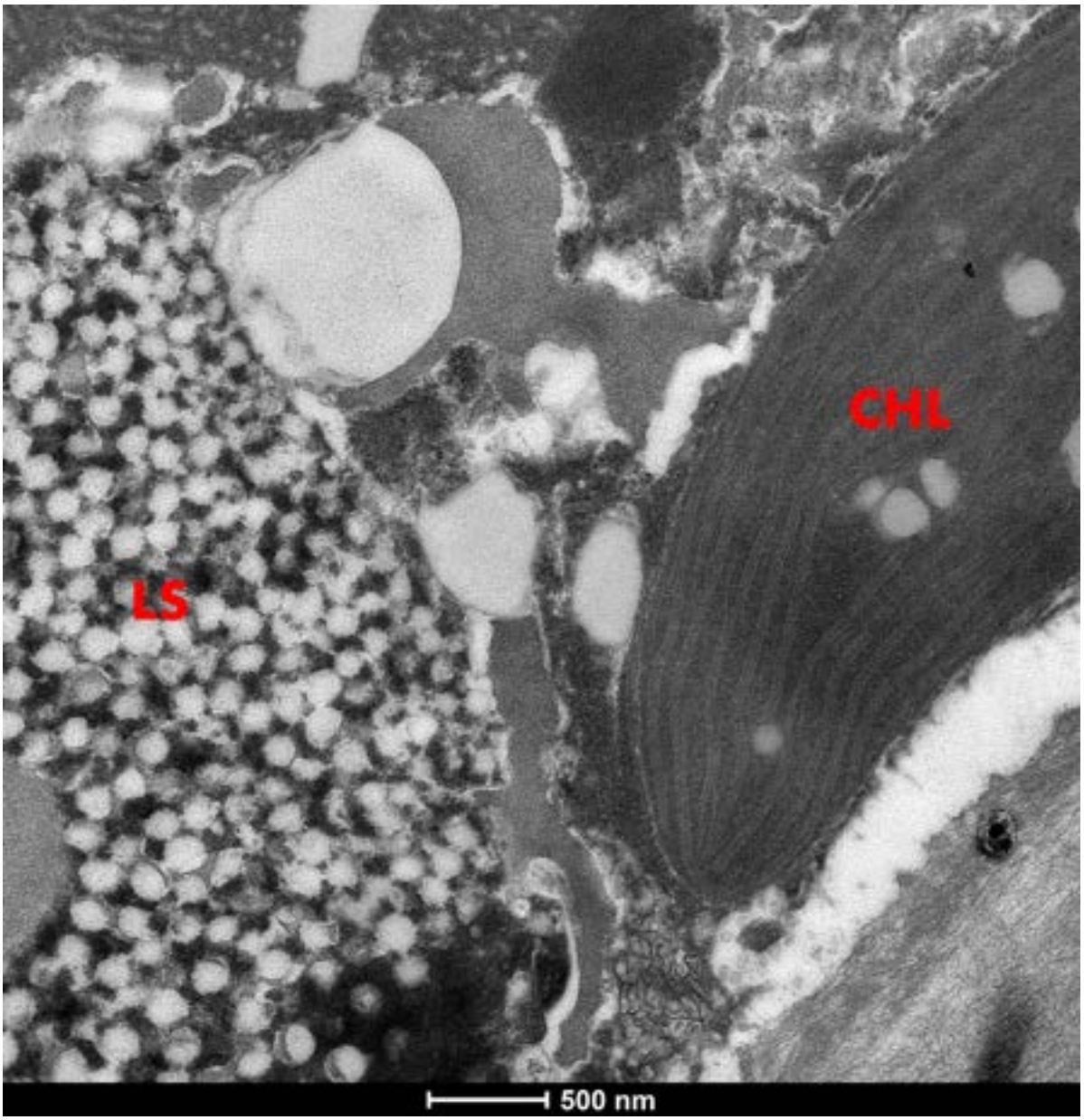

FIGURE 5.1. Ordered multilayer chloroplasts in the epidermal cells of *Ericaria selaginoides* (previously *Cystoseira tamariscifolia*) seen next to the 3D photonic opal-like structure in chemically fixed TEM images. The lipid spheres which make up the 3D opal structure have been partially ruptured and their structure disrupted by chemicals involved in the fixation process, therefore no photonic crystal ordering is expected. CHL - chloroplast, LS - lipid spheres

So far iridoplasts have been identified in *Phyllagathis rotundafolia* [79] and 32 species in the Begonia genus [88, 98]. The ordered multilayer structure of extended grana separated by stroma is found in bizonoplasts, has been optically characterised in *Selaginella erythropus* [91] and it has been reported that bizonoplast structures are common among Selaginella species [89]. There are indications that similar chloroplast structures are found in the brown algae *Ericaria selaginoides* (previously *Cystoseira tamariscifolia*). Firstly, from the doctoral thesis of Nathan Masters [153] and secondly, in a study of chloroplast morphology in Fucales [154], an order of Phaeophyceae (brown algae) in which *Ericaria selaginoides* (*C. tam.*) is found. A number of TEM images were taken during the work presented here, before the COVID-19 pandemic, which showed indications of chloroplasts with long, extended grana made up of 2-3 thylakoid subunits. Grana were separated by what is assumed to be a stromal medium, with some regions showing a periodicity of roughly $100nm$. This period is not dissimilar to measurements taken from Begonia iridoplasts imaged using TEM which found an average period of $137 \pm 26nm$ [88]. This can be seen in figure 5.1.

Lopez-Garcia and Masters suggested that the reversible 3D opal structure found in *E. selaginoides* may be a tool to enhance light scattering to the surrounding chloroplasts in the low light state [74]. It may also be possible that those chloroplasts have photonic multilayer structure which aids in the capture of light, as another measure to deal with a highly variable light environment, and low light conditions. Conveniently, a study by Chandler *et al* presented a review of structural colour in marine algae and found that many species of Phaeophyceae (brown algae) and Rhodophyta (red algae) showed iridescence from 'globular iridescent bodies' [71]. TEM images of the supposed source of this iridescence from Chandler's review showed an array of circular bodies. It may be possible that many of the species said to have this type of iridescence have a structure similar to the 3D opal-like structure reported in *E. selaginoides*, and by extension may also have iridoplast-like chloroplasts surrounding them. One factor that may have made these connections difficult to make is that the commonly used chemical fixation method used for TEM generally destroys many of the lipid vesicles that make up the 3D photonic crystal (PC) opal structure [74, 153]. To mitigate this, and get the best preserved images of the 3D PC, Lopez-Garcia *et al* used high-pressure cryo-fixation methods. This resulted in poorly contrasted, and therefore difficult to resolve chloroplast structures, which would be easily seen in chemically fixed samples.

The 3D photonic opal-like structure found in *E. selaginoides* is reported to act as a tool to scatter light in the cell when in its ordered state [74]. This same feature is seen in the leaves of some species which contain druses or cystoliths made from crystalline calcium oxalate or calcium carbonate [155–157], and in one case larger crystalline biosilica bodies [158]. These are all reported to scatter the light within cells or over intra-cellular distances, likely with the purpose of evenly distributing light throughout the plant leaf. Due to the similarity in the

proposed purpose of these bodies to those in *E. selaginoides*, it may also be fruitful to search for photonically structured chloroplasts in these same species.

5.3 Conclusion

Iridoplasts are found in many Begonia species, and in the case of green-reflecting iridoplasts these may be very difficult to identify leading to the possibility that these are even more widespread than currently assumed. Iridoplasts retain their photonically ordered structure in low light under diverse spectral qualities, which would illicit strong ultrastructural changes in normal mesophyll chloroplasts. It is not yet well understood exactly how the iridoplast contributes to the overall photosynthesis that occurs in the plant, but chlorophyll fluorometry measurement methods such as PAM and TCSCP will help elucidate some of the mysteries. As well as spectrally poor, low light conditions, it may be that highly changeable light environments with a large range in possible PAR irradiance levels are a driver for this type of photonically structured chloroplasts. There is evidence for chloroplasts with ordered multilayer structures in the brown algae *Ericaria selaginoides*, which exist in the presence of a 3D opal-like photonic structure thought to enhance scattering of PAR light in the cell under low light conditions. Some plant species show evidence for crystalline light scattering bodies in their leaves, thought to have a similar purpose. This may be a fruitful area to search for iridoplast-like photosynthetic bodies in different species.

APPENDIX

APPENDIX A

A.1 Complex refractive index for thylakoid membranes

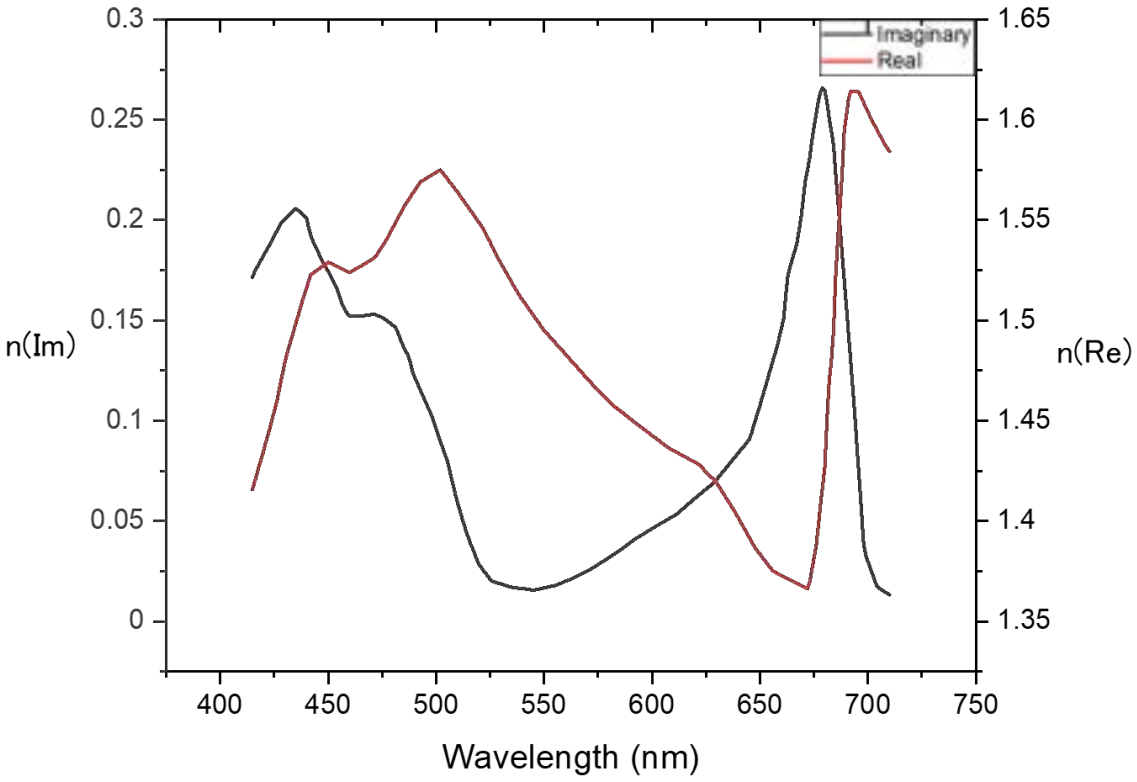

FIGURE A.1. Complex Refractive index values for thylakoid membranes used in TMM calculations. Cited from [95] and interpolated over the wavelength range used in TMM calculations ($415:710nm$) in steps of $1nm$. The complex refractive index is given by

$$n(\lambda) = n_{Re}(\lambda) - in_{Im}(\lambda),$$

where n_{Re} is the real part of the refractive index, n_{Im} is the imaginary part of the complex refractive index and i is the imaginary unit number

A.2 Comparison of reflectance calculated by TMM for different types of iridoplast structure

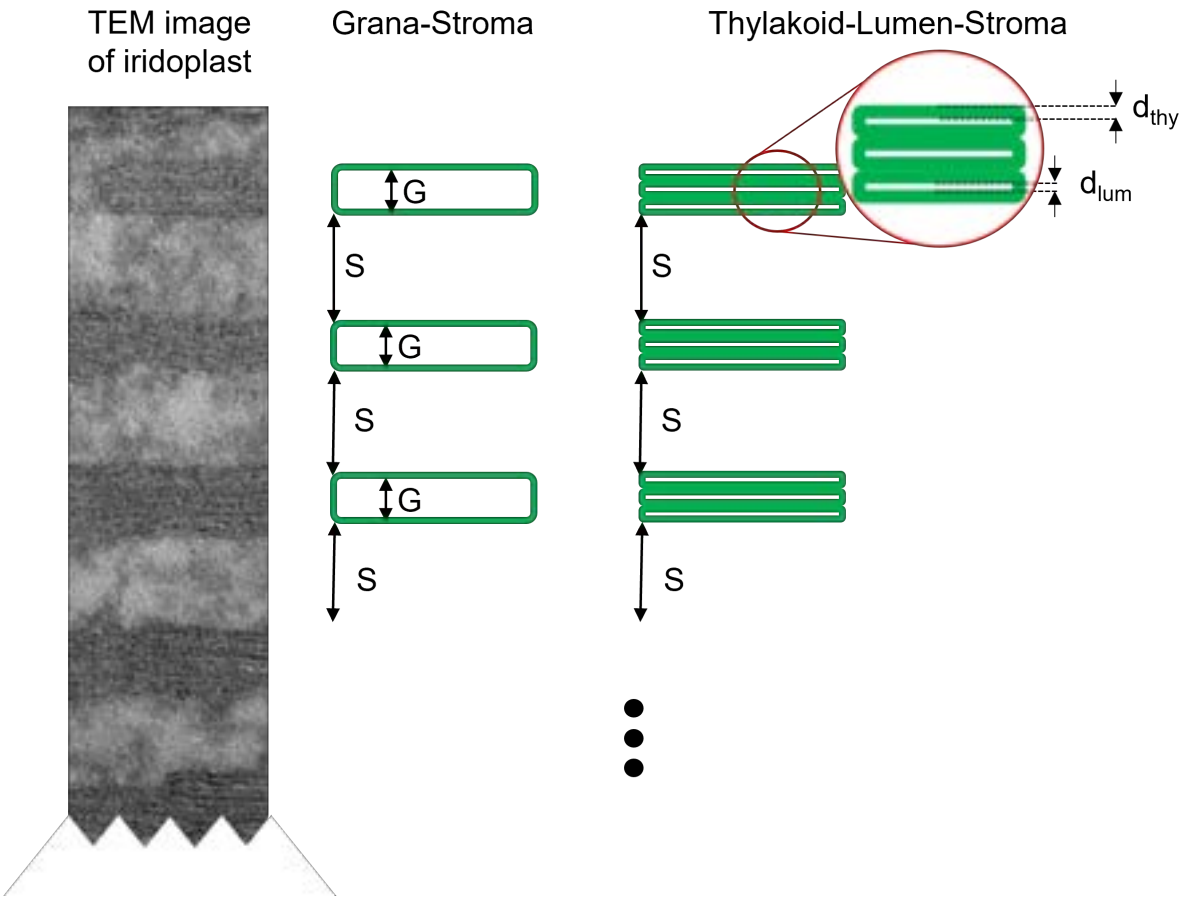

FIGURE A.2. Showing the different types of iridoplast structure, which were used when inputting iridoplast structural data into the transfer matrix method (TMM) to calculate the optical characteristics. **Grana-Stroma** A structure where the grana is treated as a uniform layer, with effective refractive index calculated from the refractive indices for lumen and thylakoid membrane, using the average ratio of thylakoid thickness to lumen thickness, 55 : 45. Calculation of the effective refractive index is shown in section 2.3. **Thylakoid-Lumen-Stroma** A structure in which the thylakoid and lumen are treated as individual layers in the iridoplast. G - grana thickness; S - stroma thickness; d_{thy} - single thylakoid membrane thickness; d_{lum} - lumen thickness.

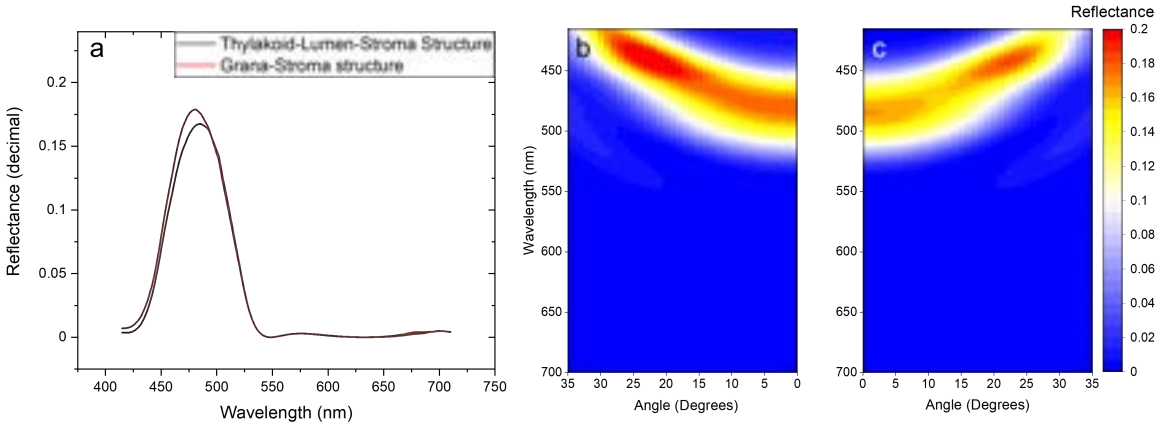

FIGURE A.3. Reflectance for iridoplast calculated using TMM at normal incidence and over wide angular range for both types of iridoplast structure: Grana-Stroma and Thylakoid-Lumen-Stroma (see figure A.2) **a)** Thylakoid-Lumen-Stroma reflectance spectra has maximum reflectance at $484 \pm 0.5nm$ and $16.7 \pm 0.05\%$
Grana-Stroma structure has maximum reflectance at $480 \pm 0.05nm$ and $17.8 \pm 0.05\%$. **b)** Reflectance between $0:35°$ for Grana-Stroma structure **c)** Reflectance between $0:35°$ for Thylakoid-Lumen-Stroma structure.

.

The dimensions used in these calculations for each structure were:

Thylakoid-Lumen-Stroma S - 125nm; d_{thy} - $4.5nm$; d_{lum} - $7nm$.

Grana-Stroma S - 125nm; G - $49.5nm$.

The dimensions and layer structure for the Thylakoid-Lumen-Stroma structure used here were the same as those determined by Jacobs *et al* [88]. The grana thickness, G, used here is the same thickness as the grana in the Thylakoid-Lumen-Stroma structure: $G = (6 \times d_{thy}) + (3 \times d_{lum})$.

A.3 TMM calculated transmission spectra for disordered iridoplast structures

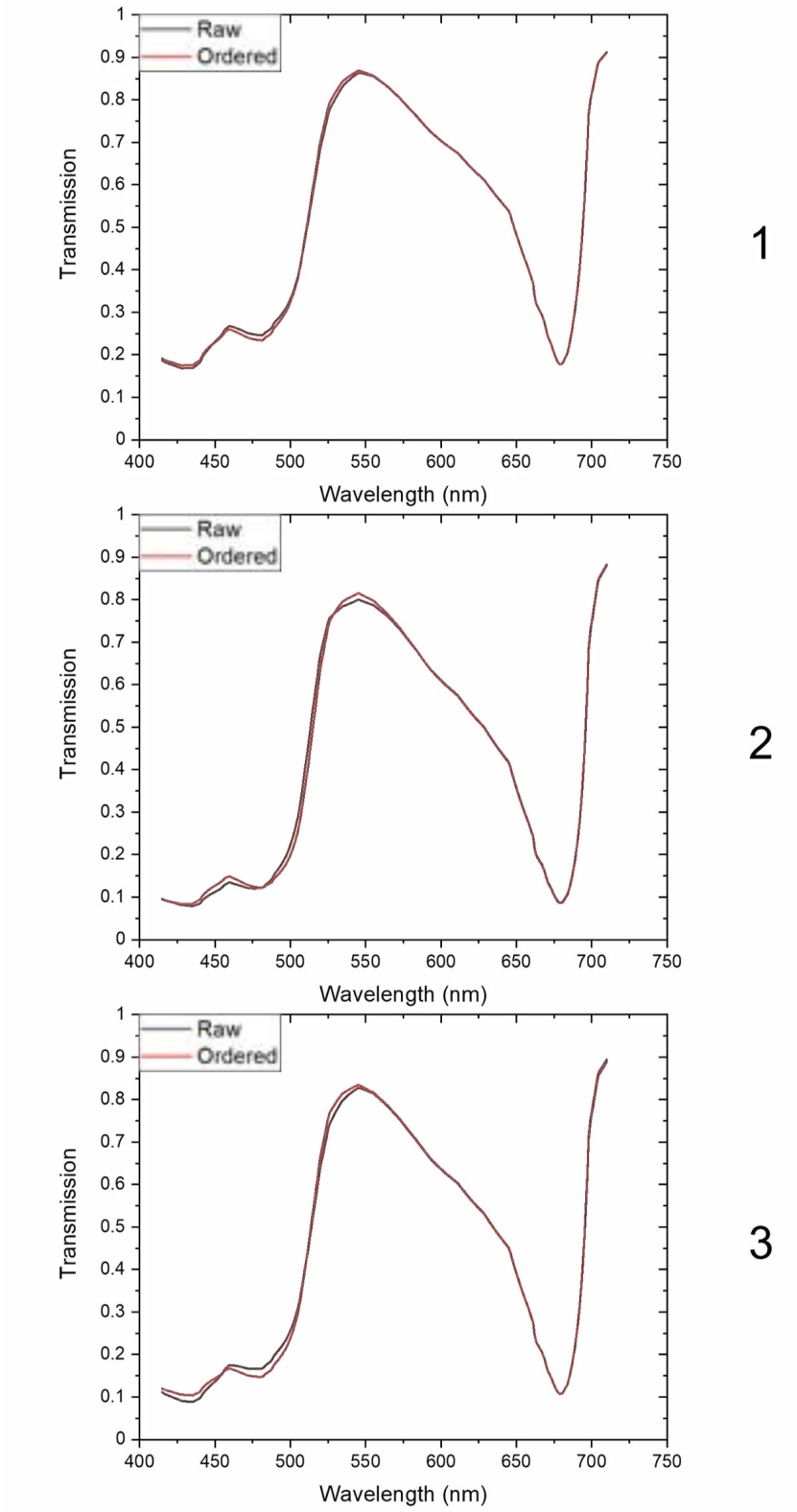

FIGURE A.4. Transmission spectra calculated by TMM for the same iridoplast structures as presented in figure 4.12. Each figure shows the transmission calculated for the disordered structure (Raw data) and the equivalent ordered structure (Ordered).

BIBLIOGRAPHY

[1] Martin Stevens.
Predator perception and the interrelation between different forms of protective coloration.
Proceedings of the Royal Society B: Biological Sciences, 274(1617):1457–1464, 6 2007.

[2] Corri Waitt, Anthony C. Little, Sarah Wolfensohn, Paul Honess, Anthony P. Brown, Hannah M. Buchanan-Smith, and David I. Perrett.
Evidence from rhesus macaques suggests that male coloration plays a role in female primate mate choice.
Proceedings of the Royal Society of London. Series B: Biological Sciences, 270(SUPPL. 2), 2003.

[3] Ulrike E. Siebeck.
Communication in coral reef fish: the role of ultraviolet colour patterns in damselfish territorial behaviour.
Animal Behaviour, 68(2):273–282, 8 2004.

[4] Melissa S. Gerald.
Primate colour predicts social status and aggressive outcome.
Animal Behaviour, 61(3):559–566, 3 2001.

[5] JOHN A. ENDLER.
An overview of the relationships between mimicry and crypsis.
Biological Journal of the Linnean Society, 16(1):25–31, 8 1981.

[6] Martha R. Weiss.
Innate colour preferences and flexible colour learning in the pipevine swallowtail.
Animal Behaviour, 53(5):1043–1052, 1997.

[7] Barbara Snow and David Snow.
Birds and berries.
A&C Black, 2010.

[8] H. M. Schaefer, K. McGraw, and C. Catoni.
Birds use fruit colour as honest signal of dietary antioxidant rewards.

Functional Ecology, 22(2):303–310, 4 2008.

[9] W. J. Steyn, S. J.E. Wand, D. M. Holcroft, and G. Jacobs.
Anthocyanins in vegetative tissues: a proposed unified function in photoprotection.
New Phytologist, 155(3):349–361, 9 2002.

[10] Keith T. Killingbeck.
Nutrients in Senesced Leaves: Keys to the Search for Potential Resorption and Resorption Proficiency.
Ecology, 77(6):1716–1727, 9 1996.

[11] T. S. Feild, D. W. Lee, and N. M. Holbrook.
Why Leaves Turn Red in Autumn. The Role of Anthocyanins in Senescing Leaves of Red-Osier Dogwood.
Plant Physiology, 127(2):566–574, 10 2001.

[12] Carlos A Mazza, Miriam M Izaguirre, Jorge Zavala, Ana L Scopel, and Carlos L Ballaré.
Insect perception of ambient ultraviolet-b radiation.
Ecology Letters, 5(6):722–726, 2002.

[13] Matthew H Koski and Tia-Lynn Ashman.
Dissecting pollinator responses to a ubiquitous ultraviolet floral pattern in the wild.
Functional Ecology, 28(4):868–877, 2014.

[14] Ronald H Douglas, Conrad W Mullineaux, and Julien C Partridge.
Long–wave sensitivity in deep–sea stomiid dragonfish with far–red bioluminescence: evidence for a dietary origin of the chlorophyll–derived retinal photosensitizer of malacosteus niger.
Philosophical Transactions of the Royal Society of London. Series B: Biological Sciences, 355(1401):1269–1272, 2000.

[15] Denis Shcherbakov, Alexandra Knörzer, Svenja Espenhahn, Reinhard Hilbig, Ulrich Haas, and Martin Blum.
Sensitivity differences in fish offer near-infrared vision as an adaptable evolutionary trait.
PloS one, 8(5):e64429, 2013.

[16] Thérèse Wilson and J Woodland Hastings.
Bioluminescence.
Annual review of cell and developmental biology, 14(1):197–230, 1998.

[17] P. J. Herring.
Systematic distribution of bioluminescence in living organisms.
Journal of Bioluminescence and Chemiluminescence, 1(3):147–163, 5 1987.

[18] E. A. Widder.
Bioluminescence in the ocean: Origins of biological, chemical, and ecological diversity.
Science, 328(5979):704–708, 5 2010.

[19] S Kinoshita, Shinya Yoshioka, and J Miyazaki.
Physics of structural colors.
Reports on Progress in Physics, 71(7):076401, 2008.

[20] Shuichi Kinoshita and Shinya Yoshioka.
Structural colors in nature: the role of regularity and irregularity in the structure.
ChemPhysChem, 6(8):1442–1459, 2005.

[21] MH Freeman, CC Hull, and W. N. Charman.
Optics (11 edn), 2003.

[22] Bodo D. Wilts, Hein L. Leertouwer, and Doekele G. Stavenga.
Imaging scatterometry and microspectrophotometry of lycaenid butterfly wing scales with perforated multilayers.
Journal of The Royal Society Interface, 6(SUPPL. 2), 4 2008.

[23] Silvia Vignolini, Edwige Moyroud, Beverley J. Glover, and Ullrich Steiner.
Analysing photonic structures in plants.
Journal of The Royal Society Interface, 10(87), 10 2013.

[24] P. Vukusic and D. G. Stavenga.
Physical methods for investigating structural colours in biological systems.
Journal of the Royal Society Interface, 6(SUPPL. 2), 2009.

[25] Amy E. Goodling, Sara Nagelberg, Bryan Kaehr, Caleb H. Meredith, Seong Ik Cheon, Ashley P. Saunders, Mathias Kolle, and Lauren D. Zarzar.
Colouration by total internal reflection and interference at microscale concave interfaces.
Nature 2019 566:7745, 566(7745):523–527, 2 2019.

[26] Matthew Jacobs, Martin Lopez-Garcia, O. Phart Phrathep, Tracy Lawson, Ruth Oulton, and Heather M. Whitney.
Photonic multilayer structure of Begonia chloroplasts enhances photosynthetic efficiency.
Nature Plants, 2(October):1–6, 2016.

[27] Gerald E Jellison Jr.
Data analysis for spectroscopic ellipsometry.
Thin Solid Films, 234(1-2):416–422, 1993.

[28] Pochi Yeh.

Optical waves in layered media, volume 61.
Wiley-Interscience, 2005.

[29] Amnon Yariv, Chi-Shain Hong, and Pochi Yeh.
Electromagnetic propagation in periodic stratified media. I. General theory*.
JOSA, Vol. 67, Issue 4, pp. 423-438, 67(4):423–438, 4 1977.

[30] Jotham R Austin and L Andrew Staehelin.
Three-dimensional architecture of grana and stroma thylakoids of higher plants as determined by electron tomography.
Plant physiology, 155(4):1601–1611, 2011.

[31] Ethan Weiner, Justine M Pinskey, Daniela Nicastro, and Marisa S Otegui.
Electron microscopy for imaging organelles in plants and algae.
Plant Physiology, 188(2):713–725, 2022.

[32] L Andrew Staehelin and Dominick J Paolillo.
A brief history of how microscopic studies led to the elucidation of the 3d architecture and macromolecular organization of higher plant thylakoids.
Photosynthesis research, 145(3):237–258, 2020.

[33] Richard O. Prum and Rodolfo H. Torres.
A fourier tool for the analysis of coherent light scattering by bio-optical nanostructures.
Integrative and Comparative Biology, 43(4):591–602, 2003.

[34] Richard O Prum and Rodolfo H Torres.
Fourier blues: Structural coloration of biological tissues.
In *Excursions in Harmonic Analysis, Volume 2*, pages 401–421. Springer, 2013.

[35] Richard O Prum, Rodolfo Torres, Scott Williamson, and Jan Dyck.
Two-dimensional fourier analysis of the spongy medullary keratin of structurally coloured feather barbs.
Proceedings of the Royal Society of London. Series B: Biological Sciences, 266(1414):13–22, 1999.

[36] Richard O Prum, Staffan Andersson, and Rodolfo H Torres.
Coherent scattering of ultraviolet light by avian feather barbs.
The Auk, 120(1):163–170, 2003.

[37] Richard O Prum, Jeff A Cole, and Rodolfo H Torres.
Blue integumentary structural colours in dragonflies (odonata) are not produced by incoherent tyndall scattering.
Journal of Experimental Biology, 207(22):3999–4009, 2004.

[38] Richard O Prum, Tim Quinn, and Rodolfo H Torres.
Anatomically diverse butterfly scales all produce structural colours by coherent scattering.
Journal of Experimental Biology, 209(4):748–765, 2006.

[39] S. A. Jewell, P. Vukusic, and N. W. Roberts.
Circularly polarized colour reflection from helicoidal structures in the beetle Plusiotis boucardi.
New Journal of Physics, 9(4):99, 4 2007.

[40] Jiyu Sun, Bharat Bhushan, and Jin Tong.
Structural coloration in nature.
RSC Advances, 3(35):14862–14889, 8 2013.

[41] E. J. Denton and J. A.C. Nicol.
Studies on reflexion of light from silvery surfaces of fishes, with special reference to the bleak, Alburnus alburnus.
Journal of the Marine Biological Association of the United Kingdom, 45(3):683–703, 1965.

[42] E J Denton.
Review lecture: On the organization of reflecting surfaces in some marine animals.
Philosophical Transactions of the Royal Society of London. B, Biological Sciences, 258(824):285–313, 5 1970.

[43] Helen Ghiradella.
Light and color on the wing: structural colors in butterflies and moths.
Applied Optics, 30(24):3492, 8 1991.

[44] P. Vukusic, J. R. Sambles, C. R. Lawrence, and R. J. Wootton.
Quantified interference and diffraction in single Morpho butterfly scales.
Proceedings of the Royal Society of London. Series B: Biological Sciences, 266(1427):1403–1411, 7 1999.

[45] Alison Sweeney, Christopher Jiggins, and Sönke Johnsen.
Polarized light as a butterfly mating signal.
Nature 2003 423:6935, 423(6935):31–32, 2003.

[46] Kathryn D. Feller, Thomas M. Jordan, David Wilby, and Nicholas W. Roberts.
Selection of the intrinsic polarization properties of animal optical materials creates enhanced structural reflectivity and camouflage.
Philosophical Transactions of the Royal Society B: Biological Sciences, 372(1724), 2017.

[47] Joanna Aizenberg, Alexei Tkachenko, Steve Weiner, Lia Addadi, and Gordon Hendler.
Calcitic microlenses as part of the photoreceptor system in brittlestars.

Nature 2001 412:6849, 412(6849):819–822, 8 2001.

[48] Wendy J. Crookes, Lin Lin Ding, Qing Ling Huang, Jennifer R. Kimbell, Joseph Horwitz, and Margaret J. HcFall-Ngai.
Reflectins: The Unusual Proteins of Squid Reflective Tissues.
Science, 303(5655):235–238, 1 2004.

[49] Johannes W Goessling, William P Wardley, Martin Lopez-Garcia, J W Goessling, W P Wardley, and M Lopez-Garcia.
Highly Reproducible, Bio-Based Slab Photonic Crystals Grown by Diatoms.
Advanced Science, 7(10):1903726, 5 2020.

[50] ANDREW R Parker.
The diversity and implications of animal structural colours.
Journal of Experimental Biology, 201(16):2343–2347, 1998.

[51] Andrew R. Parker, David R. Mckenzie, and Maryanne C.J. Large.
Multilayer reflectors in animals using green and gold beetles as contrasting examples.
Journal of Experimental Biology, 201(9):1307–1313, 5 1998.

[52] Richard O. Prum and Rodolfo H. Torres.
Structural colouration of mammalian skin: convergent evolution of coherently scattering dermal collagen arrays.
Journal of Experimental Biology, 207(12):2157–2172, 5 2004.

[53] Priscilla Simonis and Serge Berthier.
How Nature Produces Blue Color.
In Dr Alessandro Massaro, editor, *Photonic crystals: Introduction, applications and theory*, chapter How Nature. InTech, 2012.

[54] Amanda L. Holt, Sanaz Vahidinia, Yakir Luc Gagnon, Daniel E. Morse, and Alison M. Sweeney.
Photosymbiotic giant clams are transformers of solar flux.
Journal of the Royal Society Interface, 11(101), 2014.

[55] Amitabh Ghoshal, Elizabeth Eck, Michael Gordon, and Daniel E. Morse.
Wavelength-specific forward scattering of light by Bragg-reflective iridocytes in giant clams.
Journal of the Royal Society Interface, 13(120), 2016.

[56] Johannes W Goessling, Yanyan Su, Paulo Cartaxana, Christian Maibohm, Lars F Rickelt, Erik C L Trampe, Sandra L Walby, Daniel Wangpraseurt, Xia Wu, Marianne Ellegaard, Michael K€ Uhl, and Michael K€.

Structure-based optics of centric diatom frustules: modulation of the in vivo light field for efficient diatom photosynthesis.
New Phytologist, 219:122–134, 2018.

[57] Christopher I. Cazzonelli.
Carotenoids in nature: insights from plants and beyond.
Functional Plant Biology, 38(11):833–847, 10 2011.

[58] Beverley J. Glover and Heather M. Whitney.
Structural colour and iridescence in plants: the poorly studied relations of pigment colour.
Annals of Botany, 105(4):505–511, 4 2010.

[59] Holly L. Gorton and Thomas C. Vogelmann.
Effects of Epidermal Cell Shape and Pigmentation on Optical Properties of Antirrhinum Petals at Visible and Ultraviolet Wavelengths.
Plant Physiology, 112(3):879–888, 11 1996.

[60] Saskia Wilmsen, Adrian G. Dyer, and Klaus Lunau.
Conical flower cells reduce surface gloss and improve colour signal integrity for free-flying bumblebees.
Journal of Pollination Ecology, 28:108–126, 7 2021.

[61] Heather M. Whitney, K. M.Veronica Bennett, Matthew Dorling, Lucy Sandbach, David Prince, Lars Chittka, and Beverley J. Glover.
Why do so many petals have conical epidermal cells?
Annals of Botany, 108(4):609–616, 9 2011.

[62] Silvia Vignolini, Edwige Moyroud, Thomas Hingant, Hannah Banks, Paula J. Rudall, Ullrich Steiner, and Beverley J. Glover.
The flower of Hibiscus trionum is both visibly and measurably iridescent.
New Phytologist, 205(1):97–101, 2015.

[63] Edwige Moyroud, Tobias Wenzel, Rox Middleton, Paula J. Rudall, Hannah Banks, Alison Reed, Greg Mellers, Patrick Killoran, M. Murphy Westwood, Ullrich Steiner, Silvia Vignolini, and Beverley J. Glover.
Disorder in convergent floral nanostructures enhances signalling to bees.
Nature, 550(7677):469–474, 10 2017.

[64] Heather M. Whitney, Alison Reed, Sean A. Rands, Lars Chittka, and Beverley J. Glover.
Flower iridescence increases object detection in the insect visual system without compromising object identity.
Current Biology, 26(6):802–808, 3 2016.

[65] Casper J. van der Kooi, Bodo D. Wilts, Hein L. Leertouwer, Marten Staal, J. Theo M. Elzenga, and Doekele G. Stavenga.
Iridescent flowers? Contribution of surface structures to optical signaling.
New Phytologist, 203(2):667–673, 7 2014.

[66] Rox Middleton, Miranda Sinnott-Armstrong, Yu Ogawa, Gianni Jacucci, Edwige Moyroud, Paula J. Rudall, Chrissie Prychid, Maria Conejero, Beverley J. Glover, Michael J. Donoghue, and Silvia Vignolini.
Viburnum tinus Fruits Use Lipids to Produce Metallic Blue Structural Color.
Current Biology, 30(19):3804–3810, 10 2020.

[67] Silvia Vignolini, Paula J. Rudall, Alice V. Rowland, Alison Reed, Edwige Moyroud, Robert B. Faden, Jeremy J. Baumberg, Beverley J. Glover, and Ullrich Steiner.
Pointillist structural color in Pollia fruit.
Proceedings of the National Academy of Sciences of the United States of America, 109(39):15712–15715, 9 2012.

[68] David W. Lee.
Ultrastructural basis and function of iridescent blue colour of fruits inElaeocarpus.
Nature 1991 349:6306, 349(6306):260–262, 1991.

[69] David W. Lee, George T. Taylor, and Anthony K. Irvine.
Structural fruit coloration in Delarbrea michieana (Araliaceae).
International Journal of Plant Sciences, 161(2):297–300, 7 2000.

[70] Silvia Vignolini, Thomas Gregory, Mathias Kolle, Alfie Lethbridge, Edwige Moyroud, Ullrich Steiner, Beverley J. Glover, Peter Vukusic, and Paula J. Rudall.
Structural colour from helicoidal cell-wall architecture in fruits of Margaritaria nobilis.
Journal of The Royal Society Interface, 13(124), 11 2016.

[71] Chris J. Chandler, Bodo D. Wilts, Juliet Brodie, and Silvia Vignolini.
Structural Color in Marine Algae.
Advanced Optical Materials, 2017.

[72] Chris J. Chandler, Bodo D. Wilts, Silvia Vignolini, Juliet Brodie, Ullrich Steiner, Paula J. Rudall, Beverley J. Glover, Thomas Gregory, and Rachel H. Walker.
Structural colour in Chondrus crispus.
Scientific Reports, 5(1):11645, 12 2015.

[73] William H Gerwick and Norma J Lang.
Structural, chemical and ecological studies on iridescence in iridaea (rhodophyta) 1.
Journal of Phycology, 13(2):121–127, 1977.

[74] Martin Lopez-Garcia, Nathan Masters, Heath E O'Brien, Joseph Lennon, George Atkinson, Martin J Cryan, Ruth Oulton, and Heather M Whitney.
Light-induced dynamic structural color by intracellular 3d photonic crystals in brown algae.
Science advances, 4(4):eaan8917, 2018.

[75] Fabian Fischer, Evelyne Zufferey, Jean Marc Bourgeois, Julien Héritier, and Fabrice Micaux.
UV-ABC screens of luteolin derivatives compared to edelweiss extract.
Journal of Photochemistry and Photobiology B: Biology, 103(1):8–15, 4 2011.

[76] Jean Pol Vigneron, Marie Rassart, Zofia Vértesy, Krisztián Kertész, Michael Sarrazin, László P. Biró, Damien Ertz, and Virginie Lousse.
Optical structure and function of the white filamentary hair covering the edelweiss bracts.
Physical Review E - Statistical, Nonlinear, and Soft Matter Physics, 71(1), 1 2005.

[77] John B. Clark and Geoffrey R. Lister.
Photosynthetic Action Spectra of TreesII. The Relationship of Cuticle Structure to the Visible and Ultraviolet Spectral Properties of Needles from Four Coniferous Species.
Plant Physiology, 55(2):407–413, 2 1975.

[78] Charles Hébant and David W. Lee.
ULTRASTRUCTURAL BASIS AND DEVELOPMENTAL CONTROL OF BLUE IRIDESCENCE IN SELAGINELLA LEAVES.
American Journal of Botany, 71(2):216–219, 2 1984.

[79] Kevin S. Gould and David W. Lee.
Physical and ultrastructural basis of blue leaf iridescence in four Malaysian understory plants.
American Journal of Botany, 83(1):45–50, 1 1996.

[80] Rita M. Graham, David W. Lee, and Knut Norstog.
PHYSICAL AND ULTRASTRUCTURAL BASIS OF BLUE LEAF IRIDESCENCE IN TWO NEOTROPICAL FERNS.
American Journal of Botany, 80(2):198–203, 2 1993.

[81] Lisa Maria Steiner, Yu Ogawa, Villads Egede Johansen, Clive R. Lundquist, Heather Whitney, and Silvia Vignolini.
Structural colours in the frond of Microsorum thailandicum.
Journal of the Royal Society Interface Focus, 9(1), 2 2019.

[82] John A Endler.

The color of light in forests and its implications.
Ecological monographs, 63(1):1–27, 1993.

[83] Olaf Karthaus.
Biomimetics in photonics.
CRC press, 2012.

[84] Katherine R. Thomas, Mathias Kolle, Heather M. Whitney, Beverley J. Glover, and Ullrich Steiner.
Function of blue iridescence in tropical understorey plants.
Journal of The Royal Society Interface, 7(53):1699–1707, 12 2010.

[85] Karin Kjernsmo, Joanna R. Hall, Cara Doyle, Nadia Khuzayim, Innes C. Cuthill, Nicholas E. Scott-Samuel, and Heather M. Whitney.
Iridescence impairs object recognition in bumblebees.
Scientific Reports 2018 8:1, 8(1):1–5, 5 2018.

[86] Robert R Wise.
The diversity of plastid form and function.
In *The structure and function of plastids*, pages 3–26. Springer, 2007.

[87] Debashish Bhattacharya, Hwan Su Yoon, and Jeremiah D Hackett.
Photosynthetic eukaryotes unite: endosymbiosis connects the dots.
Bioessays, 26(1):50–60, 2004.

[88] Matthew Jacobs, Martin Lopez-Garcia, O. Phart Phrathep, Tracy Lawson, Ruth Oulton, and Heather M. Whitney.
Photonic multilayer structure of Begonia chloroplasts enhances photosynthetic efficiency.
Nature Plants, 2(October):1–6, 2016.

[89] Jian Wei Liu, Shau Fu Li, Chin Ting Wu, Iván A. Valdespino, Jia Fang Ho, Yeh Hua Wu, Ho Ming Chang, Te Yu Guu, Mei Fang Kao, Clive Chesson, Sauren Das, Hank Oppenheimer, Ane Bakutis, Peter Saenger, Noris Salazar Allen, Jean W.H. Yong, Bayu Adjie, Ruth Kiew, Nalini Nadkarni, Chun Lin Huang, Peter Chesson, and Chiou Rong Sheue.
Gigantic chloroplasts, including bizonoplasts, are common in shade-adapted species of the ancient vascular plant family Selaginellaceae.
American Journal of Botany, 107(4):562–576, 4 2020.

[90] Chiou Rong Sheue, Vassilios Sarafis, Ruth Kiew, Ho Yih Liu, Alexandre Salino, Ling Long Kuo-Huang, Yuen Po Yang, Chi Chu Tsai, Chun Hung Lin, Jean W.H. Yong, and Maurice S.B. Ku.

Bizonoplast, a unique chloroplast in the epidermal cells of microphylls in the shade plant Selaginella erythropus (Selaginellaceae).
American Journal of Botany, 94(12):1922–1929, 2007.

[91] Nathan J. Masters, Martin Lopez-Garcia, Ruth Oulton, and Heather M. Whitney.
Characterization of chloroplast iridescence in Selaginella erythropus.
Journal of The Royal Society Interface, 15(148):20180559, 11 2018.

[92] Rabia Ghaffar, Marieluise Weidinger, Barbara Mähnert, Michael Schagerl, and Irene Lichtscheidl.
Adaptive responses of mature giant chloroplasts in the deep-shade lycopod Selaginella erythropus to prolonged light and dark periods.
Plant, Cell & Environment, 41(8):1791–1805, 8 2018.

[93] O-Phart Phrathep et al.
Biodiversity and physiology of Begonia iridoplasts.
PhD thesis, University of Bristol, 2020.

[94] Miguel A. Castillo, William P. Wardley, and Martin Lopez-Garcia.
Light-Dependent Morphological Changes Can Tune Light Absorption in Iridescent Plant Chloroplasts: A Numerical Study Using Biologically Realistic Data.
ACS Photonics, 8(4):1058–1068, 4 2021.

[95] G Paillotin, W Leibl, Jacek Gapiński, J Breton, and Andrzej Dobek.
Light gradients in spherical photosynthetic vesicles.
Biophysical journal, 75(1):124–133, 1998.

[96] Kiah A Barton, Martin H Schattat, Torsten Jakob, Gerd Hause, Christian Wilhelm, Joseph F Mckenna, Csaba Máthé, John Runions, Daniel Van Damme, and Jaideep Mathur.
Epidermal pavement cells of arabidopsis have chloroplasts, 2016.

[97] D. W. Lee and J. B. Lowry.
Physical basis and ecological significance of iridescence in blue plants.
Nature 1975 254:5495, 254(5495):50–51, 1975.

[98] Shang-Hung Pao, Ping-Yun Tsai, Ching-I Peng, Pei-Ju Chen, Chi-Chu Tsai, En-Cheng Yang, Ming-Chih Shih, Jiannyeu Chen, Jun-Yi Yang, Peter Chesson, and others.
Lamelloplasts and minichloroplasts in Begoniaceae: iridescence and photosynthetic functioning.
Journal of plant research, pages 1–16, 2018.

[99] Mark C Tebbitt.
Begonias: cultivation, identification, and natural history.
Timber Press (OR), 2005.

[100] Mark Hughes, Peter M Hollingsworth, and J Squirrell.
Isolation of polymorphic microsatellite markers for begonia sutherlandii hook. f.
Molecular Ecology Notes, 2(2):185–186, 2002.

[101] Kiah A Barton, Martin H Schattat, Torsten Jakob, Gerd Hause, Christian Wilhelm, Joseph F Mckenna, Csaba Máthé, John Runions, Daniel Van Damme, and Jaideep Mathur.
Epidermal pavement cells of arabidopsis have chloroplasts, 2016.

[102] Jacob O Brunkard, Anne M Runkel, and Patricia C Zambryski.
Chloroplasts extend stromules independently and in response to internal redox signals.
Proceedings of the National Academy of Sciences, 112(32):10044–10049, 2015.

[103] Elizabeth J Robertson, Stephen M Rutherford, and Rachel M Leech.
Characterization of chloroplast division using the arabidopsis mutant arc5.
Plant Physiology, 112(1):149–159, 1996.

[104] Paul Dupree, Keng-Hock Pwee, and John C Gray.
Expression of photosynthesis gene-promoter fusions in leaf epidermal cells of transgenic tobacco plants.
The Plant Journal, 1(1):115–120, 1991.

[105] Helmut Kirchhoff, Chris Hall, Magnus Wood, Miroslava Herbstová, Onie Tsabari, Reinat Nevo, Dana Charuvi, Eyal Shimoni, and Ziv Reich.
Dynamic control of protein diffusion within the granal thylakoid lumen.
Proceedings of the National Academy of Sciences of the United States of America, 108(50):20248–20253, 12 2011.

[106] William HJ Wood, Craig MacGregor-Chatwin, Samuel FH Barnett, Guy E Mayneord, Xia Huang, Jamie K Hobbs, C Neil Hunter, and Matthew P Johnson.
Dynamic thylakoid stacking regulates the balance between linear and cyclic photosynthetic electron transfer.
Nature plants, 4(2):116–127, 2018.

[107] Alexander V Ruban and Matthew P Johnson.
Dynamics of higher plant photosystem cross-section associated with state transitions.
Photosynthesis Research, 99(3):173–183, 2009.

[108] Matthew James Jacobs.
The development and function of \textit{Begonia} leaf iridescence.
PhD thesis, School of Biological Sciences, University of Bristol, 2017.

[109] A. Capretti, A. K. Ringsmuth, J. F. van Velzen, A. Rosnik, R. Croce, and T. Gregorkiewicz.
Nanophotonics of higher-plant photosynthetic membranes.
Light: Science & Applications, 8(1):5, 12 2019.

[110] Bing Quan Huang and Edward C. Yeung.
Chemical and Physical Fixation of Cells and Tissues: An Overview.
Plant Microtechniques and Protocols, pages 23–43, 9 2015.

[111] Mark E Stearns and EB Wagenaar.
Ultrastructural changes in chloroplasts of autumn leaves.
Canadian Journal of Genetics and Cytology, 13(3):550–559, 1971.

[112] Hartmut K Lichtenthaler and Fatbardha Babani.
Light adaptation and senescence of the photosynthetic apparatus. changes in pigment composition, chlorophyll fluorescence parameters and photosynthetic activity.
In *Chlorophyll a fluorescence*, pages 713–736. Springer, 2004.

[113] Hartmut K Lichtenthaler and Alan R Wellburn.
Determinations of total carotenoids and chlorophylls a and b of leaf extracts in different solvents, 1983.

[114] Casper J van der Kooi, J Theo M Elzenga, Jan Dijksterhuis, and Doekele G Stavenga.
Functional optics of glossy buttercup flowers.
Journal of the Royal Society Interface, 14(127):20160933, 2017.

[115] Kerstin Koch, Bharat Bhushan, and Wilhelm Barthlott.
Multifunctional surface structures of plants: an inspiration for biomimetics.
Progress in Materials science, 54(2):137–178, 2009.

[116] Sakkia Wilmsen, Adrian G Dyer, and Klaus Lunau.
Conical flower cells reduce surface gloss and improve colour signal integrity for free-flying bumblebees.
Journal of Pollination Ecology, 28:108–126, 2021.

[117] A Nasrulhaq-Boyce and JG Duckett.
Dimorphic epidermal cell chloroplasts in the mesophyll-less leaves of an extreme–shade tropical fern, teratophyllum rotundifoliatum (r. bonap.) holtt.: a light and electron microscope study.
New Phytologist, 119(3):433–444, 1991.

[118] Denis L Fox and James R Wells.
Schemochromic blue leaf-surfaces of selaginella.
American Fern Journal, 61(3):137–139, 1971.

[119] Kevin S Gould, David W Lee, Understory Plants, Kevin S Gould, and David W Lee.
Physical and ultrastructural basis of blue leaf iridescence in four Malaysian understory plants.
American Journal of Botany, 83(1):45–50, 1996.

[120] Lyman B Smith and Bernice G Schubert.
The begoniaceae of colombia.
Contributions from the Gray Herbarium of Harvard University, (164):1–209, 1946.

[121] Jacob B Khurgin.
Slow light in various media: a tutorial.
Advances in Optics and Photonics, 2(3):287–318, 2010.

[122] Robert W Boyd.
Material slow light and structural slow light: similarities and differences for nonlinear optics.
JOSA B, 28(12):A38–A44, 2011.

[123] Suzushi Nishimura, Neal Abrams, Bradley A Lewis, Lara I Halaoui, Thomas E Mallouk, Kurt D Benkstein, Jao Van de Lagemaat, and Arthur J Frank.
Standing wave enhancement of red absorbance and photocurrent in dye-sensitized titanium dioxide photoelectrodes coupled to photonic crystals.
Journal of the American Chemical Society, 125(20):6306–6310, 2003.

[124] Jesper Pedersen, Sanshui Xiao, and Niels Asger Mortensen.
Slow-light enhanced absorption for bio-chemical sensing applications: potential of low-contrast lossy materials.
arXiv preprint arXiv:0802.0558, 2008.

[125] Qingwu Meng, Nathan Kelly, and Erik S. Runkle.
Substituting green or far-red radiation for blue radiation induces shade avoidance and promotes growth in lettuce and kale.
Environmental and Experimental Botany, 162:383–391, 6 2019.

[126] Woo Hyun Kang, Jong Seok Park, Kyung Sub Park, and Jung Eek Son.
Leaf photosynthetic rate, growth, and morphology of lettuce under different fractions of red, blue, and green light from light-emitting diodes (LEDs).
Horticulture, Environment, and Biotechnology 2016 57:6, 57(6):573–579, 12 2016.

[127] Jan M Anderson.
Photoregulation of the composition, function, and structure of thylakoid membranes.
Annual review of plant physiology, 37(1):93–136, 1986.

[128] XY Wang, XM Xu, and J Cui.
The importance of blue light for leaf area expansion, development of photosynthetic apparatus, and chloroplast ultrastructure of cucumis sativus grown under weak light.
Photosynthetica, 53(2):213–222, 2015.

[129] Chun-Xia Li, Zhi-Gang Xu, Rui-Qi Dong, Sheng-Xin Chang, Lian-Zhen Wang, Muhammad Khalil-Ur-Rehman, and Jian-Min Tao.
An rna-seq analysis of grape plantlets grown in vitro reveals different responses to blue, green, red led light, and white fluorescent light.
Frontiers in plant science, 8:78, 2017.

[130] A. Melis and G. W. Harvey.
Regulation of photosystem stoichiometry, chlorophyll a and chlorophyll b content and relation to chloroplast ultrastructure.
BBA - Bioenergetics, 1981.

[131] Jack Myers, Jo-Ruth Graham, and Richard T. Wang.
Light Harvesting in Anacystis nidulans Studied in Pigment Mutants.
Plant Physiology, 66(6):1144–1149, 12 1980.

[132] Miroslava Herbstová, Stefanie Tietz, Christopher Kinzel, Maria V. Turkina, and Helmut Kirchhoff.
Architectural switch in plant photosynthetic membranes induced by light stress.
Proceedings of the National Academy of Sciences of the United States of America, 109(49):20130–20135, 12 2012.

[133] Helmut Kirchhoff.
Architectural switches in plant thylakoid membranes.
Photosynthesis Research, 116(2-3):481–487, 10 2013.

[134] Sébastien R. Mouchet, Stephen Luke, Luke T. McDonald, and Pete Vukusic.
Optical costs and benefits of disorder in biological photonic crystals.
Faraday Discussions, 223(0):9–48, 10 2020.

[135] Maximilian Rothammer, Cordt Zollfrank, Kurt Busch, and Georg von Freymann.
Tailored Disorder in Photonics: Learning from Nature.
Advanced Optical Materials, 9(19):2100787, 10 2021.

[136] Edwige Moyroud, Tobias Wenzel, Rox Middleton, Paula J Rudall, Hannah Banks, Alison Reed, Greg Mellers, Patrick Killoran, M Murphy Westwood, Ullrich Steiner, et al.
Disorder in convergent floral nanostructures enhances signalling to bees.
Nature, 550(7677):469–474, 2017.

[137] Matteo Burresi, Lorenzo Cortese, Lorenzo Pattelli, Mathias Kolle, Peter Vukusic, Diederik S. Wiersma, Ullrich Steiner, and Silvia Vignolini.
Bright-White Beetle Scales Optimise Multiple Scattering of Light.
Scientific Reports 2014 4:1, 4(1):1–8, 8 2014.

[138] C Pouya, D G Stavenga, P Vukusic, J D Joannopoulos, S G Johnson, J N Winn, and R D Meade.
Discovery of ordered and quasi-ordered photonic crystal structures in the scales of the beetle Eupholus magnificus.
Optics Express, Vol. 19, Issue 12, pp. 11355-11364, 19(12):11355–11364, 6 2011.

[139] Jan P. Dekker and Egbert J. Boekema.
Supramolecular organization of thylakoid membrane proteins in green plants.
Biochimica et Biophysica Acta (BBA) - Bioenergetics, 1706(1-2):12–39, 1 2005.

[140] Seng Fatt Liew and Hui Cao.
Optical properties of 1D photonic crystals with correlated and uncorrelated disorder.
Journal of Optics, 12(2):024011, 1 2010.

[141] Nathan J Masters, Martin Lopez-Garcia, Ruth Oulton, and Heather M Whitney.
Characterization of chloroplast iridescence in selaginella erythropus.
Journal of the Royal Society Interface, 15(148):20180559, 2018.

[142] Helmut Kirchhoff, Chris Hall, Magnus Wood, Miroslava Herbstová, Onie Tsabari, Reinat Nevo, Dana Charuvi, Eyal Shimoni, and Ziv Reich.
Dynamic control of protein diffusion within the granal thylakoid lumen.
Proceedings of the National Academy of Sciences, 108(50):20248–20253, 2011.

[143] Yasuko Kaneko and Paul Walther.
Comparison of ultrastructure of germinating pea leaves prepared by high-pressure freezing–freeze substitution and conventional chemical fixation.
Microscopy, 44(2):104–109, 1995.

[144] Dimitri Vanhecke, Werner Graber, and Daniel Studer.
Close-to-native ultrastructural preservation by high pressure freezing.
Methods in cell biology, 88:151–164, 2008.

[145] Robert A Grassucci, Derek J Taylor, and Joachim Frank.
Preparation of macromolecular complexes for cryo-electron microscopy.
Nature protocols, 2(12):3239–3246, 2007.

[146] Satoru Murakami and Lester Packer.
Protonation and chloroplast membrane structure.
The Journal of cell biology, 47(2):332–351, 1970.

[147] Phillip A. Davis, Steven Caylor, Craig W. Whippo, and Roger P. Hangarter.
Changes in leaf optical properties associated with light-dependent chloroplast movements.
Plant, Cell & Environment, 34(12):2047–2059, 12 2011.

[148] Ta Yan Leong, David J. Goodchild, and Jan M. Anderson.
Effect of Light Quality on the Composition, Function, and Structure of Photosynthetic Thylakoid Membranes of Asplenium australasicum (Sm.) Hook.
Plant Physiology, 78(3):561–567, 7 1985.

[149] Ute C Vothknecht and Peter Westhoff.
Biogenesis and origin of thylakoid membranes.
Biochimica et Biophysica Acta (BBA)-Molecular Cell Research, 1541(1-2):91–101, 2001.

[150] Wah Soon Chow, Eun-Ha Kim, Peter Horton, and Jan M Anderson.
Granal stacking of thylakoid membranes in higher plant chloroplasts: the physicochemical forces at work and the functional consequences that ensue.
Photochemical & Photobiological Sciences, 4(12):1081–1090, 2005.

[151] Thomas C Vogelmann, Greg Martin, Guoying Chen, and Daniel Buttry.
Fibre optic microprobes and measurement of the light microenvironment within plant tissues.
In *Advances in Botanical Research*, volume 18, pages 255–295. Elsevier, 1991.

[152] Fabiola Cardoso Delgado.
Dynamic iridescence of Phyllagathis rotundifolia.
PhD thesis, University of Bristol, 2022.

[153] Nathan Masters.
Structural colour in plants and algae.
PhD thesis, University of Bristol, 2020.

[154] LV Evans.
Chloroplast morphology and fine structure in british fucoids.
New Phytologist, 67(1):173–178, 1968.

[155] George Karabourniotis, Harry T Horner, Panagiota Bresta, Dimosthenis Nikolopoulos, and Georgios Liakopoulos.
New insights into the functions of carbon–calcium inclusions in plants.
New Phytologist, 228(3):845–854, 2020.

[156] Assaf Gal, Vlad Brumfeld, Steve Weiner, Lia Addadi, and Dan Oron.
Certain biominerals in leaves function as light scatterers.
Advanced Materials, 24(10):OP77–OP83, 2012.

[157] Maria Pierantoni, Ron Tenne, Vlad Brumfeld, Vladimir Kiss, Dan Oron, Lia Addadi, and Steve Weiner.
Plants and light manipulation: the integrated mineral system in okra leaves.
Advanced Science, 4(5):1600416, 2017.

[158] Kanako Sato, Akira Yamauchi, Noriaki Ozaki, Takaaki Ishigure, Yuya Oaki, and Hiroaki Imai.
Optical properties of biosilicas in rice plants.
RSC advances, 6(110):109168–109173, 2016.